THREE NEW DESIGNS OF COVALENT CAGES

STUDY OF SYNTHESIS, LUMINESCENCE, COORDINATION AND CATALYSIS

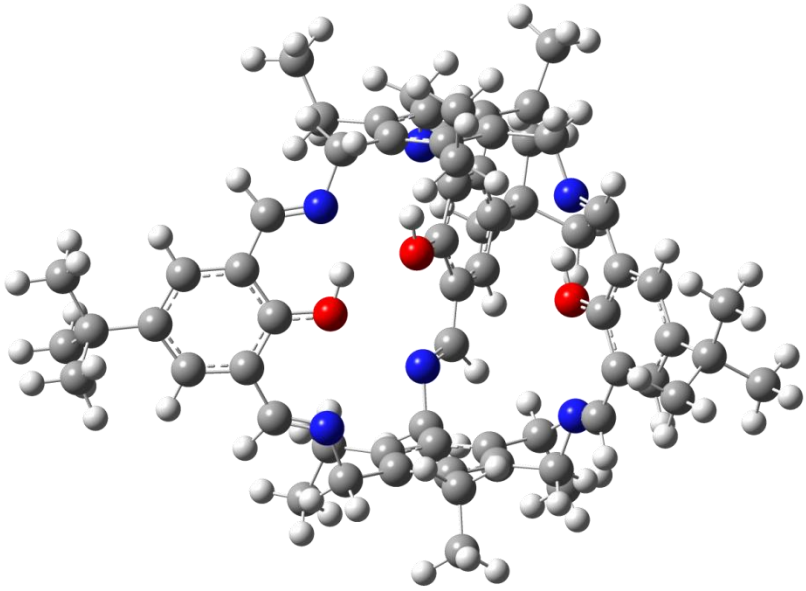

Masterthesis
S.J. van Dijk, BSc

28-02-2017

Dr. M. Otte,
Dr. M.-E. Moret,
Prof. dr. R.J.M. Klein Gebbink

Organic Chemistry and Catalysis
Debye Institute for Nanomaterials Science

ABSTRACT

Organic cages provide regularly well-defined cavities, which have the potential for many applications such as catalysis or sensoring. In recent years, dynamic covalent chemistry (DCC) has become an important approach for the synthesis of purely organic cages. This study focuses on three new designs: **A**, **B** and **C** (Figure 1). The designs are heterosequenced and/or contain a functionalized interior to stimulate versatile catalysis. They are analyzed with retrosynthesis and separated in building blocks. The synthesis of building blocks is studied as well as the coupling reactions between building blocks (DCC). Unfortunately, cage **A** and **B** could not be synthesized as the coupling reaction(s) failed. Cage **C** is successfully synthesized with a quantitative yield (**C1**) as well as the imine analogue (**C2**). **C2** shows luminescence with addition of acid. This property is further studied and quantified. In addition, both cages show the ability to coordinate zinc ions. Other metals have been tested for **C2**. However, only indirect evidence of coordination is found due to solubility issues. Catalytic testing for a possible **C2** with Fe(III) leads to inconclusive results.

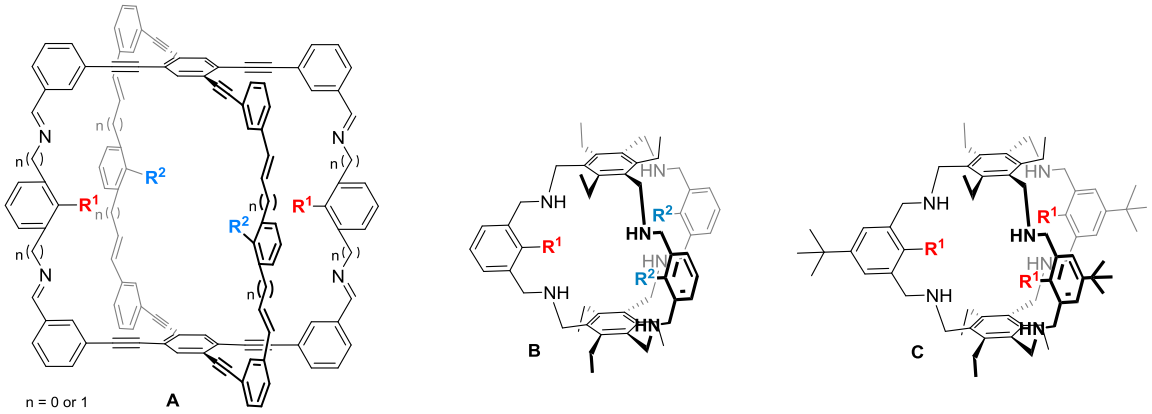

Figure 1: *Three new designs of organic covalent cages (a) Cage compound **A**. (b) Cage compound **B**. (c) Cage Compound **C**.*

TABLE OF CONTENT

LIST OF ABBREVIATIONS

COF = Covalent Organic Framework
DCC = Dynamic Covalent Chemistry
FGI = Functional Group Interconversion
FLP = Frustrated Lewis pair
HOMO = Highest Occupied Molecular Orbital
LUMO = Lowest Unoccupied Molecular Orbital
ODCC = Orthogonal Dynamic Covalent Chemistry

°C = Degrees Celsius
h = Hour
RT = Room temperature
eq = Equivalent

DEAD = diethyl azodicarboxylate
DMF = Dimethylformamide
FA = Formic acid
TBAF = Tetra-*n*-butylammoniumfluoride
^{t}Bu = *tert*-butyl
TCB = 1,3,4-trichlorobenzene
TFA = Trifluoroacetic acid
TMS = trimethylsilyl

NMR = Nuclear Magnetic Resonance
^{13}C MAS NMR = ^{13}C Magic Angle Spinning - NMR
COSY NMR = Correlation Spectroscopy NMR
DFT = Density Function Theory
DOSY NMR = Diffusion Ordered Spectroscopy NMR
ESI-MS = ElectroSpray Ionization Mass Spectroscopy
IR = Infrared
MALDI-TOF = Matrix assisted laser desorption/ionisation - time of flight mass spectrometry
TLC = Thin layer chromatography
UV-VIS = Ultra Violet - Visual

Å = Angstrom
g = gram
mg = milligram
mmol = millimol
m/z = mass-to-charge ratio
nm = nanometer

1. INTRODUCTION

1.1. ALL ORGANIC MATERIALS

Supramolecular chemistry is a widely studied field of research. It significance is emphasized by two Nobel prizes for contribution in this area (1987 and 2016) [1]. This multidisciplinary field combines knowledge from organic chemistry, inorganic chemistry, biology, computational chemistry and others. It is focused on the assembly of relatively small building blocks into large, ordered structures; which are based on non-covalent intermolecular interactions. Consequently, very dynamic structures are formed with well-defined cavities. The compounds could provide molecular recognition via these cavities, comparable to enzymes. Specifically, the reactive site of enzymes could be mimicked. Research might lead to development of new, enzyme-mimicked catalysts or a better understanding of the mechanisms of enzymes based on models of their active sites. More information can be found in the many reviews written on supramolecular chemistry [2–7]. In addition, Mirkin *et al.* [8] provides a high quality review on enzyme mimicking.

Dynamic covalent chemistry (DCC) studies similar large, dynamic structures. However, the building blocks are linked with covalent bonds. The structures are dynamic due to reversible formation and breaking of covalent bonds [9] (see sections 2.1 and 2.2). The use of covalent bonds provides very rigid structures.

All organic materials designed with DCC can be categorized in 2-D (flat) and 3-D structures. The first subclass of materials are macrocycles. These 2-D structures are defined by IUPAC as, "*cyclic macromolecule or a macromolecular cyclic portion of a molecule*" [10]. A crownether, as shown in figure 2a, is an example of a small macrocycle. Individual macrocycles are mostly studied for the single molecule applications, such as recognition. However, they are also known to align in long channels (3-D) though π-stacking of the individual macrocycles [11–13]. Another interesting subclass of materials are the covalent organic frameworks (COFs), which can be described as layers consisting of linked macrocycles [1]. Also, these 2-D structures can form channels via π-stacking. The last subclass are organic cages, which are defined by IUPAC as, "*polycyclic compounds with a shape of a cage*" [14]. Cryptands were the first synthesized organic cages. An example is shown in figure 2b. The previously mentioned Nobel prize of 1987 was given for the discovery of cryptands. Our work mainly concentrates on organic cages, which did not reached full potential yet. Therefore, a lot of knowledge on this topic can be gained. Although, many of the concepts will also apply for macrocycles. Additional information on macrocycles [15–17] and COFs [18,19] can be found in respective reviews.

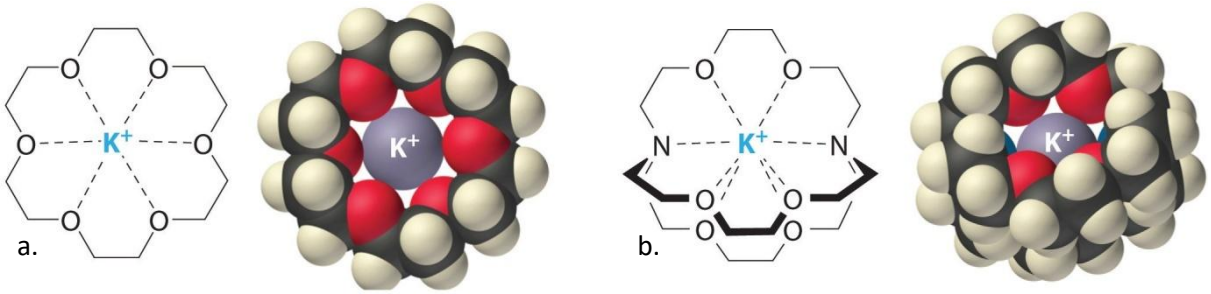

Figure 2: *(a) The crown ether 18-crown-6. Crown ethers can be classified as a macrocycle. (b) The cryptand crypt-222. Cryptands are an example of organic cages* [4].

[1] There are some examples known in which COFs are formed of linked cages (e.g. Li *et al.*[102]) .

1.2 POSSIBLE APPLICATIONS

Cage compounds are mainly synthesized for scientific interest. In general, the research is more fundamental and it is, to my knowledge, not applied in industry yet. However, they are intensively studied for possible applications. The possible applications can be split in four main groups: stabilization, recognition, porous materials and catalysis [14]. The categories will be discussed individually and an example will be given for each category.

- ***1.2.1. STABILIZATION***

  Reactive species can be stabilized by storage within the cavity of the cage, which protects them against harmful environments. This results in a longer lifetime of the reactive compounds.

  Warmuth *et al.* [20] provides a nice example. Highly reactive compounds are stabilized by the imine cage shown in figure 3. It is used as a molecular reaction flask for photochemical reactions. An encapsulated precursor is irradiated leading to the formation of Bredt olefins adamantene and 1-noradamantyldiazomethane, of which adamantene is a highly strained, reactive compound. However, it is observed that the products are stable for days at room temperature if DMSO-d_6/CD_3CN is used as solvent. The cage protects the reactive adamantene from the bulk solvent. Consequently, the products have a lifetime of minutes if D_2O is used, due to the hydrolysis of the imine bonds. The cage compound can no longer supply a protected cavity.

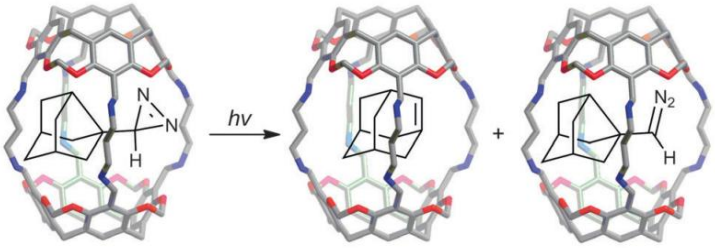

Figure 3: *Cage compound used as molecular reaction flask by Warmuth et al. 3-Noradamantyldiazirine encapsulated by a dynamic octaimine hemicarcerand is irradiated resulting in Bredt olefins adamantene and 1-noradamantyldiazomethane both still encapsulated in the cage.*

- ***1.2.2. RECOGNITION***

  Many investigators have been focused on selective recognition of guest molecules or ions through interaction with the cavity of a cage. Cages are great hosts for recognition due to many factors: rigidity, a well defined cavity and the possibility to vary size and shape of the cage as well as position and nature of interaction with guests [21]. A large range of guest molecules from small ions to even polymers are suited for recognition due to the variation in cages. A good interaction between guest and host requires an ideal match in size and interactions, which can be influenced by design of the cage or choice in guest. Especially anionic recognition is widely studied due to their important role in cell biology; 70% of all cofactors and substrates are anionic. Multiple methods are developed to make a cage suitable for anionic guests such as protonation of amine based cages [22]. Guests can bind in different ways depending on the cage. Interior binding and exterior binding is shown in the following example. In addition, a hybrid form is possible, in which a guest binds in a side pocket [22].

An example is given by Severin *et al.* [23], who conducted research on another cage compound (figure 4). It is found that the cage contains two different binding sites. The exterior of the cage can bind smaller cations such as Li^+, and the interior, which can bind larger cations such as Cs^+. Complexation with cesium cations are known to give color change. Therefore, the complex can be used as a selective sensor for cesium ions which can be read out with the naked eye.

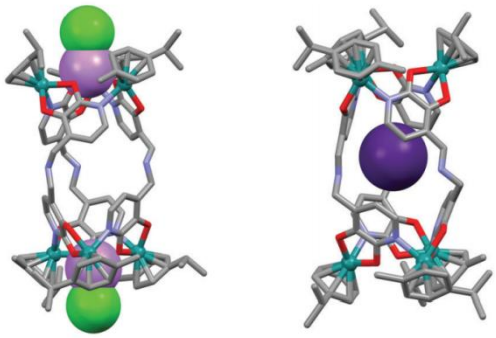

Figure 4: *Left: bis-LiCl adduct of the cage, Right: Cs^+ adduct of the cage.*

- ***1.2.3. POROUS MATERIALS***

The specific surface area of organic cage compounds is relativity large, which makes them interesting as new porous materials. Porosity in solution is possible if the cage compound is soluble. Although, the main interest remains in gas based absorption, which requires removal of solvents. Many cages collapse after solvent is removed. Shape persistent organic cage compounds must be specially designed for this purpose. They must have a defined interior, large enough to host other molecules, and does not collapse to a more dense or twisted structure. Rigid building blocks are required for shape persistent cages. It is shown that the created pores of the cages can remain after the solvent is removed with the right design. Permanent pores can be formed [14,24–26].

Systematic studies by Cooper and Mastalerz *et al*. show the influence of morphologies on the specific surface areas [14,27]. Varying in precipitation ratios, mixing time, solvent and reactant ratios resulted in many different structures which mainly varied in grade of crystallinity. In general, more amorphous samples have more surface area with a maximum of 859 m^2g^{-1}. Varying with the morphology of the periphery-substituted cages appears to be crucial in the magnitude of the specific surface area of crystalline compounds. More bulky substituents lead to lower surface areas. The highest surface area of 2071 m^2g^{-1} was found for a second polymorph of the *t*-butyl substituted cage compound shown in figure 5.

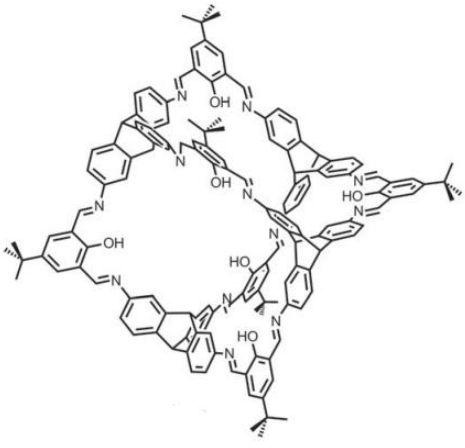

Figure 5: The *t*-butyl substituted cage which is found to have a great specific surface area if it is grown in crystalline structures.

- ***1.2.4. CATALYSIS***

Catalysis is of major importance, 80% of all chemical and pharmaceutical products are made with the use of catalysts. Organometallic catalysts are used for synthesis of a broad range of compounds, from fine to bulk [28]. The majority of organometallic catalysts still contain precious metals e.g. palladium and rhodium are used despite the high prices and toxicity. The demand is high to substitute precious metals for cheaper and overall less toxic base metals. Base metals include manganese, iron, cobalt, nickel, copper and zinc.

Cages can act as molecular flask which can prepare and store chemicals. The flasks are of similar size as the reactants (several nanometers). Molecular flasks are inspired by natures' enzymes, whose active sited are well defined pockets which can bind, order and modify a substrate [29]. These confined spaces can mediate or catalyze reactions [30]. There are two approaches to mimic the active site of an enzyme. The first approach aims for incorporation of an catalytic moiety into the cage, which then controls the environment of the active site [8]. Incorporation can be done by encapsulation of an active catalyst or by including a catalytically active center in the building blocks (metals or active organic groups) making the cage itself the catalyst. Size-selective catalysis is possible if the cages are well designed. The pores should let substrates selectively pass based on their size, where after they will be converted [30]. The second approach is to mimic the pocket of an enzyme without pre-defined catalytic moieties: structural mimics. The reaction speed is increased though effects as substrate concentration and reorganization of substrates [8].

Martinez and Dufaud *et al.* [31,32] describe the effects of cages by comparing catalytic activities of an encapsulated and a bare catalyst. The catalytic moiety in these studies are azaphosphatrane groups, which are highlighted in figure 6. They are catalytically active in neutral and protonated state. The neutral state can catalyze the Diels-Alder reaction whereas the protonated state can catalyze the synthesis of cyclic carbonates from CO_2 and epoxides. The active site is incorporated in a cage structure (figure 6a) or the active site is only surrounded by substituents (figure 6b). Catalytic testing for the neutral catalyst showed a similar catalytic activity. However, the diastereoselectivity is significantly higher for the cage complex. The protonated catalyst demonstrated that the confinement of the active site results in higher catalytic activity and lower degradation rates by protecting the catalyst from its environment. These experiments showcase the remarkable effect of caging on activity, stability and selectivity. It shows the relevance of cages in catalysis.

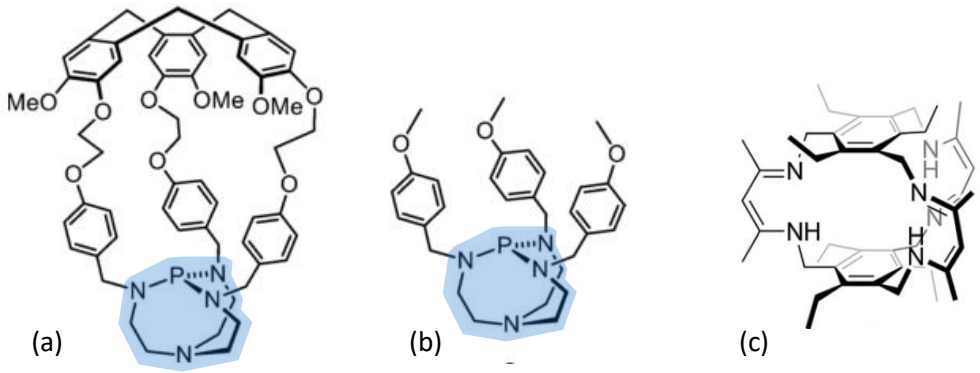

Figure 6: *(a) Caged catalyst of Martinez and Dufaud et al. The catalytic center is shown in blue. (b) Uncaged catalyst of Martinez and Dufaud et al. (c) Cage by Murray et al.*

Many researchers sough after small molecule activation as small molecules are generally readily available and inexpensive (e.g. O_2, CO_2, NH_3). Yet, due to their stability it is difficult to utilize activation. Murray *et al.* designed an organic cage, which shows evidence for small molecule activation. The structure is shown in figure 6c. The cage is made catalytic active though coordination of different base metals in the interior of the cage [33]. A strong base, benzyl potassium, is used for deprotonation after which a metal salt is added. A range of multiple metal complexes is synthesized and tested on small molecule activation. The copper cage was found to

coordinate nitrogen via the Cu(I) ions [34], which is a promising result. Coordination is the first step for activation. In another study, the iron analogue was found to coordinate and activate dinitrogen after reduction with KC_8, as three bridging nitrides were found in the product [35,36]. Finally, treatment with hydrides leads to the formation of metal hydride complexes, which are able to insert CO_2 (M=Fe,Co,Zn) [37,38]. These remarkable results show small molecule activation is feasible with the use of functionalized cages.

1.3 SYNTHESIS

1.3.1. MAIN ROUTES

The synthesis of cages is divided into two main routes: irreversible and reversible [5]. (I) The irreversible route makes use of irreversible bond formations; For instance, cross-coupling reactions ensure a stable cage against reactive chemicals. However, irreversible reactions are less used since the product yield is generally low [14]. Examples of irreversible reactions include Heck reaction and Sonogashira reaction.

(II) The reversible route is based on reversible covalent bond formation, and is named Dynamic Covalent Chemistry (DCC). The dynamic feature of reversible bonds enables molecular components to achieve the thermodynamic minimum of the energy landscape via an equilibrium state. In contrast to the irreversible route, high yields can be obtained due to 'self-healing', in which selective formation of a specific product is favored by thermodynamics [39]. Less byproducts are formed and many cages only require a one-step-synthesis from basic building blocks. Examples of reversible reactions include imine condensation and disulfide exchange.

DCC is an interesting combination of the error-correcting of supramolecular chemistry with the robustness of covalent bonds [9]. Although the number of studies on the synthesis of cages via DCC is increasing, it remains an area that has not yet reached its full potential. The next paragraphs will discuss DCC in more detail.

1.3.2. THEORY OF DYNAMIC COVALENT CHEMISTRY (DCC)

In a reaction mixture competing pathways tend to lead to different products (figure 7). Kinetic products (P1) are formed faster due to lower activation energy ($\Delta G^{\ddagger}$), whereas thermodynamic products (P2) are once formed more stable (ΔG^{0}). Product selectivity can be gained through kinetic or thermodynamic control, which both depend on reaction conditions.

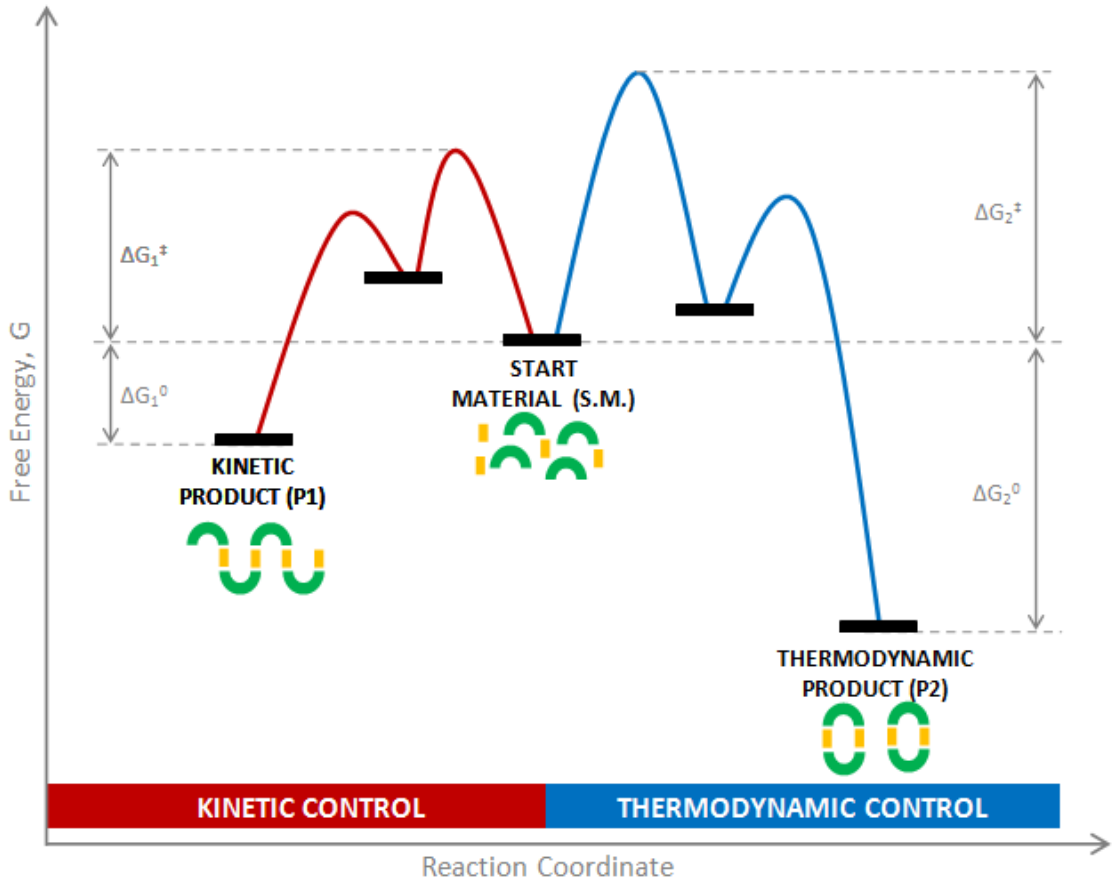

Figure 7: *Schematic representation of kinetic control and thermodynamic control in which the reaction coordinate and the free energy are plotted. The kinetic product is faster formed, where the thermodynamic product is more stable.*

As described before, the characteristic feature of DCC is based on the free exchange at a equilibrium state to achieve the thermodynamic minima of a system: thermodynamic control [40]. Consequently, the self-assembly of complex molecular architectures is determined by the stability of the equilibrium states. Therefore, dynamic covalent reactions with fast kinetics are generally preferred to reach the thermodynamic equilibrium within a reasonable time. Catalysts are often required to achieve a fast equilibrium. The composition of reaction mixtures can have large contrasts between pre-equilibrium and equilibrium [40].

Thermodynamic control requires a pathway independent product distribution at equilibrium. This can be easily disrupted by kinetic trapped products, which cannot freely interact with other compounds, for example insoluble compounds. Therefore, the thermodynamic equilibrium will not be reached. Kinetic traps are often undesired. They can be prevented by careful product design or modification [9].

The position of the equilibrium depends on the reaction environment. Factors can significantly change the equilibrium state as type of solvent, temperature, light, templates and metal ions. These factors can be tuned to aim for desired products. DCC is an adaptable strategy, which is a great advantage in synthesis. The equilibrium must be readily stopped to isolate the desired product; common methods to stop the exchange process are temperature control, pH control, removal of catalysts, or kinetically trapping the products by oxidation or reduction [9].

1.3.3. REVERSIBLE COVALENT REACTIONS

The formed covalent bonds should be stable enough to keep the cage intact, but should still have dynamic character which can be utilized with DCC. Therefore, the life span of the reversible covalent bonds must be between one millisecond and one minute [9]. Covalent bonds reported to be of dynamic nature include the following bonds: C-C, C-N, C-O, C-S, S-S and B-O. Dynamic covalent bonds can be created by two types of reactions, (I) exchange reactions, where one compound is exchanged for another (e.g. disulfide exchange, imine exchange). (II) formation of new dynamic covalent bonds (e.g. imine condensation, boronic acid condensation, olefin metathesis) [9,39].

This work mainly explores two reversible reactions. At first, imine condensation, also named imine formation, where aldehydes and amines react together to generate imines. The reaction mechanism is shown in scheme 1a. Imine condensation is catalyzed by Brønsted or Lewis acids. Trifluoroacetic acid (TFA) or MeOH are widely used for this purpose. In the first reaction step (step a), an aldehyde is protonated by acid to lead to a more electrophilic carbonyl. Subsequently, the amine attacks the carbonyl (step b), followed by a proton shift (step c), which enables the condensation step (step d). Last, deprotonation results in the desired imine (step e). Imine condensation is frequently used in DCC due to commonly high yields and simplicity of the reaction. Imine bonds are relative rigid, but still dynamic enough for DCC [14,39].

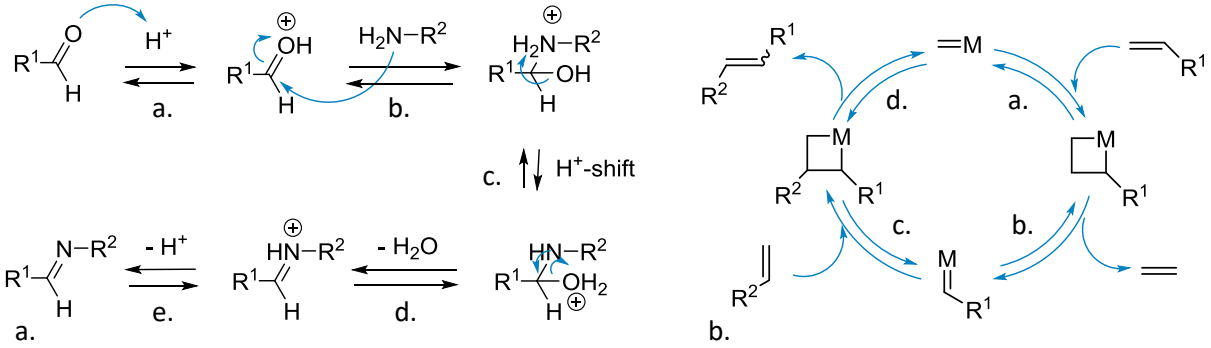

Scheme 1: *Reaction mechanism of (a) imine condensation, (b) olefin metathesis.*

The second reaction explored reaction is olefin metathesis, which is most often catalyzed by a Grubbs catalyst. The catalytic cycle is shown in scheme 1b. The first step is a cycloaddition of an olefin into the catalyst (step a). Followed by rearrangement of electrons resulting in elimination of ethylene (step b), a by-product in this reaction. Consequently, another cycloaddition takes place with another olefin (step c) and electron rearrangement finally leads to product elimination (step d). In contrast to imine condensation, olefin metathesis is still underexplored for DCC. The dynamic nature and error correcting character of this reaction was proven when Grubbs and co-workers reported template-directed depolymerisation of polymers to form cyclic oligomers in 1997 [40]. Ethylene should be removed from the reaction by using vacuum or adding nitrogen to allow the equilibrium to complete. Olefin metathesis is widely studied [9], the high number of studies on metathesis is a great advantage in exploring olefin metathesis for DCC. Other advantages include mild reaction conditions, availability of different catalysts and high functional group tolerance.

1.4. BUILDING BLOCKS

1.4.1. DESIGN

As mentioned before, complex cages are generally constructed from basic building blocks. The variety of building blocks is enormous. Building blocks are interchangeable as long as the functional groups for coupling remain the same. Many different building blocks are already stored in libraries for DCC [14]. Generally, building blocks are commercially available or synthesized via well-known organic reactions. Some building blocks must still be designed due to incompleteness or inaccessibility of the libraries. Some important considerations for design are discussed in the rest of this section.

The building blocks determine the structure and properties of the cages. Therefore, they must be carefully selected or designed. The formation of the most thermodynamic stable product is favored in DCC (see section 2.2). Building blocks can be specifically designed for the desired product to be the most thermodynamically stable product. Critical factors include rigidity, geometrical features (e.g. angle), and solubility of intermediates in the solvent [40]. Rigid building blocks are essential for shape persistent cages (see section 1.2.3). Rigidity can be achieved by incorporating multiple bonds and aromatic groups. Shape-persistence of a cage can be predicted by calculation, for example, with Density Function Theory (DFT). However, these calculations could be complex due to the many possible permutations within one cage.

The choice of building blocks could prediction of the geometry of a cage. Geometry of self-sorted cages are mainly based on bite angles of reactants and their stoichiometric ratio. The design can be based on this. Examples of regulating geometry are found in literature. Klotzbach *et al.* [41] studied the co-condensation of a TBTQ which diboronic acid building blocks with varying angles of reactive sites (figure 8). They found indeed the different angles lead to different compositions of cages. Generally, wider angles correspond to more building blocks per cage. In addition, competitive building blocks could result either in narcissistic or social self-sorting. Narcissistic self-sorting selectively forms cages from specific building blocks and ignores other building blocks. In contrast, social self-sorting results in cage formation of all available building blocks. More research is needed for a better prediction of geometry. Still, angles in building blocks should be taken into consideration while designing new cages. In addition, angles are related with ring strain [9]. Higher ring strain results in less thermodynamically stable products and these are less favored in DCC.

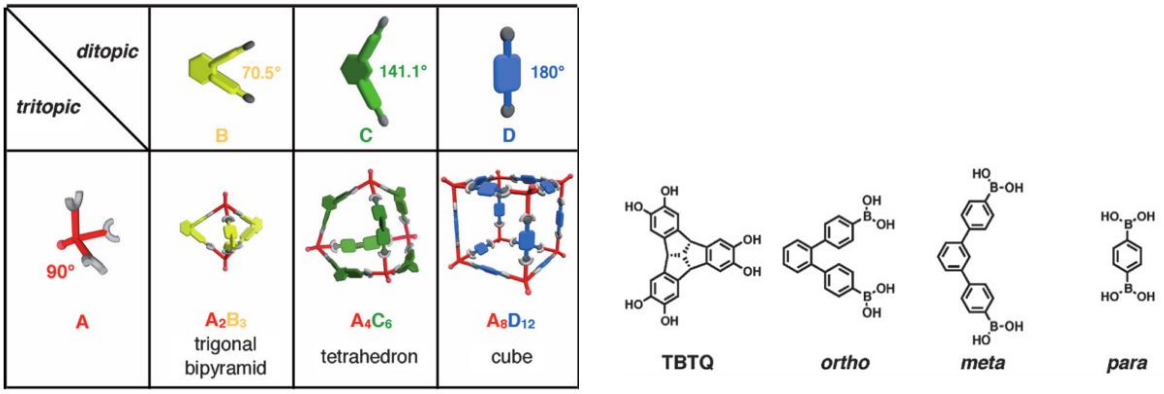

Figure 8: Formation of different organic cages based on the angles of the building blocks [41].

Another method to direct reactions towards the desired product is template directed synthesis. Templates organizes atoms or molecules with non-covalent interactions in a certain geometry to achieve a particular arrangement. Therefore, it favors the formation of a single product. The template can generally be removed after synthesis. However, it can become interlocked in the structure as well. Templates can be divided into two categories. Thermodynamic templates shift an equilibrium of a reversible reaction, whereas kinetic templates stabilize reaction intermediates in irreversible reactions. The first category would affect cage formation via DCC. Differences in nature or amount of template can result in completely different products. Therefore, in the design of the cage careful template considerations should be made [42,43].

Interiors of cages are often apolar and provide little interactions for most substrates. Hence, the scope of substrates is limited for many cages. More research on functionalized interiors has been done in recent years, yet more variation is desired [44]. Functionalized interiors can act as active centers of enzyme-mimics providing directed attraction between substrate and cage. Applications in catalysis are within reach.

Functionalized groups could be introduced before or after cage synthesis. Introduction before cage synthesis is feasible by incorporating functional groups in the starting material. In the cage synthesis they are installed into the cage via DCC. Introduction after cage synthesis is possible by modification of functional groups. The start material should contain simple functional groups (e.g. halides, alcohols), which can be after cage synthesis modified to the desired functional group. Mastalerz *et al.* [45] showed that post synthetic modification of cages to be feasible. They constructed a cage bearing six phenol motives, in with the alcohol groups are pointing inwards. They showed that Williamson ether synthesis remains possible on the hydroxygroups after cage synthesis. Post-modification for halides is to our knowledge not known for all organic cage compounds, but it is expected to be feasible. Post-modification is used for instance if the desired functional group cannot tolerate reaction conditions necessary for cage synthesis. In general, the design of building block(s) and coupling reaction(s) must be well-matched for all functional groups. Overall, mild reaction conditions are preferred that are compatible with a broad range of functional groups [9]. Some examples of desired functionalities in cages include Brønsted pairs, Frustrated Lewis Pairs (FLP) and multiple metal centers.

For this work, functionalities are desired on the inside of the cage to enhance selectivity. Rigid structures tend to prevent rotation from the interior to the exterior: exo-rotation. Exo-rotation could be hindered by the use of 1,3-substituted aromatic building blocks well as bulky substituents on the exterior.

The use of phenol groups is one possibilities to enable hydrogen bonding in the cavity as well as metal coordination[46]. Phenol groups can influence the spectroscopic and coordination properties of compounds. Two metals could coordinate to a single phenol group with bridging. Furthermore, it has potential to become fluorescent with the interaction of a guest or a metal. Therefore, the cage could act as a switch [47].

1.4.2 RETROSYNTHESIS

Retrosynthesis is a technique to plan a synthesis based on the product instead of the start material. It is often used to find synthetic routes for complex molecular structures. The technique focuses on strategically breaking down of products. This is done by the recognition of key structural elements in

complex products, which relate to synthetic transformations [48]. An example is shown in figure 9. The aim is a synthetic route for production of the potent opioid Ocfentanil. An amide is recognized in the which could be synthesized from an amine and a acid chloride. A C/N disconnection is made (marked as a red wavy line) and the appropriate reagents are made. A functional group interconversion (FGI) is made for the next retrosynthetic step in which the amine is converted into an imine. Imines could be synthesized with amines and ketones, which results in the starting material for this route. Translation into synthesis can be done by changing the direction of the scheme: imine condensation, imine reduction and amide formation. It is a valuable technique for translating designs into actual compounds. Therefore, retrosynthetic analysis will also be applied for this work. An high-quality review on retrosynthesis is provides by Schreiber [48].

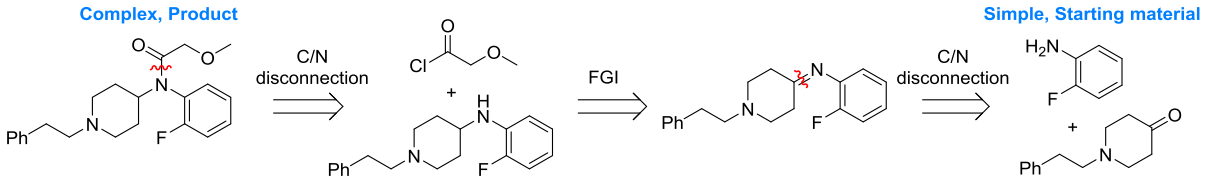

Figure 9: *Retrosynthetic analysis of Ocfentanil.*

1.4.3. HOMOSEQUENCED VS. HETEROSEQUENCED STRUCTURES

Studies of DCC focus mainly on highly symmetric cages that are constructed from one or two kinds of building blocks: homosequenced cages. Their synthesis are of often facile, but cages are limited to a single type of functionality (figure 10a). Cages consisting of two of more different building blocks, called hetero sequenced cages, have been gaining more popularity in the last years. Nonetheless, they remain rare in literature [49]. More building blocks can add to the level of sophistication of the cage. Each type of building block can bare a type of functional group; multiple types of building blocks correlates to multiple types of functionalities (see figure 10b) [49]. Heterosequenced cages could execute complex chemistry as cooperative catalysis. Therefore, heterosequenced cages are highly desired.

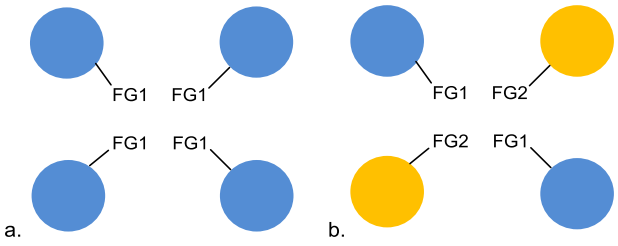

Figure 10: *Schematic representation a cross section of a homosequenced cage (a) on the left, containing one functional group, and a heterosequenced cage (b) on the right, containing two functional groups.*

Synthesis of heterosequenced cages has proven to be difficult. Until very recent, they where synthesized under kinetically controlled reactions resulting in low yields [49]. DCC is currently explored to synthesize heterosequenced cages in higher yields. Two dynamic covalent coupling reactions are used in a one-pot fashion. In this method, it is of utmost importance that the reactions conditions of the two individual reactions are compatible with each other. This concept of creating heterosequenced cages is becoming known as orthogonal dynamic covalent chemistry (ODCC) [49].

Imine formation and olefin metathesis seem to be very suitable candidates for heterosequenced cages. Both reactions are individually discussed in section *1.3.3. Reversible covalent bonds* The combination is previously investigated by Zhang *et al.* [50] for the formation of a heterosequenced macrocycle. The order of these reactions can be very significant. Two problems may arise: I. imine formation results in water and some remaining acid which might decrease reactivity of the metathesis catalyst, II. primary amines can inhibit the activity of the metathesis. Zhang *et al.* found the highest yield is obtained when first imine condensation is executed followed by high vacuum to eliminate the water. Subsequently olefin metathesis is carried out.

Another impediment is described by Skowronek *et al.* [51]. They demonstrate that higher symmetric cages are more favorable entropically than one of lower symmetry. Therefore, heterosequenced cages could be more difficult to synthesis. Still, thermodynamics are not effortlessly reduced to parameters which requires caution

1.4.4. SONOGASHIRA REACTION

In this study, the Sonogashira reaction is often used for the synthesis of building blocks. This palladium catalyzed cross-coupling reaction is used for carbon-carbon bond formation. It is one of only a few routes towards alkyn formation.

The overall reaction and mechanism are shown in scheme 2. The mechanism consists of a copper cycle and a palladium cycle. The palladium cycle starts with the oxidative addition of an organohalide across a palladium metal center. The oxidation state of palladium increases by two. Meanwhile, in the copper cycle a copper(I) salt reacts with an alkyne in the presence of a base to form a cuprate. In the next step a transmetallation occurs between the copper complex and palladium complex resulting again in the copper(I) salt and a palladium complex with both R-groups. The product is obtained after a cis-trans isomerization followed by a reductive elimination.

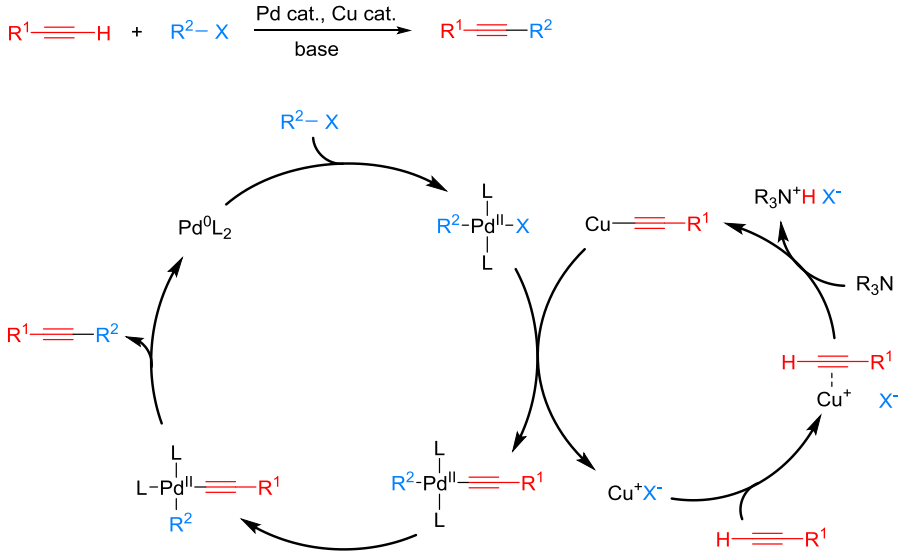

Scheme 2: *Mechanism of the Sonogashira reaction. On top the overall reaction and on the bottom the catalytic cycle. R^2 = aryl or vinyl, X= I, Br, Cl or OTf.*

1.5. SALEN LIGAND

Salen ligands describe a family of ligands derived from *N,N'*-bis(salicylidine)ethylenediamine **3**, and contains two phenolic and two imine moieties (scheme 3). Variations are seen in different groups of the aromatic rings and on the imine backbone. Salen was first reported by Pfeiffer *et al.* [52] in 1933 and became a popular chelating ligand since then. The ligand is synthesized via an imine condensation of silylaldehyde **1** and 1,2-diamine **2**, as shown in scheme 3. The straightforward synthesis of the ligands makes it possible to easily introduce other substituents, to add bulky groups, or to regulate the Lewis acidity of the metal ions by introducing electron withdrawing or donating groups [53]. The alterations have influence on which reactions are preferred by the corresponding complexes. Salen ligands are prone to hydrolysis catalyzed by acid, however, the stability increases tremendously upon coordination of metal ions. Therefore, it is even possible to carry out reactions in wet solvents [54].

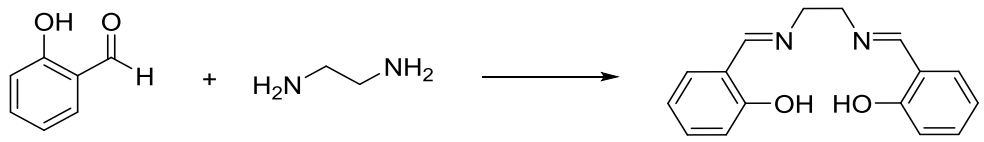

1 **2** **3**

Scheme 3: Synthesis of a salen ligand.

Coordination complexes of salen ligands with many metals are reported in literature including basemetals: V, Cr, Mn, Fe, Co, Ni, Cu and Zn. The metal ion is bound to two oxygen atoms and two nitrogen atoms in a ONNO fashion. Depending on the metal and oxidation state a N_2O_2 or N_2O_2X coordination is formed with a distorted square planar or square pyramidal geometry [54]. Many synthesizes of metal-salen complexes exist. Two routes are most commonly used: I. Complexation with $M(OAc)_n$. II. Complexation with MX_n and base [55]. Advantages of these methods are availability of reactants and in some cases insensitivity to air. Other less used methods include use of metal alkoxides, metal amides, and metal halides after deprotonation with lithium salts.

Salen complexes can catalyze many different reactions including epoxidation, benzylation, Michael addition, cycloaddition and Diels-Alder reaction [53,56,57]. In catalysis salen ligands had a big breakthrough when Jacobsen and Katsuki discovered a chiral Mn(Salen) **4** (figure 11a) which could catalyze selective epoxidation of alkenes. The Jacobsen catalyst is currently used to convert prochiral alkenes into epoxides with enantiomeric excesses of over 90%. The reaction does not require additional direction groups as in the alternative Sharpless oxidation. Also Cr(Salen) and Co(Salen) prove to be highly enantiomeric catalyst for ring opening of epoxides [58]. Salcomine **5** is a Co(Salen) which is commercially available and is used as oxygen transporter or oxidizer (figure 11b).

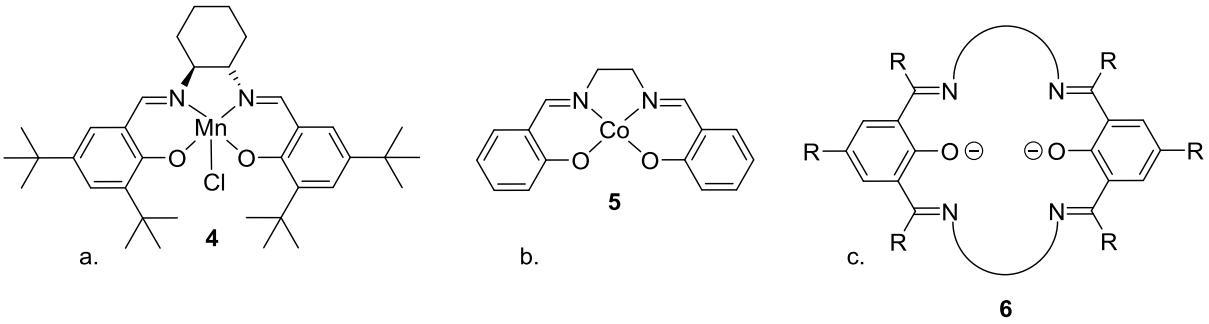

Figure 11: (a) Jacobsen's catalyst. (b) Salcomine. (c) $N(imine)_4O_2$ type macrocycle.

Although Salen complexes are much more stable than the ligand itself it could still degrade. Acid causes demetallation by protonation of the phenols. Oxidizing conditions could result in oxidation of the imine groups which also significantly reduces the stability of the complexes [54].

Closely related are the $N(imine)_4O_2$ type macrocycles **6**, which are synthesized from a phenol containing dialdehydes and diamines (figure 11c). These binucleating ligands are able to coordinate two metal ions in close proximity, as well as their reduced form. They could serve as synthetic versions of bimetallobiosites present in enzymes [59].

2. PROJECT AIM

Organic cages seem promising for multiple applications, especially catalysis. Three new cages have been drafted to promote new catalysis through a functionalized interior and/or heterosequenced nature (figure 12). The objective of this study is the synthesis of these cages. Retrosynthesis will be used as a convenient tool to propose building blocks and plan the overall synthesis routes. Building blocks that are not yet available will be synthesized. Coupling reactions are examined as well to favor cage synthesis (DCC).

We aimed at selective catalysis, which can be achieved through metal coordination in the cavities of cages, resembling enzymes. Therefore, a diversity of metals is attempted to coordinate in the cavities of cages. Catalytic activity of any complexes will be tested by sulfoxidation of thioanisole.

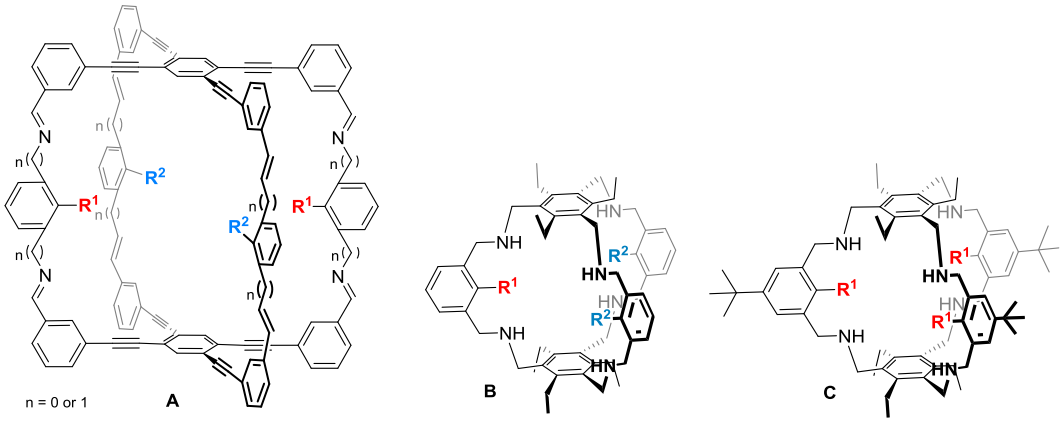

Figure 12: *Three new designs of organic covalent cages (a) Cage compound **A**. (b) Cage compound **B**. (c) Cage Compound **C**.*

3. CAGE COMPOUND A

Cage compound **A** is the design of a heterosequenced cage compound with a relative large cavity (figure 13). Each type of linker could bare one type functional group. Basic functional groups will be introduced, which could be altered by post-modification in a later stage. The functionalities are cross-positioned. The design probably prohibits exo-rotation of functionalities due to 1,3-substitution of the functionalized aromatics. Moreover, many multiple bonds and aromatics are introduced to aim for shape persistency. The rigid centered building block provides the basis for a large stable cavity. The cavity provides a basis for multimetal coordination and/or large cage-guest interaction.

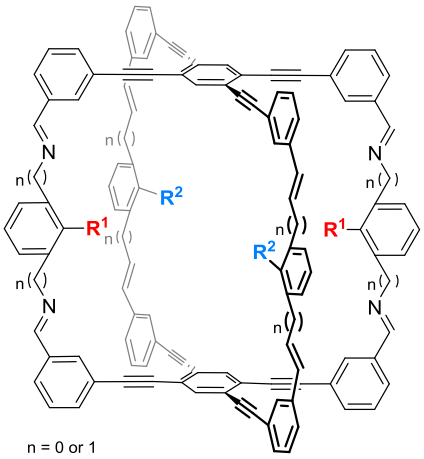

Figure 13: *Cage compound A*

3.1. RETROSYNTHESIS

Disconnections can be made on all imine groups and olefins of cage A, all reversible covalent bonds. Retrosynthetic analysis results in three types of functional groups in the building blocks: olefins, aldehydes and amines. All building blocks can be joined by imine condensation and olefin metathesis. Two routes are suggested by alteration alignment of the imine groups, hence, alternation electrophiles and nucleophiles. Consequently, translation of synthons into reagents gives different outcomes (scheme 1 and 3). The two routes will be called route 1 and route 2, and are discussed separately.

3.2. ROUTE 1

Retrosynthesis leads to three reagents, as is shown in scheme 4. Compounds **8** and **9** are basic building blocks. Several compounds with these motives are commercially available and will not be discussed (e.g. R^1 = H,Br and R^2 = H). In contrast, **7** is a complex building block which needs to be synthesized from scratch.

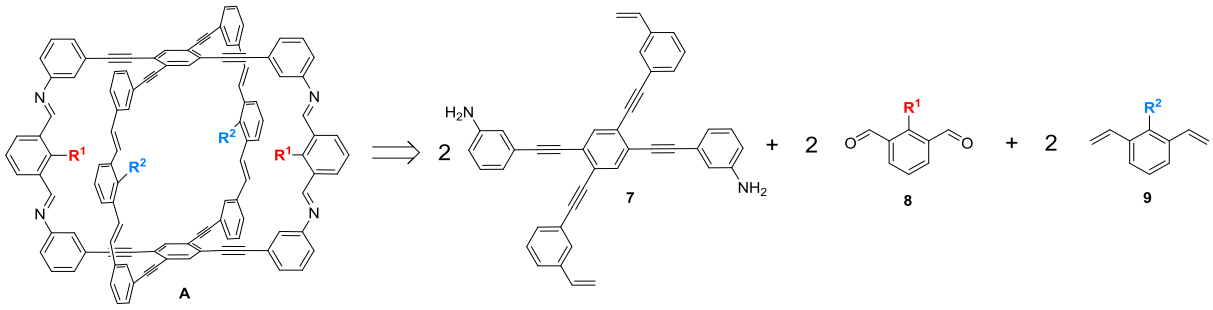

Scheme 4: *Retrosynthesis of compound A into building blocks via route 1.*

The proposed synthesis for **7** is shown in Scheme 5. Iodation of 1,4-dibromobenzene **10** was carried out according to literature [60]. The *para*-substituted product **11** is obtained with a yield of 29%. Lower yields are common for this particular reaction. Selectivity is achieved with a difference in reactivity between bromide and iodide. Sonogashira coupling with 3-ethynylanaline is done successfully (30%), resulting in **12**. Poor solubility of the product could clarify the relative low yield.

Much product is lost during the purification (column chromatography). **12** is not described in literature, but full analysis proves the desired compound is formed (see experimental). **15** is synthesized via a second Sonogashira reaction with 1-bromo-3-vinylbenzene and ethynyltrimethylsilane. Subsequently, tetra-*n*-butylammoniumfluoride (TBAF) is added to remove the trimethylsilane protecting group, resulting in product formation with 41% yield.

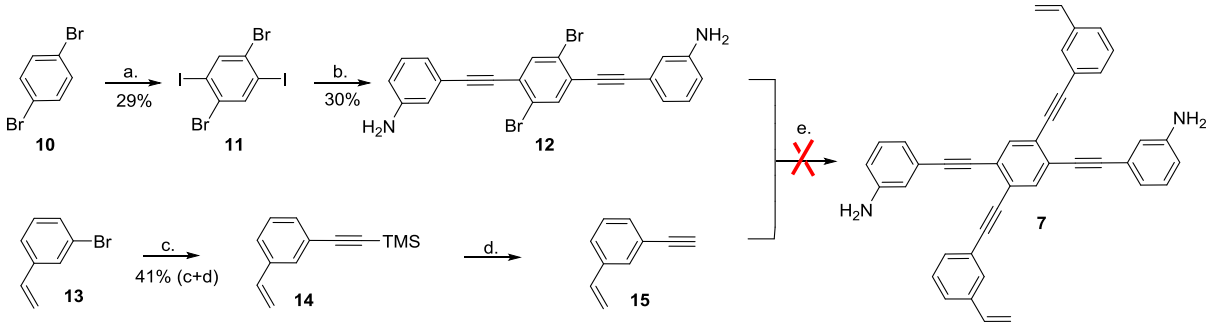

Scheme 5: *Proposed synthesis for the large building block in route 1.* ***a)*** *H_2SO_4, I_2* ***b)*** *3-Ethynylaniline, $Pd(PPh_3)_2Cl_2$, CuI, $NH(^iPr)_2$, THF.* ***c)*** *Ethynyltrimethylsilane, $Pd(PPh_3)_2Cl_2$, CuI, NEt_3.* ***d)*** *K_2CO_3, MeOH, CH_2Cl_2.* ***e)*** *$Pd(PPh_3)_2Cl_2$, CuI, NEt_3.*

The final proposed reaction step, another Sonogashira coupling, did not result in **7**. Analysis with ^{1}H-NMR revealed mainly start material and no products. No reaction took place. The same result is obtained after variation in base and catalyst ($NH(^ipr)_2$ and $Pd(PPh_3)_4$). The lack of reaction could have been caused by two factors: reactivity and solubility. At first, the bromides might be not reactive enough; it is less reactive than iodide. Poor reactivity due to sterics might be possible. **12** supports two large bulky groups, which might hinder oxidative addition on the catalyst (see mechanism *1.4.3*, p.15); especially in combination with the large groups present on the catalyst. Second, functional group intolerance between amines and olefins result in insoluble side products. Amination of alkenes can occur in the presence of a catalyst as described by Müller and Beller *et al*. [61] The alkali hydride could act as pre-catalysts. Lastly, poor solubility is most probable to be the origin of the problem. Analysis of compound **12** was proven to be difficult due to poor solubility. Similarly, compound **12** could not be visually solved in the required reaction conditions for the final reaction, which decreases reactivity. Aromatic amines are known for their low solubility in common organic solvents. Therefore, the amine functional group could be the origin of the low solubility of **12**.

Further investigation with regard of route 1 are not done due to better results in route 2.

3.3. ROUTE 2

The second retrosynthesis provides building blocks **16**, **17**, and **9** (scheme 6). Compound **16** does not contain the amines as in compound **7**, which is beneficial for its synthesis. **17** is commercially available, although, the high prices make synthesis appealing. Finally, **18** can be synthesized in a two-step synthesis, which will be later on discussed on p. 58-59. The other synthesizes are discussed in this chapter.

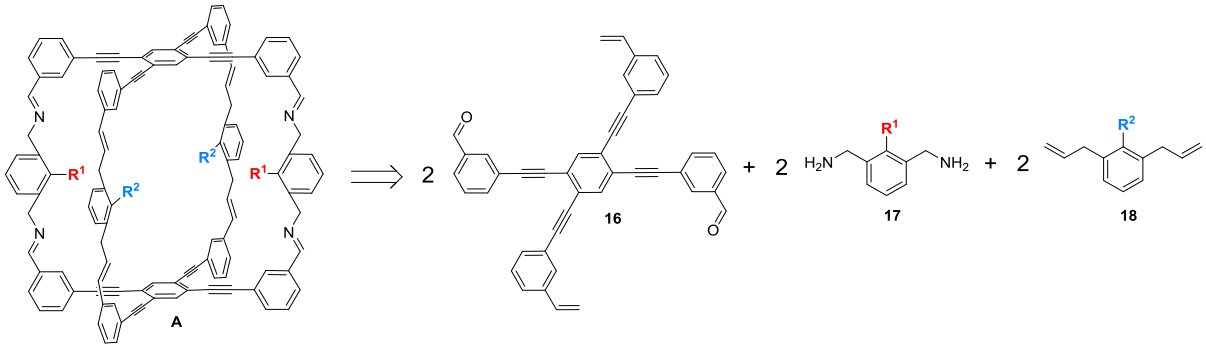

Scheme 6: *Retrosynthesis of compound A into building blocks via route 2.*

This chapter will first discus several simplified imine condensation followed by macrocycle synthesis to gain knowledge on the topics. This will be continued with the synthesis of building blocks **16** and **17** and attempted imine condensation with the building blocks.

Reductive amination is carried out with benzaldehyde **21** and either *m*-xylylenediamine **19** or pyridine-2,6-diyldimethanamine **20** (Scheme 7).

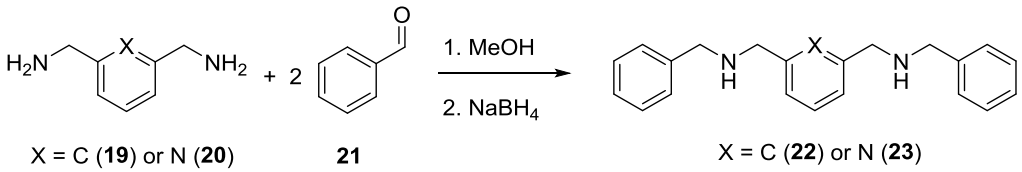

entry	Diamine	# mmol diamine	# mmol **21**	$NaBH_4$	Product(s)
1	**19**	0.10	0.20	Wet	Imine analogue of **22**
2	**19**	0.515	1.00	Dry	**22** + monosubstituted analogue
3	**20**	0.10	0.35	Wet	Imine analogue of **23** + **21**

Scheme 7: *Imine condensation followed by reduction.*

Three experiments are executed with slightly different reaction conditions resulting in other products. The first observed difference is the nature of $NaBH_4$. In entries **1** and **3** is an old source used, which has soaked up moisture from the atmosphere for years. The analysis of the reaction mixtures revealed imine analogues of the desired products has formed. Therefore, we can conclude imine formation was successful in contrast to the reduction. Dry $NaBH_4$ is essential for product formation. In entry **2** is dry $NaBH_4$ used, which leads indeed to the desired product **22**. In addition, is the mono-substituted analogue found with NMR and ESI-MS. The ratio varies in different NMR solvents, probably due to a difference in solubility (monosubstituted product : **22** is 1:1.86 for $CDCl_3$ and 1:1.50 for CD_2Cl_2). The monosubstituted product is explained by the excess of **19** as can be seen in scheme 7. The opposite is shown for entry **20** were the excess of **21** leads to remaining **21** in the reaction mixture. Benzaldehyde should probably be in a minimal excess for an optimal result. The difference in starting material (either **19** or **20**) does not lead to a difference in results. Unfortunately, yields could not be determined due to overlapping signals in impurities or other products. However, it is shown imine condensation with a (functionalized) diamine is possible. This might have been previously a problem in the synthesis of **7**. The gained experience in imine condensation is applied in further experiments.

A synthesis of macrocycle **25** [62] is carried out to gain advanced knowledge of this reaction type (Scheme 8). For entry **1** are M-xylylenediamine **19** and isophtaldehyde **24** solutions are slowly added to additional solvent with a syringe pump over the course of 7h. White solid is formed. Slow addition drives the equilibrium of this reaction towards the thermodynamic product. Hereby, less kinetically trapped products, such as polymers, are formed. The reaction mixture contains multiple compounds after 60 hours stirring and a work-up. The desired compound **25** is not found in ESI-MS. Therefore, the desired reaction did not occur or the imines are hydrolyzed in the process. Traces of water in the solvent and/or the work-up are the most probable cause for hydrolysis of the imines. Accordingly, further attempts are directly reduced after imine formation (Scheme 8). Analysis of entry **2** show indeed the formation of the desired [2+2] macrocycle in 63% yield (see experimental) and traces of the [1+1] analogue. It can be concluded that the reaction can take place in dry methanol and direct reduction is beneficial for the stability of the product. Solvent mixtures of CH_2CL_2 and MeOH are tested to increase solubility. MeOH / CH_2CL_2 mixtures of 1:1 (entry **3**) and 1:4 (entry **4**) both give similar results.

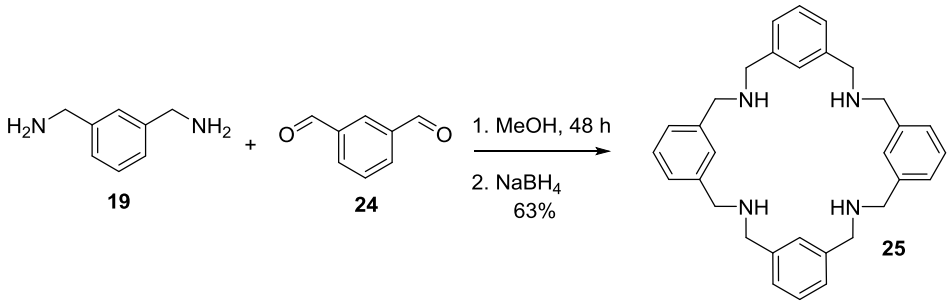

entry	$NaBH_4$	Solvent(s)	Product(s)
1	No	EtOH[1]	No distinguishable products
2	Yes	MeOH[2]	**25** (63%)[3]
3	Yes	MeOH[2]: CH_2Cl_2[2] = 1 : 1	**25** (52%)[3]
4	Yes	MeOH[2]: CH_2Cl_2[2] = 1 : 4	**25** (61%)[3]

Scheme 8: *Formation of a macrocycle with imine condensation and reduction in 63% yield.* [1] *104.6 ppm water,* [2] *Dry solvent.* [3] *Formation of [1+1] is not taken into account for the yield calculation.*

Compound **16** is synthesized by Dr. M. Otte at Organic Chemistry and Chemistry in Utrecht according to Scheme 9. 1,4-dibromobenzene **10** is iodized (step a), similar to route 1, followed by a Sonogashira reaction with ethynyltrimethylsilane (step b). The remaining bromides in **26** are converted into iodides with *n*-BuLi and iodide to increase reactivity (step c). **27** and 1-ethynyl-3-vinylbenzene react together in a Sonogashira reaction to obtain product **28** in 91% yield (step d). Finally, the TMS protecting groups are removed with potassium hydroxide (step e). The resulting reactive alkynes are used in a third Sonogashira coupling with 3-iodobenzaldehyde to obtain **16** in an 87% yield (step f).

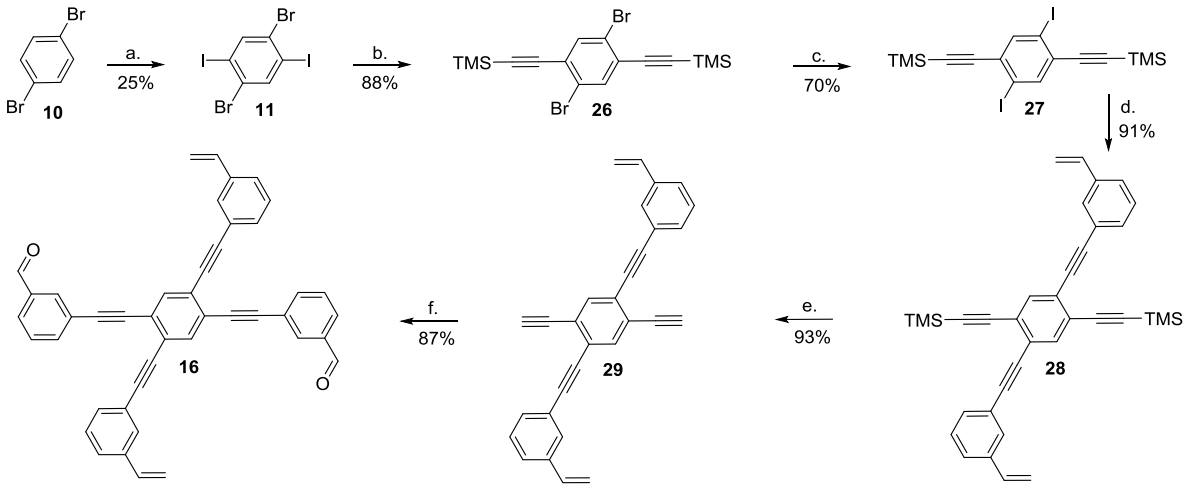

Scheme 9**: Proposed synthesis for the large building block in route 2.* ***a) *H_2SO_4, I_2, 25%* ***b)*** *Ethynyltrimethylsilane, $Pd(PPh_3)_2Cl_2$, CuI, $NH(^iPr)_2$, THF., 88%* ***c) 1.*** *n-BuLi, THF, -79 °C.* ***2.*** *I_2 THF, -79 °C., together 70%* ***d)*** *ethynyl-3-vinylbenzene, $Pd(PPh_3)_2Cl_2$, CuI, $NH(^iPr)_2$, THF. 91%* ***e)*** *KOH, THF, EtOH. 93 %* ***f)*** *3-iodobenzaldehyde, $Pd(PPh_3)_2Cl_2$, CuI, NH_3, THF. 87 %.*

An attempt is made to synthesize macrocycle **31** with **16** and unfunctionalized diamine **19** (Scheme 10, entry **1**) using similar conditions as for the successful synthesis of macrocycle **25** (scheme 8). Due to the poor solubility of compound **16**, the order of addition is adapted such that **19** and MeOH were slowly added to **16** with a syringe pump. After 60 h of stirring, the supposedly formed imines are reduced with $NaBH_4$ at 0 °C and a work-up with CH_2Cl_2 is followed. Unfortunately, poorly soluble products are formed, which could not be analyzed with NMR. ESI-MS does not measure the desired compound but instead over 50 compounds with different isotope patterns are observed, which represent probably impurities. A second attempt, entry **2**, is done with TFA as proton source instead of MeOH. In addition, 1,2,4-trichlorobenzene (TCB) is used as solvent to enhance the solubility of **16** and **31**. Still, a suspension is obtained. Reduction with $LiAlH_4$ is completed after two days of stirring. The high boiling point of TCB is inconvenient due to difficult separation of the solvent from other compounds, therefore no analysis could be done. Addition of acid to the mixture resulted in yellow flakes, which were not soluble in any common organic solvents. Three scenarios could be considered, (I) Building block **16** is not reactive due to solubility issues. It contains many aromatic rings which could cause insolubility through π-stacking, as can be seen in figure 15. (II) **31** is not soluble. The formed macrocycle could form large structures though π-stacking. (III) Poorly soluble polymers are formed during the imine condensation.

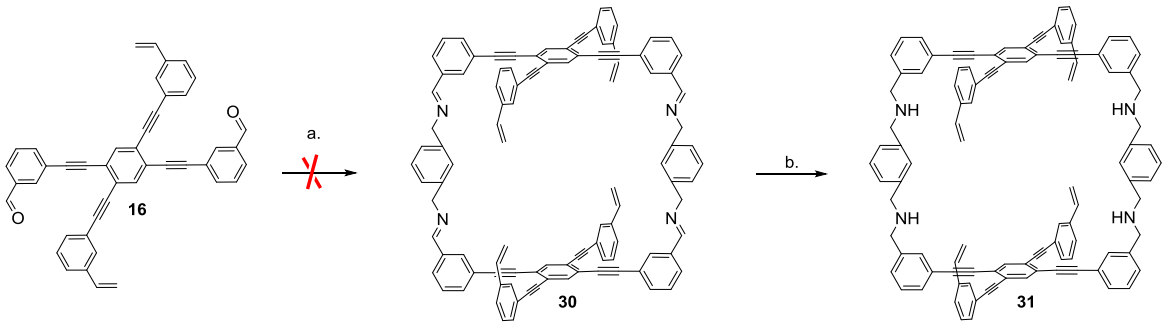

entry	Solvent	Reductant	Product(s)
1	CH_2Cl_2	$NaBH_4$	No distinguishable products
2	TCB	$LiAlH_4$	No analysis possible

***Scheme 10**: Probably failed synthesis of a macrocycle with imine condensation.* ***a)** m-Xylylenediamine **19**, MeOH or THF.* ***b)** $NaBH_4$ or $LiAlH_4$.*

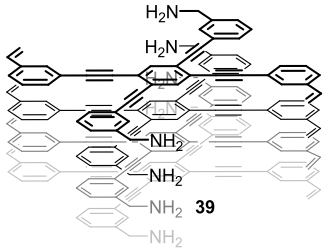

***Figure 15**: Representation of π-stacking of **16**. Similar stacking as described by Moore et al.* [11]

Since imine condensation of **16** with **19** did not seem to be promising, a different diamine building block was attempted to be used in macrocycle synthesis. pyridine-2,6-diyldimethanamine **20,** the pyridine analogue of **19** is used in next attempts. Its incorporation into a cage structure could lead to a Brønsted pair functionalized cage if a Brønsted acid (e.g. carboxylic acid) is added as R^2. As mentioned before, **20** is commercially available. However, it is very expensive. Therefore, a synthetic attempt to obtain **20** in reasonable amounts was made. Synthesis of **20** is first attempted via Gabriel synthesis (Scheme 11).

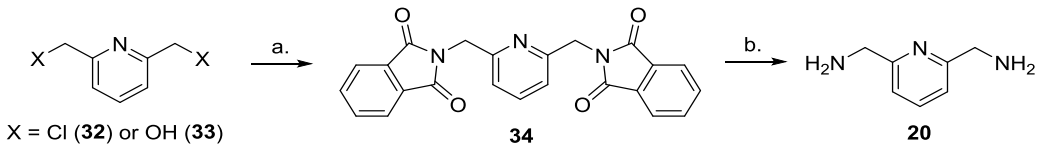

entry	Start material	Reactants step a.	Reactants step b.	Product(s)	Total yield
1	**32**	phtalimide K salt, K_2CO_3	$N_2H_4 \cdot H_2O$	**20**	34% [1]
2	**33**	PPh_3, DEAD, phtalimide	$N_2H_4 \cdot H_2O$	**20**, DEAD derivative	5%

***Scheme 11**: Synthesis* of pyridine-2,6-diyldimethanamine ***a)** phtalimide K salt, K_2CO_3, DMF, 140 °C, 16 h or PPh_3, DEAD, phtalimide, THF.* ***b)** $N_2H_4 \cdot H_2O$, EtOH, 90°C, 16 h or $N_2H_4 \cdot H_2O$, EtOH/H_2O, 90°C, 16 h.* [1] *any water is not taken into account.*

For entry **1** is 2,6-Bis(chloromethyl)pyridine **32** combined with phtalimide K-salt and K_2CO_3 in DMF and stirred at 140 °C for 16 h. White solid forms over time, which is poorly soluble and consequently difficult to characterize. The solid is reacted with hydrazine hydrate. Again, solid forms and analysis with NMR is attempted. The solid only contains **20** in low concentration. The water content of could not be determined with NMR as. The product could be synthesized in a total yield of 34% if the solid

is assumed dry. Recrystallization in acetone/water (1:1) does not improve the concentration. Meanwhile, another attempt (entry **2**) is done with 2,6-bis(hydroxymethyl)pyridine **33**, phtalimide, triphenylphosphine (PPh_3) and diethyl azodicarboxylate (DEAD) (Scheme 11). Compound **34** is formed in this Mitsunobu reaction in a 59% yield, which was confirmed by NMR. Cleavage with hydrazine hydrate results in a mixture of the desired product and a DEAD derivative (see appendix C). **20** is obtained in a poor yield of 9%. Both attempts result in the synthesis **20**. However, impurities are present which could not have been removed yet. Therefore, another direction is taken.

20 can also be synthesized in another two-step synthesis, which consists of a nucleophilic substitution with an azide followed by reduction (Scheme 12). In entry **1** is 2,6-bis(chloromethyl)pyridine **32** reacted with sodium azide in the presents of 18-crown-6 and tetrabutylammoniumbromide in DMF. After an overnight reaction and work up pure **36** is obtained in a 75% yield. Subsequently, **36** is reduced by Pd/C catalyzed hydrogenation with H_2 gas (1 bar, static pressure). ^{1}H-NMR show the formation of a single product next to the signals for the unconverted starting material. However, the ppm values do not match with the limited available data of the literature [63], which a deviation of 0.40 ppm ± 0.02. The obtained product may be the protonated amine. $CDCl_3$ as proton source is doubtful since the same compound is observed in CD_2Cl_2 (less prone to contain HCl). The ^{1}H-NMR spectrum overlaps with the purchased **20**. We assume **20** is formed for entry **1** with a yield of 47%. Entry **2** is carried out with 2,6-bis(bromomethyl)pyridine **35** (scheme 12). Reduction is obtained by reaction with PPh_3. It reacts with the azide to generate phosphazide, followed by loss of nitrogen to form an iminophosphorane. Addition of water lead to product as the formation of very stable PPh_3O provides the driving force. This reduction is known as Staudinger reduction. Full conversion of **35** to form **20** is observed ^{1}H-NMR (Yield = 93%). ESI-MS confirms that **20** is formed. However, the use of this technique does not exclude the formation of a protonated product.

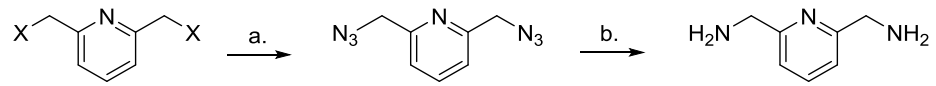

X = Cl (**32**) or Br (**35**) **36** **20**

entry	Start material	Reactants step a.	Yield step a.	Reactants step b.	Yield step b.
1	**32**	NaN_3, 18-crown-6, $N(C_4H_9)^+Br^-$	75%	$Pd/C/H_2$	47%
2	**33**	NaN_3	93%	PPh_3, H_2O	47%

***Scheme 12**: Synthesis* of pyridine-2,6-diyldimethanamine ***a)** NaN_3, 18-crown-6, $N(C_4H_9)^+Br^-$, DMF or NaN_3, DMF. **b)** $Pd/C/H_2$, EtOH or PPh_3, H_2O, THF.*

In conclusion, **20** can be obtained in reasonable purity via both routes as shown in scheme 11 and 12. Both routes shown in scheme 11 are less efficient due to the formation of impurities, which are difficult to remove. NMR analysis of the reactions suggest protonation or a slip in literature.

Synthesis of a macrocycle is attempted three times with **16** and **20** (Scheme 13). The first attempt is carried out with **16** and the synthesized **20** in CH_2CL_2/MeOH. Combining all reactants gives a bright yellow suspension, which is refluxed for 18 h and results in a suspension of a brown solid and a yellow liquid. Separate analysis can be done after filtration. The yellow liquid contains only starting material, indicated by the aldehyde signal in ^{1}H-NMR. The brown solid shows no visible solubility. ^{1}H-NMR show traces of compound, which probably originates from impurities (two singlets at 7.01 ppm and 4.74 ppm are distinguished). In ESI-MS the desired compound is not or cannot be protonated.

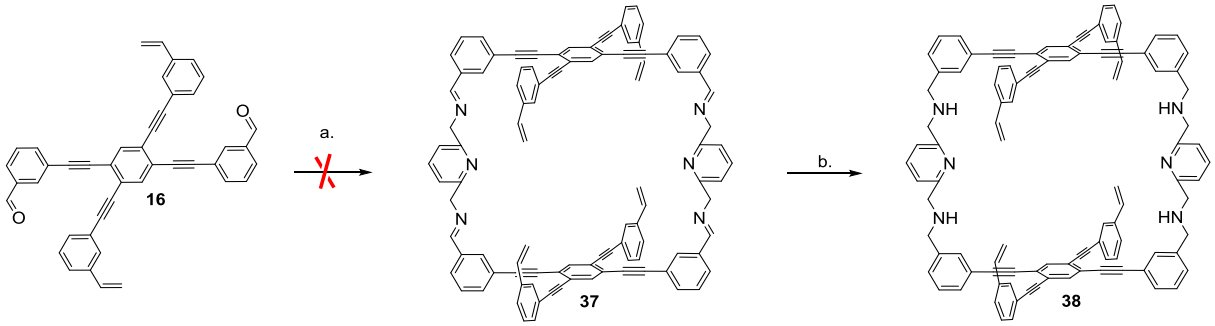

entry	**20**	Solvent(s)	Atmosphere	Product(s)
1	synthesized	CH_2Cl_2 / MeOH	Air	Insoluble products
2	purchased	$CHCl_3$[2]	Nitrogen	Insoluble products
3	purchased	TCB	Air	Insoluble products

Scheme 13**: Probably failed synthesis of a macrocycle with imine condensation.* ***a) *pyridine-2,6-diyldimethanamine* ***20**, MeOH/CH_2Cl_2.* ***b)*** *$NaBH_4$ or $LiAlH_4$.*

In the second attempt the purchased **20** was used. In addition, the reaction is carried out in degassed chloroform[2] as solvent and under nitrogen atmosphere. The reaction is stirred for 16 h while blocked from light to prevent polymerization by the olefins. The cloudy mixture is separated with canula filtration. The filtrate mainly contains **16** and no **20** while the residue is again insoluble and remains to be characterized.

The third reaction is carried out in 1,2,4-trichlorobenzene to improve solubility and is monitored with thin layer chromatography (TLC). TLC analysis is done every half hour over a total period of six hours. No change in the observed spots is seen (quantity, shape or intensity). Even after an additional 8 hours a similar TLC is obtained. Canula filtration separates the dark yellow filtrate from the orange solid. Again, the solid cannot be solved. The same three considerations can be made for this reaction as for the similar reaction discussed on page 22-23. No strong conclusions can be made at this point.

Cage compound A appears to be much more complex than was thought, especially due to solubility issues. Due to restricted time the synthesis of Cage A was not further investigated.

[2] 74,3 ppm water

4. CAGE COMPOUND B

Cage compound **B** is designed to be a smaller heterosequenced cage compound (figure 16). The design is made with considerations on rigidity, rotation and building block angles. The cage in which $R^1 = R^2 = H$ was studied before as homosequenced cage by Roelens *et al.* [64] and Delgado *et al.* [65]. Therefore, we can conclude the geometry of **B** is able to form. In addition, literature describes interaction with small molecules and ions as acetone and sulfate. We expect selective binding of metal ions and substrates can be achieved when the appropriate R-groups are selected.

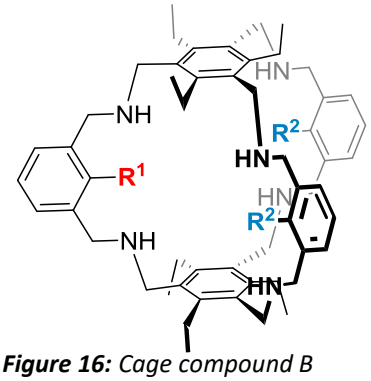

Figure 16: *Cage compound B*

The retrosynthesis of cage compound **B** is shown in scheme 14. **B** contains six amine groups of which two are converted into imines by FGI. Four C/N disconnections are made and the synthons are translated into building block **8** and **41**. Another two C/N disconnections are subsequently made yielding Building block **42** and **43**.

Reversing the order of retrosynthesis leads to a synthesis results in a synthetic plan: an S_N2 between **42** and **43** is followed by an imine formation with **8** after which **40** is reduced to **B**. The S_N2 reaction is not a covalent reversible reaction and can therefore not be used in DCC. Self-healing is not possible, so it will not lead to the most thermodynamic stable product. However, DCC is most essential in the cage-closing step, which is executed with imine formation, which can be controlled by DCC.

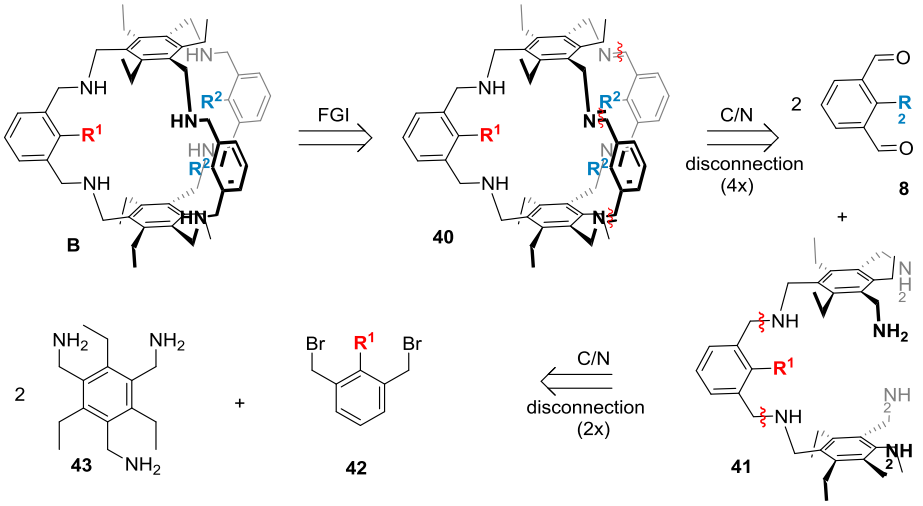

Scheme 14*: Schematic representation of the retrosynthesis of cage compound B.*

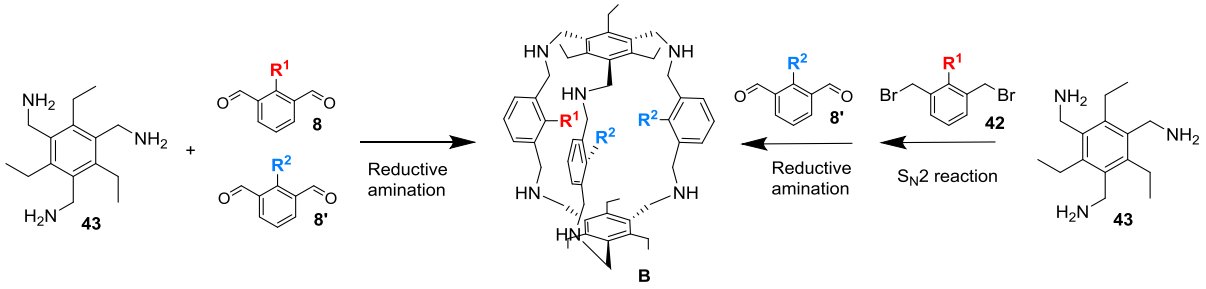

Scheme 15*: Schematic representation of proposed two routes for cage **B** formation.*

In previous research, synthesis of heterosequenced cage compound **B** was attempted via another route; by imine formation of two different aldehydes and **43** (Scheme 15) Control over the stereochemical ratio between **8** and **8'** was expected to give selectivity. Unfortunately, selectivity was poor in practice and all combinations of R^1 and R^2 was found. In this work, two coupling reactions are used, which are expected to give better selectivity (scheme 15). The synthesis of the intermediate could be controlled to by the choice of ratio's. A completely selective synthesis probably requires purification of the intermediate, but this is not tested in this study.

Compound **43** can be synthesized according to scheme 16. Triethylbenzene **44** undergoes an electrophilic aromatic substitution with formaldehyde, which is formed by heating paraformaldehyde. Zinc bromide acts as Lewis acid which activates carbonyls. HBr can act similarly in addition to providing bromide ions to undergo the final S_N2 reaction resulting in **45**. Compound **45** is obtained pure after an overnight heated reaction and work-up water in a yield of 99%. A Gabriel synthesis subsequently performed in which **45** reacts with an excess of a potassium phtalimide salt and 18-crown-6 in an overnight reaction at 100 °C. Further purification is achieved by column chromatography (Acetone : CH_2Cl_2 = 1 : 20). Analysis confirms **46** is formed with a yield of 81%. Finally, cleavage of the phtalimide groups with hydrazine results in **43** with a yield of 81%.

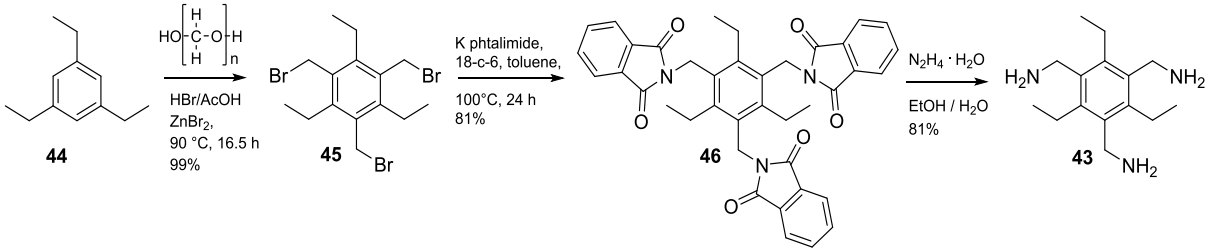

Scheme 16: Synthesis of triamine building block **43**.

Column chromatography after the Gabriel Synthesis (scheme 16, second reaction) separates the reaction mixture of three compounds: product **46**, the added excess of phtalimide and a side product (15-20 mol%). The side product is identified as compound **50** with ^{1}H-NMR, ^{13}C-NMR, COSY and ESI-MS (Scheme 17) and is quantified as 15-20 mol% of the mixture. A reaction proposed to explain side product formation is shown in scheme 17. First, an acid-base reaction between deprotonated phtalimide **47** and water results in hydroxide ions. This ion attacks the tribromide **45**, pushing a bromide out in an S_N2 reaction. **49** reacts as in a normal Gabriel synthesis, in which phtalimide ions directly attack the neighboring carbon of the bromides. Compound **50** could be interesting to use in the synthesis of other heterosequenced cages, an example is shown in the outlook.

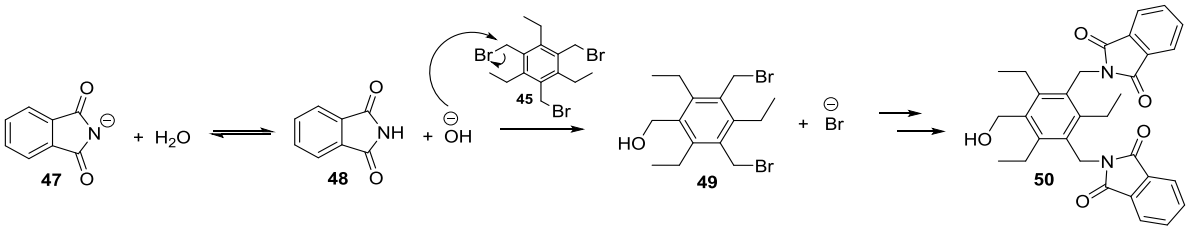

Scheme 17: Side reaction of the Gabriel synthesis used to synthesize **43**.

The triamine **43** and **51** are added together (1 : 0.45) with NEt_3 in CH_2CL_2 and stirred for 48 h (scheme 18). ^{1}H-NMR spectra show formation of many compounds, and compound **52** could not be found with ESI-MS. The experiment was repeated with the pyridine analogue, again without formation of

the desired product. Nevertheless, **53** could be synthesized when imine condensation is immediately followed as a one-pot synthesis. Isophtaldehyde is directly added to the reaction mixture of **43** and **51** and any formed imines are reduced to amines with $NaBH_4$ during overnight stirring at RT or 40 °C. (Scheme 18). Triamine **43**, 1,3-bis(bromomethyl)benzene **51** and a base are stirred overnight on room temperature at 40 °C. A small excess of isophtaldehyde (1 : 2,2) is used and the reduction is carried out in an ice bath for 3 hours. Both NMR [65] and ESI-MS confirm the product is present in the mixture. Interestingly, the mixture obtained from the reaction at 40 °C contains more impurities than the reaction at RT. The yield is high, but could not be exactly determined due to unknown impurities. Compound **53** could also be formed if only one of two reactions could has occurred.

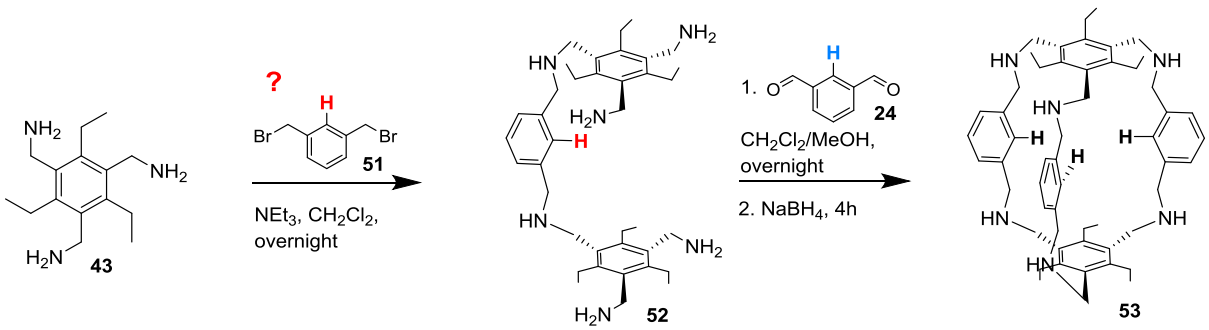

***Scheme 18**: Desired synthesis of cage B ($R^1 = R^2 = H$)*

An experiment with one bromo-substituted reactant is followed to investigate if both reaction took place or only the reductive amination. **43**, **51** and a base are stirred overnight at RT (Scheme 19). The following day a small excess of 2-bromoisophtaldehyde **54** was added and stirred overnight again. The obtained mixture is reduced with $NaBH_4$ at 0 °C for 3 hours. ESI-MS shows the no formation of desired cage **C**. Instead, the analogue cage with three bromides is found (**55**). Therefore, we can conclude that the imine condensation was successful, but that the desired S_N2 reaction did not take place.

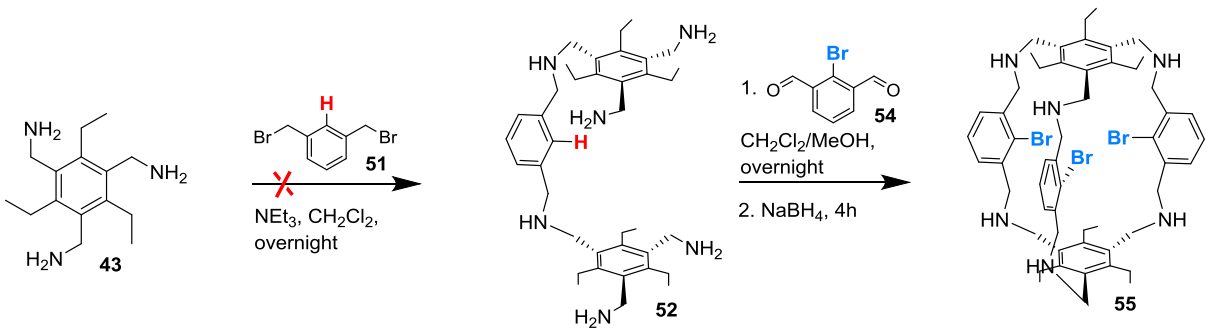

***Scheme 19**: Desired synthesis of cage B ($R^1 = H$, $R^2 = Br$)*

In general, amines are good nucleophiles for S_N2 reactions; possibly too good resulting in overalkylation. In addition, an S_N2 reaction is between all primary groups, therefore, no steric hindrance is expected. In this case, it was difficult to achieve an S_N2 reaction without any clear reasons. Therefore, the research was continued in another direction.

5. CAGE COMPOUND C

Cage compound **C** is similar to cage compound **B**; the same cavity size is obtained (figure 17). However, **C** is of a homosequenced nature. In addition, the bulk of ^{t}Bu-groups inhibit rotation even more than 1,3-substitution. Compound C was synthesized before in this research group. It can be synthesized in a two-step synthesis with good yields. Coordination of metals in the cavity will be studied for this cage compound.

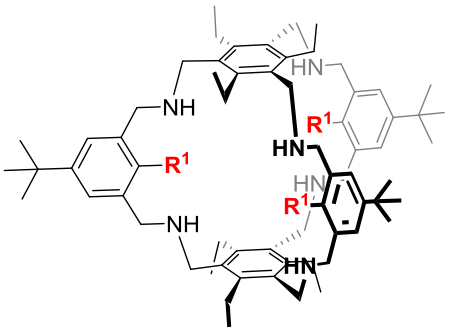

Figure 17: *Cage compound C*

5.1 RETROSYNTHESIS

Homosequenced cage **C** is designed with three phenol groups as interior and six amine groups in the skeleton. The classical retrosynthesis of this compound is shown in scheme 20; at first the amine cage (**C1**) is converted into its imine analogue, **C2**, by FGI. Subsequently, six C/N disconnections are simultaneously done over all imine bonds, which can be translated into dialdehyde **56** (4-tert-Butyl-2,6-diformylphenol) and triamine **43** (2,4,6-Triethyl-1,3,5-benzenetrimethanamine). **56** is commercially available and the synthesis of **43** is previously discussed in chapter 4 (scheme 16, p 26).

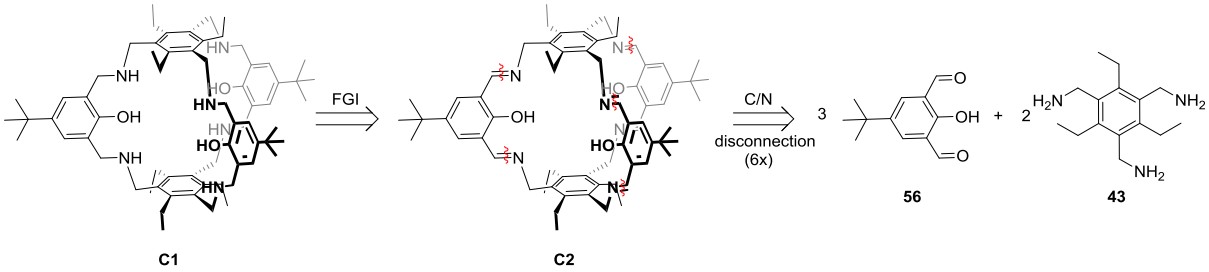

Scheme 20*: Retrosynthetic analysis of cage C.*

The corresponding synthesis is known as reductive amination. **43** and **56** react in a condensation reaction to form iminecage **C2**. The mechanism of imine formation is discussed in 1.3.3. (scheme 1, p 12). Reduction converts **C2** in **C1**. Cage **C1** and **C2** are both of interest, since they both seem suitable to coordinate metals. A difference in properties is expected. C1 and C2 will be discussed separately.

5.2 C2: IMINE CAGE

5.2.1. STRUCTURE AND SYNTHESIS OF C2

C2 is formed via a imine formation with **56** and **43** (scheme 21). The reaction conditions are of great importance in reversible reactions such as imine formation. Equilibriums can easily shift due to many factors e.g. reactant ratio, solvent, temperature and reaction time. The reaction conditions in this reaction are based on synthesis of a similar cages [46,64,65]. The reaction shown in scheme 21 is carried out in a solvent mixture of CH_2CL_2 and MeOH (2:3). Methanol is used as a solvent since it leads to rapid and near quantitative imine formation [66], whereas CH_2CL_2 is necessary to solve **C2**. In addition, dry solvents are used to diminish the hydrolysis rate. Water is formed during the synthesis, which could be evaporated or captured by drying agents.

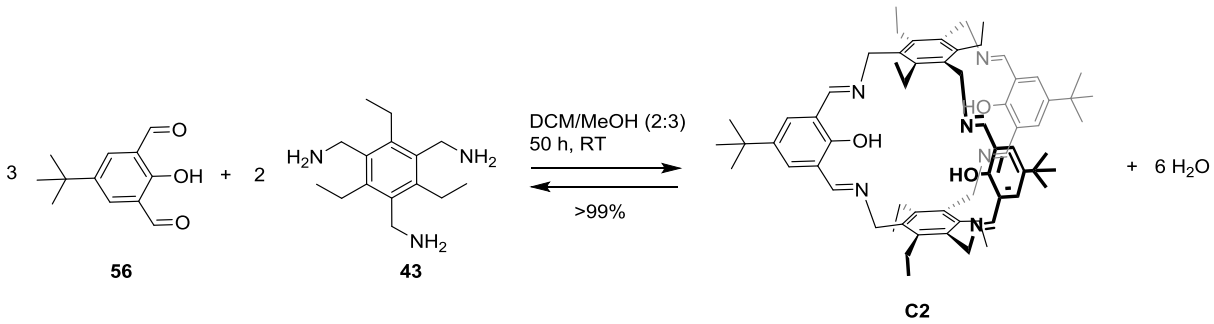

Scheme 21: *Scheme of cage synthesis C2*

Formation of side products results in lower yields. For instance, polymerization can occur if not all three linkers connect to the same two caps. A small excess of caps (**43**) suppresses polymerization, therefore, the ratio **56** : **43** = 1 : 1.49 is chosen for **C2** synthesis. Linkers will likely connect to the same caps. Consequently, formation of cages will be favored instead of polymer formation.

C2 is successful synthesized in a quantitative yield. ^{1}H-NMR and ^{13}C-NMR both show very symmetric spectra. A detailed explanation of the spectra is present in the experimental section. In ^{1}H-NMR, a broad peak is observed at 12.52 ppm, which is caused by an intramolecular H-bond (figure 18a). This H-bond can be explained by examination of the resonance structures in which the hydrogen shifts from the alcohol to the amine (18b). The H-bond decreases electron density on the alcohol group (deshielding) causing a downfield shift. In addition, the spectra shown some water and occasional solvent, which could not be evaporated. Solvent molecules might be trapped in the cage, resulting in laborious removal of solvents.

Other analyses also indicate the formation of **C2**. IR shows a clear imine vibration at 1629.90 cm^{-1} as expected and ESI-MS gives the correct masses of the mono-, di and tricationic species. Unfortunately, crystallization of **C2** has been unsuccessful. Some crystals are grown when a concentrated sample in CH_2CL_2 is stored in the freezer over three days. Unfortunately, the crystals rapidly dissolve when taken out of the freezer.

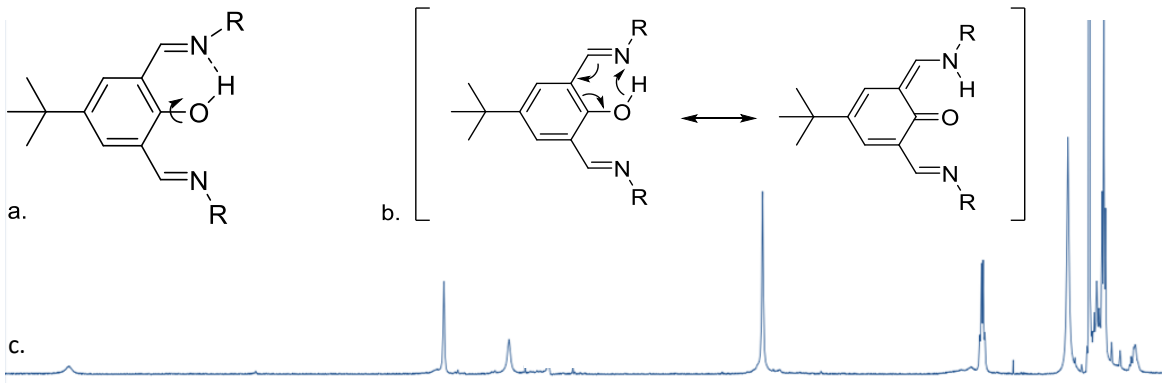

Figure 18: *Intramolecular H-bond. (a) schematic representation of the intramolecular H-bond. (b) Resonance structures.(c)* ^{1}*H-NMR spectrum with the intramolecular H-bond peak on the far left. Note: the chloroform peak is removed for clarity.*

The intramolecular H-bond stabilizes the imine bond, which could prevent rotation. However, this effect is small for **C2** which is indicated by Mastalerz *et al.* whom expected conformational isomers

for a cage with the same linker, although larger in size [27]. Other cases of Exo-rotation are seen for several cages such as another similar cage described by Murray *et al.* [33]. However, for **C2** linker rotation is not expected due to the t-butyl group which would not fit in the interior. In summary, we expect the combination of the bulk, intramolecular H-bond, cage size and restriction in bond angels to prevent rotation.

The reversible imine bonds make the structure versatile. For instance, it might enable the cage to reversibly open and close. This process is called a gate mechanism [44]. Reversible guest exchange is possible for guests, which are too large to fit though the pores.

Furthermore, DFT is used to study the structure and its flexibility [3]. Calculations were performed under vacuum, which should be taken into account during the analysis of the structures. The optimized structures of two analogues are shown in figure 19. The different confirmations are close in energy. The difference is 0.68 kcal/mol, which is the same order as vanderwaals interactions. It appears the linkers align in an optimal angle with respect to the cage (~ 57°), although the direction is random. Two orientations are possible; a symmetric cage with C3-axis (19b) and a nonsymmetrical cage with a wide angle of ~ 191° (19c). During optimization, the angle remains the same. The degree of applied distortion in the angle is not of influence in the optimized structures. This is in agreement with the design of a rigid compound ,which maintains the phenol groups endo-directed. In solution, the most symmetric orientation is probably maintained as NMR showcases a highly symmetric compound.

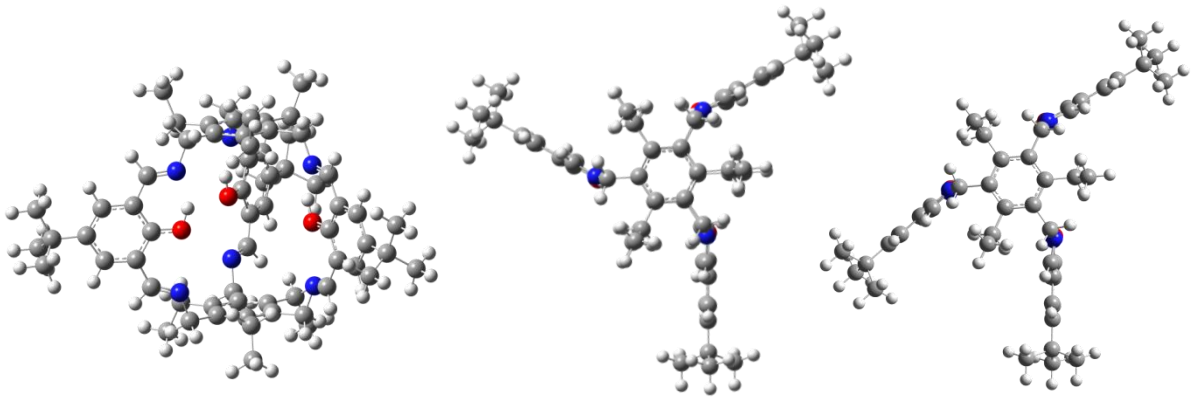

***Figure 19: C2** optimized structures with DFT. (a) side view. (b) top view 1. (c) topview 2.*

In addition, the top view of the two orientations show perfect alignment of the caps, which is possible due to the flat π-system of the linkers. Finally, the structure contains three pores open for guests. The diameter of the interior can be expressed by the distance between oxygen atoms, which is calculated as 5.79 - 5.86 Å. To give an impression, a water molecule is 2.75 Å, a typical C-C bond 1.54 Å and a benzene ring around 6.7 Å.

The **C2** synthesis is carried out multiple times and a few attempts were successful (3x success, 4x unsuccessful and 2x not clear) [4]. The cause for difference in results, while using the same reaction conditions, remains unclear. Different attempts led to different forms in appearance of the

[3] in collaboration with Léon Witteman, MSc with the program Gaussian 09 with the B3LYP functional.
[4] Only cage of successful experiments are used for further investigations to guarantee the same quality.

product(s) can be distinguished: granolas, semi-solid, film and powder (figure 20). The main difference is the solubility of the solids in CH_2CL_2; they range from not soluble (20a) to very soluble (20d). The powder did contain pure **C2**. In the next paragraphs, we will discuss possible identities of the unknown other solids and explanations of their formation. The identity of the poorly soluble solids could be explained by four possibilities: stacking, [4+6]-cages, COFs and polymers.

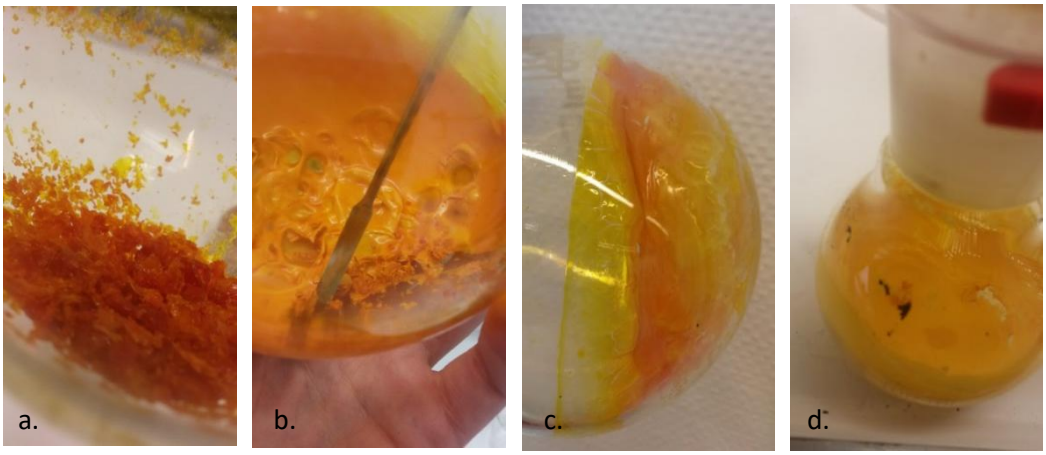

Figure 20: *Different appearances in* ***C2*** *synthesis. (a) Granolas. (b) Semi-solid. (c) Film. (d) Powder.*

- ***Stacking*****:** Stacking of molecules readily decreases solubility. We expect stacking is possible for **C2** due to the many aromatics and possibility to create a near flat side (figure 18c). Increasing sterics will reduce the degree of stacking, which are ^{t}Bu-groups for **C2**. Unstacked cages will be visual in analysis where stacked cages will not. The stacked cages might solve better over time, which is seen for the film formation (20c). The structure of the cage remains the same in stacking, which is in contrast with the next possibilities.

- ***[4+6] cage***: Secondly, another cage might form during the synthesis. Instead of the designed [2+3] cage a [4+6] cage could form. A schematic representation of [2+3] and [4+6] cages is shown in figure 21a. It is not known if the [4+6] cages will be soluble as literature reports soluble[67] as well as insoluble[27] [4+6] cages.

- ***COF:*** Formation of COFs is another alternative (figure 21b), in which all linkers react to different caps. COFs are not soluble of nature.

- ***Polymers:*** The most probable identify is formation of polymers. One form of polymerization is shown in figure 21c, which can be described as linked macrocycles. Degrees in polymerization could explain the range in solubility; oligomers are moderately soluble whereas polymers are poorly to not soluble. Polymers can be directly formed or via the reversible reactions as polymerization are kinetically trapped [9]. A combination of polymerization and stacking is shown in figure 21d.

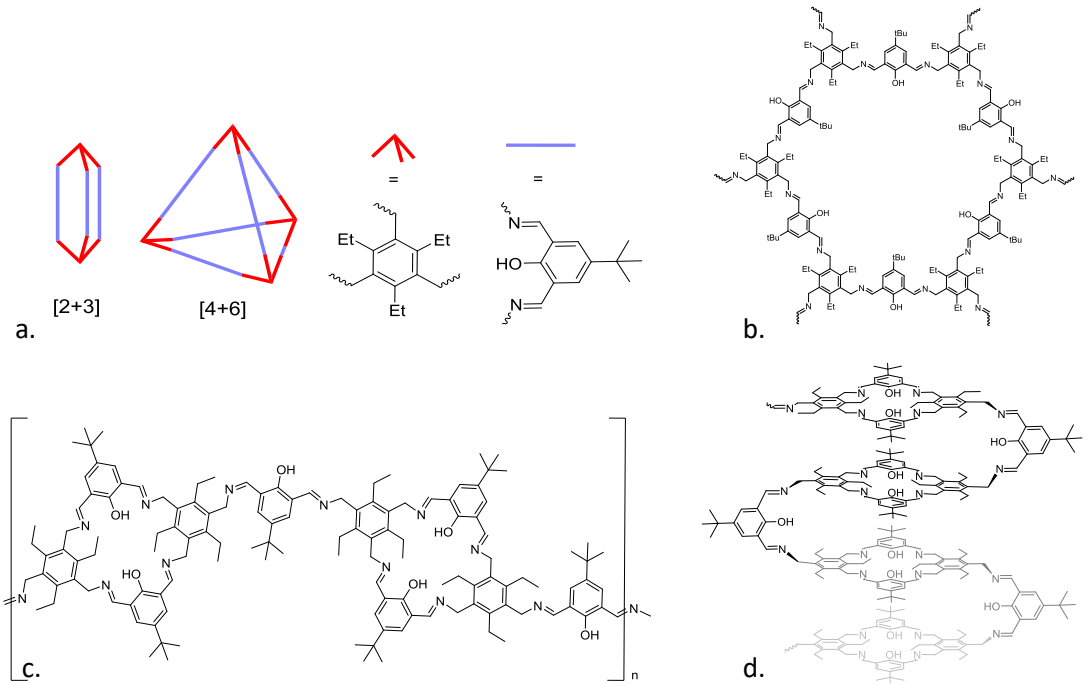

Figure 21: *Possible structures of insoluble material synthesized during* ***C2*** *synthesis. (a) schematic representations of a [2+3] and [4+6] cage. (b) Part of a COF. (c) Example of a polymerization form. (d) Stacked form of a polymer.*

All four categories will results in similar ^{1}H-NMR spectra as the other compounds are insoluble (only **C2** will be measured) or have the same chemical shifts as **C2**. Some compounds are expected to give broader signals. However, similar results could be obtained by poor tunebility due to solids in the NMR tube. In addition, ESI-MS shows a signal for the desired cage in all samples. However, this could mean the sample contains only cage, or only the cage is soluble / able to be protonated.

DOSY NMR is a method to distinguish between different species based on diffusion. In general, lower diffusion coefficients (D) correspond with larger compounds, often-heavier compounds. This method shows two compounds with D = 3 or 5 for most samples (see appendix E). The powder only has signals at D = 5, which has to correspond to the desired **C2**. The peaks at D = 3 are minor and are sometimes just over the noise level. It corresponds with a larger compound as **C2** e.g. [4+6] cages or polymers.

An attempt is made to follow the synthesis by TLC, however no clear difference is seen over time. This might be explained due to insoluble product which is not seen on TLC or the other product form during the workup. The products also might decay over the silica as it can enable hydrolysis.

Polymerization can be triggered by an ill fitted template as is described by Roelens *et al.* [46]. They expected that the addition of sugar molecules to a pyrrolic cage would lead to guest binding. Instead they observed a slow formation of oligomeric products. They suggest the molecule acts as a template, which hinders cage formation. For the reduced form, no oligomer formation was seen. Although no templates are used in this synthesis, available molecules may act as a template e.g.

solvents or small impurities. Minor changes in conditions or reagents could provide these templates and thus polymerization[5].

Another factor is concentration; the synthesis is carried out in low concentrations to favor formation of cages instead of polymers (20-30 mM). CH_2CL_2 is more volatile than MeOH and water. Therefore, the concentration of MeOH and water increases upon evaporation, which can affect the equilibrium(s). The product is poorly soluble in MeOH, which results in a yellow suspension during evaporation again able to affect the equilibrium(s) and favor polymerization.

The last factor is water content. The reaction itself produces water. The reaction mixture is dried after synthesis to study the role of water in the synthesis of **C2**. Dehydration agents should favor cage formation [55]. Again, partly soluble solids are formed after addition of drying over $MgSO_4$ (figure 20c). At least two compounds are formed, which is confirmed with DOSY NMR. It is worth noticing that sulfates are anions which binds in many cages (see 1.2.2). The sulfate ions might be binding agents or ill-fitted templates for **C2**, altering the outcome of the synthesis. In contrast, pure cage is obtained after the reaction mixture is dried over molsieves for three days.

In summary, **C2** is successfully synthesized multiple times and completely characterized. However, the reaction appears to be very sensitive as different outcomes are seen when the same reaction conditions are used. The reaction often leads to poorly soluble solids, which might be explained by stacking, [4+6]-cages, COFs or polymers. Polymerization is most likely to occur, possibly enabled by templates, concentration or water content. Removal of water directs towards cage formation if molsieves are used. Pure cage compound **C2** is used for further experiments.

5.2.2. OPTICAL PROPERTIES OF C2

The color of **56** and C**2** is bright yellow, which is caused by the conjugated π-system present (22a). Larger conjugated π-systems result in smaller HOMO/LUMO gaps. As energy is inversely proportional to the wavelength (eq. 1), larger π-systems emit higher wavelengths of light, which can go into visible light for instance around 600 nm which is seen as yellow.

$$E = \frac{h*c}{\lambda} \qquad [1]$$

Interestingly, a solution of **C2** in CH_2Cl_2 becomes fluorescent after addition of acid (figure 22b). Fluorescence is a property of molecules, which absorb a wavelength of light and subsequently emit light of a longer wavelength. For example, quinine in tonic water makes it fluorescent under a UV light. It absorbs light of 350 nm and emits light of 460 nm, which we see as blue light. The energy difference is caused by non-radiative translations. Imine moieties in **C2** are readily protonated by weak acids resulting in positive charge on the nitrogen(s). Due to the conjugated π-system this charge can be delocalized in the collective hydrogen-bond system (see sections 5.2.1. p. 30). Single protonation (**C2(1+)**) can best be stabilized by delocalization over the whole conjugated π-system (figure 22c). Even double protonation (**C2(2+)**) can even be delocalized, however in less extent (figure 22d).

[5] Differences in color intensity of purchased **56** are observed. Although, NMR spectra does not show significant difference, inorganic impurities could enable templated synthesis.

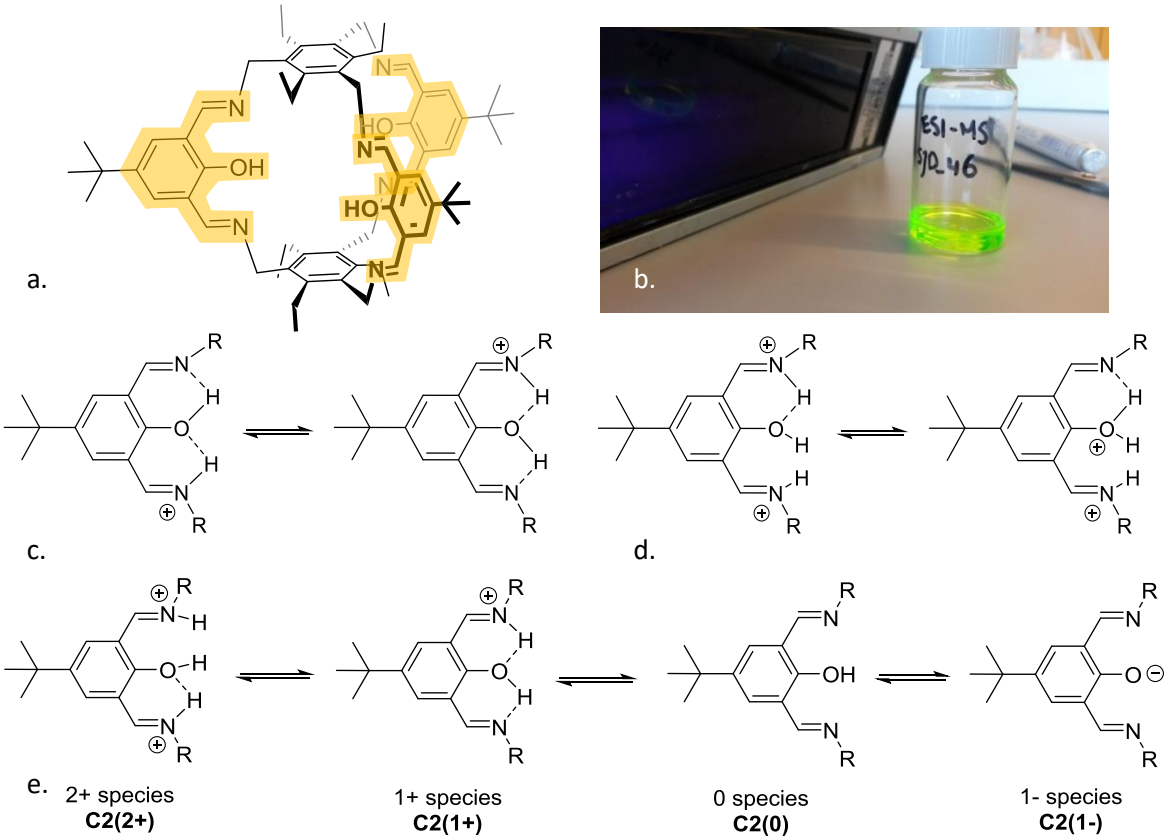

Figure 22: *Optical properties of **C2**. (a) Structure of **C2** with the conjugated π-system indicated in yellow. The same system is present in dialdehyde **56** only the nitrogen is switched for an oxygen. (b) Photograph of a vial with FA added to a solution of **C2**. (c) Collective hydrogen system for single protonation. (d) Collective hydrogen system for double protonation. (e) Theoretic formation of species with charge: +2, +1, 0 and -1.*

Optical properties can be quantified by measurement with a basic UV-VIS spectrometer and with a fluorescence spectrometer. Samples of a known concentration of **C2** in CH_2CL_2 were measured with UV-VIS spectroscopy (figure 23a, 0eq). Three main absorption peaks are observed: 1 (286 nm), 2 (347 nm) and 3 (466 nm). The molar extinction coefficients are calculated with the Beer-Lambert law (eq. 2), which relates optical properties to molecules. They are shown in figure 23b. Similar data is seen for comparable structures with one phenol and two imine motives [68]. The lack of peaks above 500 nm is also consistent with the yellow color of the compound.

$$\frac{I_1}{I_0} = e^{-\varepsilon * c * l} \qquad [2]$$

Known amounts of formic acid (FA) are added to the samples to study the influence of acid on **C2**. Low volumes are added, which should not have significant affect the concentration of **C2**. No significant change in spectrum is seen after addition of 6 eq FA, probably due to the use of the non-protic solvent CH_2CL_2. Further increasing acid concentration results in clear changes in the spectra (Figure 23a). A maximum appears to be reached at 600 eq FA.

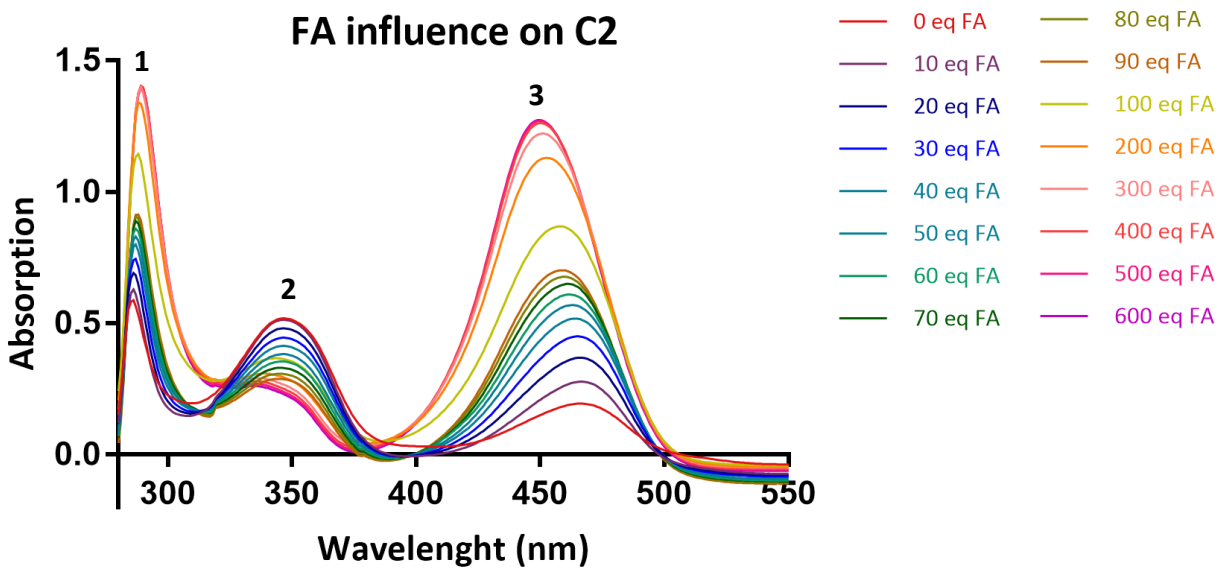

	Peak 1	Peak 2	Peak 3
Extinction coefficient (ε)	15844 $L \cdot mol^{-1} \cdot cm^{-1}$	13964 $L \cdot mol^{-1} \cdot cm^{-1}$	5224 $L \cdot mol^{-1} \cdot cm^{-1}$
0 eq FA	286 nm	347 nm	466 nm
80 eq FA	287 nm	345 nm	460 nm
400 eq FA	289 nm	335 nm	450 nm

Figure 23: *(a) UV-VIS measurements of **C2**-solution with increasing equivalents of formic acid. (b) Table of extinction coefficient and maxima of the three main peaks measured with UV-VIS spectrometry.*

Overall, peaks 1 and 3 increase in absorption and 2 decreases. In addition, slight shifts in maximum are observed, as shown in figure 23b. Minor bathochromic shifts are seen for peaks 1 and 3. A small hypsochromic shift seen for peak 2. Isosbestic points can be observed when taking a closer look. These points do not change in intensity or wavelength and indicate the equilibrium where new species are formed. The isosbestic point around 400 nm is likely to indicate the formation of a single protonated species (**C2(1+)**). This point is not crossed for samples above 90 eq FA, which means this equilibrium is no longer applicable; all molecules are protonated. A new isosbestic point is set around 380 nm, indicating a new equilibrium; the protonation of single protonated species (**C2(1+)**) to double protonated species (**C2(2+)**). The same argumentation can be made for the remaining two isosbestic points around 320 nm.

The experiment is repeated with base; deprotonation of the phenol group is expected (**C2(1-)**). 100 to 600 eq of NEt_3 are added to a solution of cage in CH_2CL_2. The yellow solution becomes colorless after addition of the base. The spectra show peak 1 decreases, peak 2 increases slightly and peak 3 completely disappears when base is added (Figure 24a). The opposite effect is observed for acid addition. The amount of added base does not seem to have a large effect, changes between 100 and 600 eq are minor. More equivalents of base correlates with peak 1 slightly increasing and peak 2 slightly decreasing. However, they are not in the same order of magnitude as for 0 eq base added. Similar effects are described in literature for acid and base addition [68]. 100 eq of base appear enough to deprotonate **C2**, although no new peaks occur corresponding to a new-formed species. The imines in **C2** could be partly protonated without any acid or base added. Therefore, the base is able to deprotonate the protonated imines, although not to deprotonate the alcohol group. This may be due to the strength of the base.

The reversibility of the equilibriums is tested by first adding acid first followed by base. The results are shown in figure 24b. The intensity for peak 3 is increased for acid addition and decreases again for base addition. The decrease is stronger than the increase resulting in absorption under the blanco. This is might be caused by an error due to low concentrations or precipitation. However, this qualitative experiment shows the change is reversible.

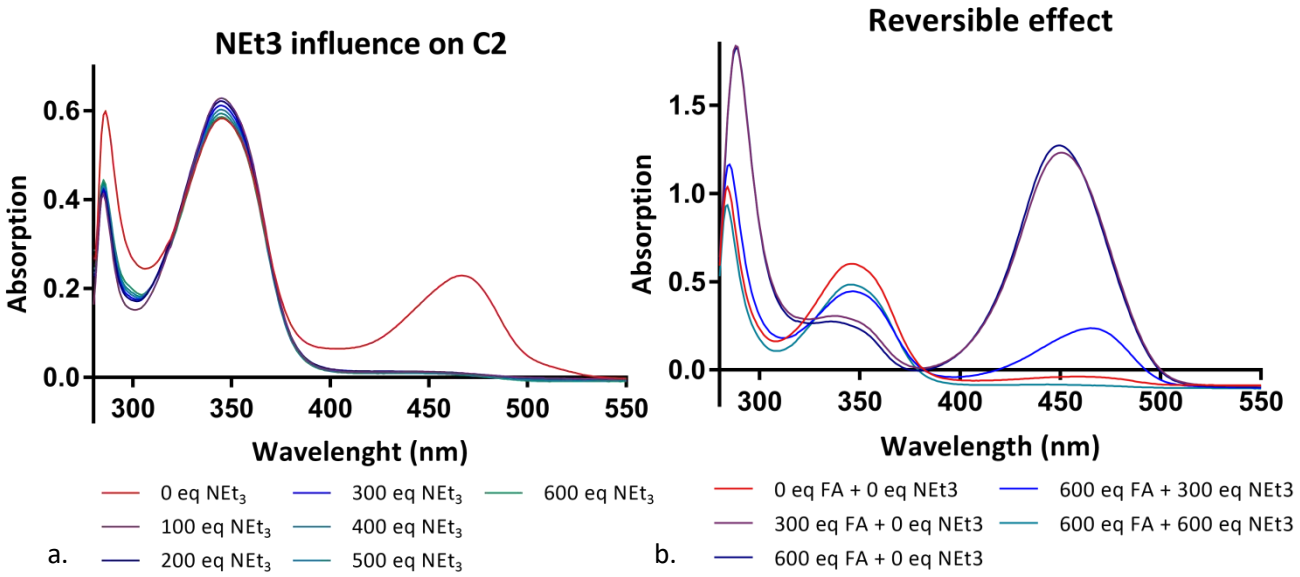

Figure 24: *UV-VIS measurements of **C2**-solution with (a) increasing equivalents of triethylamine. (b) Varying equivalents of formic acid and triethylamine.*

It should be mentioned that the species could be differently identified. In contrast to previous statements, **C2** could be already deprotonated (**C2(1-)**) without addition of acid or base, as the pKa of a phenol ranges between 4 and 11 based on the substituents. In addition, the imines will have a stabilizing effect as can be seen in the resonance structures in figure 25. Addition of acid will first form the neutral phenol (**C2(0)**) followed by the single protonated species (**C2(1+)**). **C2(2+)** is not formed, possibly as it is less stabilized. Addition of base will not change the state as the compound is already deprotonated. A change is seen between 0 and 100 eq which indicates some neutral phenol is present in the mixture; therefore, the pKa is probably slightly under the pH of measuring. Unfortunately, UV-VIS only shows formation of new species, but does not identify the species. Three species are observed, but no statement can be made if they are either **C2(2+)/C2(1+)/C2(0)** or **C2(1+)/C2(0)/C2(1-)**. All species are (highly) stabilized by the conjugated system, which complicates a definitive assignment to any one particular state.

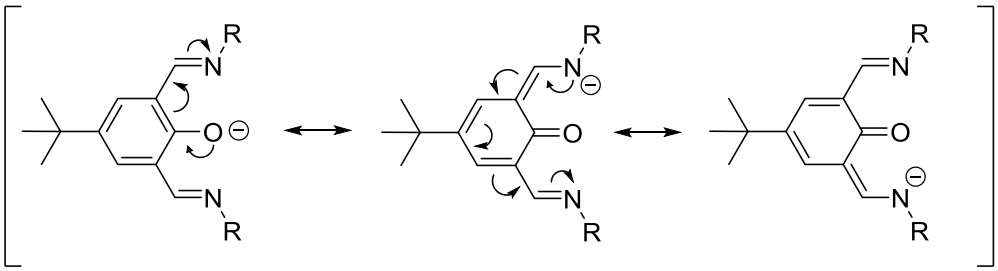

Figure 25: *Stabilization of **1-S** by resonance structures.*

Fluorescence is measured for 0, 80 and 400 eq acid which roughly corresponds to the three species found with UV-VIS spectroscopy. Overall, excitation as well as emission increases with higher acid concentration (figure 26d-e) [6]. Emission shows a small bathochromic shift with increasing acid concentration. Absorption, excitation and emission can readily be compared after normalization of the data. All data is divided by the largest data point in the series. Keep in mind that the Y-axis does not correspond with an actual quantity; the intensity of the peaks of different properties cannot be directly correlated to each other. One precondition is that excitation cannot be larger than absorption.

- 0 eq acid (26a): Three peaks are seen for absorption, but only one main peak (342 nm) is seen for excitation; Therefore, only these wavelengths are used for emission of light (fluorescence) and the absorbed wavelength lose energy in a different manner. Emission is measured with a 29 nm difference at 313 nm.
- 80 eq acid (26b): The same absorption peaks are seen with different intensities. Excitation is increased and two other peaks become more distinctive. An emission maximum of 296 nm is measured.
- For 400 eq acid (26c) is the same trend seen as described for 80 eq. An emission maximum of 294 nm is measured.

To conclude, protonation, absorption and fluorescence have been studied with spectroscopy. Three species are observed with UV-VIS (**C2(2+)**/**C2(1+)**/**C2(0)** or **C2(1+)**/**C2(0)**/**C2(1-)**).

[6] The sharp peak around 550 nm is a artifact caused by a filter

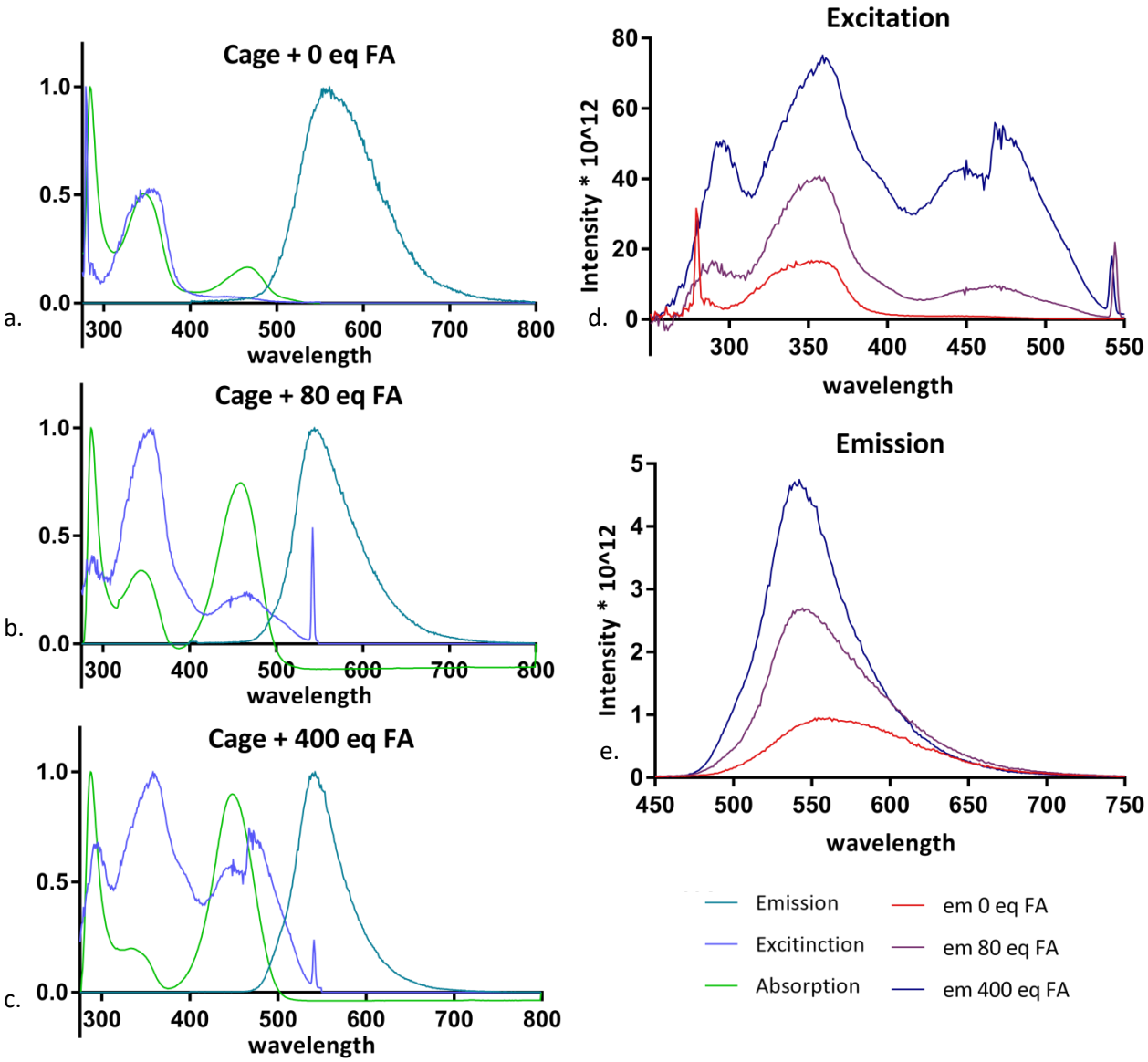

Figure 26: *Fluorescence measurements. (a)Measurements without FA. (b) Measurements with 80 eq FA. (c) Measurements with 400 eq FA. (d) Excitation measurements. (e) Emission measurements.*

5.2.3. Complexation of C2

The successful synthesis of **C2** offers opportunities to explore coordination to metal ions. The cage could be seen as a large ligand, which provides multiple coordination sites for metal ions. Multiple ways of coordination can be achieved for a cage with phenols in the interior and imines in the backbone, a few are shown in figure 27.

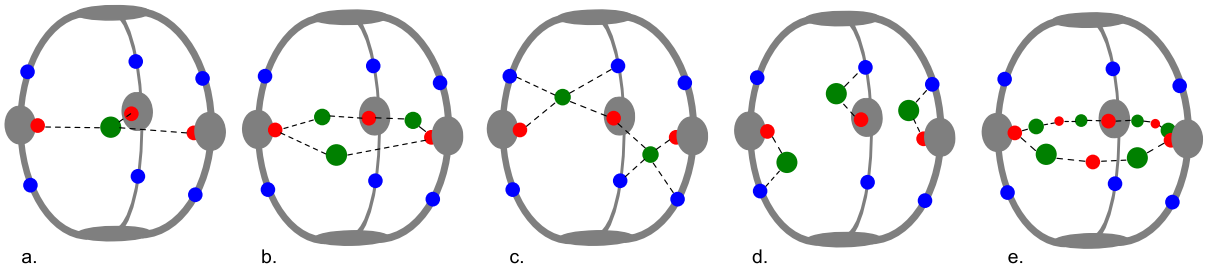

Figure 27: *Multiple possibilities of metal coordination. Other ligand on the metal ions are disregarded for clarity of the schematics.*

Previously, the distance between two oxygen was calculated with DFT to be 5.79 - 5.86 Å (figure 19, p.31). Coordinations a to c are doubtful as a single atom cannot bridge this distance, feasible

solutions which remains are represented by d to e. (d) metal ions are coordinated to a single phenol and imine (figure 27d). Coordination would be in the interior provided that the phenols are endo-orientated. Coordination of ≤ 3 metal ions is expected to be smoothly, one metal ion for each linker. However, > 3 metal ions might also coordinate by bridging the phenol groups. (e) A variation on figure 27b can be made by the addition of more bridging groups e.g. water or halides. This would result in a decrease in binding distance.

DFT calculations [7] are used to investigate if additional ligands on the metal ions would be able to fit in the cavity of **C2** and how they would orientate. The calculation is executed with a single zinc and acetate, which will also be used in actual experiments (figure 28). The calculations predict that zinc is coordinated on one deprotonated alcohol and supported by the nitrogen of the imine (coordination mode d). Zinc is coordinated in the middle of both atoms and forms a flat 6-membered ring. The acetate is located in the center of the interior, which can be seen using both side views. A metal ion can coordinate on the alcohol and imine and the interior of the cage is large enough for an acetate molecule. Up to three zinc atoms seem to fit in **C2**, however, the acetates will have to point outwards as a result of only one acetate fitting in the interior. Ghosh *et al.* [22] describe a similar size cage which shows acetone coordination. In the case of two molecules are bound in the cage; one in the center and another one inside one of the clefts. Similar behavior is expected for **C2**.

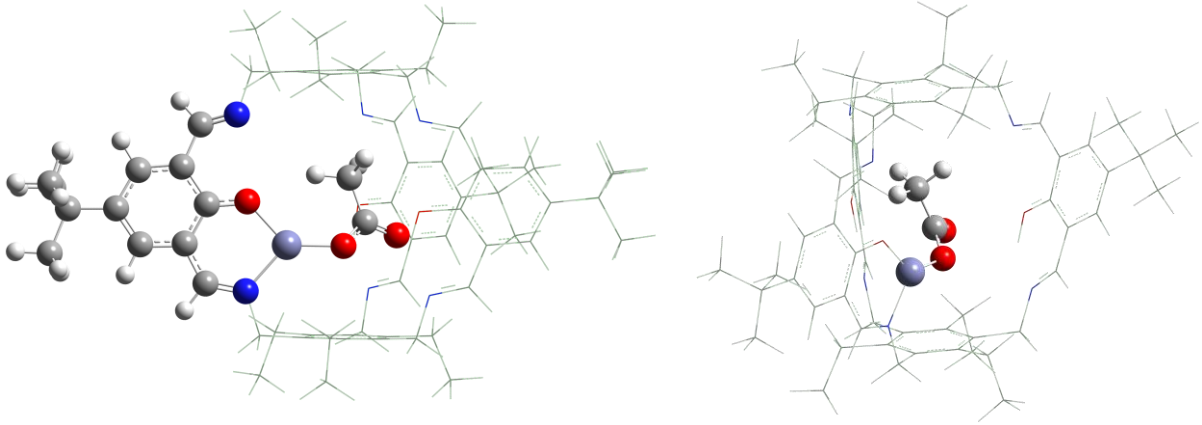

Figure 28: *Two side views of the calculate cage with ZnOAc coordinated. B is slightly more rotated than A to show the placement of acetate in the interior. Irrelevant parts of* ***C2*** *are displayed as wire frame for clarity.*

In addition, the possibility of bridging metal ions between two cages is investigated with DFT. In fact, metal bridging between cages is prevented by steric hindrance of the ethyl- and ^{t}Bu-groups of **C2**, even for the orientation with one flat side. Intermolecular bridging cannot occur for single metal ions; only when more bridging partners are introduced the distance can be overcome the distance. Some examples of multiple atom bridging are given by Murray *et al.* [33], but it is doubtful to play a role here. However, stacking can still take place resulting in solubility problems.

The following coordination experiments are based on the coordination of salen complexes. Two main routes are seen in literature [55]: I) addition of a metal acetate. Thereby the acetate acts as a base to deprotonate the phenols. II) addition of metal halides with NEt_3. Different routes can have an influence on the results, therefore both methods will be tested. Moreover, the choice of the metal salt is also of influence. Better leaving groups like anions will stimulate reaction and the larger the

[7] in collaboration with Léon Witteman, MSc with the program Gaussian 09 with the B3LYP functional.

anion the less probable to fit in the cage. Therefore, the metal could coordinate without anion by the use of other available ligands, coordinate to more available cage sites or enforce open-coordination site [69]. Note: it might also prevent any reaction as it cannot reach the coordination site.

Different base metal salts will be tested, similarly to the salen complexes (1.2.4 catalysis). Attempts are made with Fe, Co, Cu and Zn and the individual results are discussed below in the same order.

Fe: Three experiments are conducted on iron-coordination. An overview is provided by scheme 22. The first iron complex attempt is done with **C2**, $FeCl_3$ and NEt_3 under N_2 (entry **1**). The mixture is stirred overnight at 60 °C while more solid precipitates out the solution. Soluble and insoluble compounds are separated with canula filtration. The dark brown residue is not soluble in common organic solvents, which makes analysis with the available analysis techniques nearly impossible. IR spectroscopy is done for the residue; the spectrum is shown in figure 29b. Remarkable strong signals are observed at 1034.98 and 1020.22 cm^{-1}, which are assigned as C-O vibrations [8]. No change in C-O could indicate coordination without the phenolic alcohol.

The dark green, fluorescent filtrate is evaporated, brown solid remains. Resolving the solid for analysis is proven to be difficult and mainly results in suspensions. CD_2CL_2 is used for analysis as it seems to solve the most solid. ^{1}H-NMR, ^{13}C-NMR, paramagnetic NMR and ESI-MS only show the presence of NEt_3 and trace amounts of **C2.** No new compounds are observed. Although, the color suggest other compounds were present in the filtrate. As it does not show up in previous analysis, the color has to originate from organic compounds in small concentration, paramagnetic compounds with fast relaxation or inorganic material.

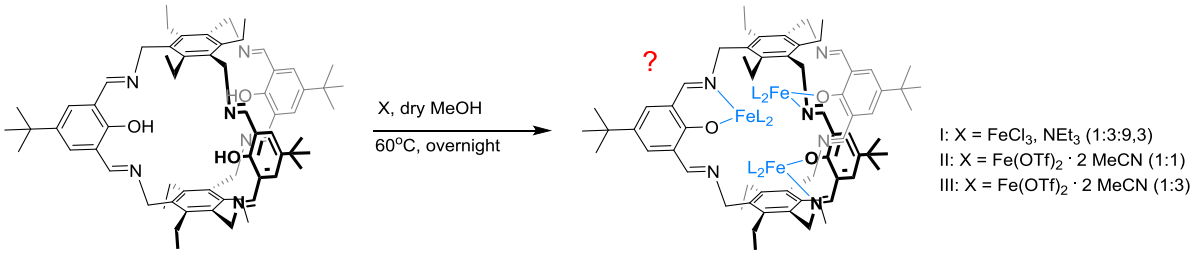

entry	Metal salt (x)	Ratio (cage : metal source : base)	Outcome
1	$FeCl_3$	1 : 3 : 9.3	Insoluble solids, **C2**, NEt_3
2	$Fe(OTf)_2 \cdot 2$ MeCN	1 : 1 : 9.3	Insoluble solids **C2**, NEt_3
3	$Fe(OTf)_2 \cdot 2$ MeCN	1 : 3 : 9.3	Insoluble solids **C2**, NEt_3, 3 Fluor sources.

Scheme 22: *Coordination of iron ions in **C2**.*

Entry **2** and **3** are executed with iron(II) triflate as metal salt. Unfortunately, the same observations are made: formation of insoluble solid and remaining base and cage in the filtrate. ^{19}F-NMR of the filtrate of entry **3** shows three peaks which would indicate three compounds. One is expected for a triflate anion. Possibly three different products are formed or triflates are oriented in different environments due to geometric restrictions.

Again, IR spectroscopy is used for further investigation of the insoluble solids (figure 29c). The spectrum is changed with respect to **C2** (figure 29a). The broad peak at 523 nm indicates a Fe-O

[8] This strong vibration is not found in other coordination experiments as is shown in figure 29.

bond, which would be present after iron coordination to phenol. A reference spectrum of rust excludes iron oxidation. In contrast, the residue spectrum does show quite some similarities to a Fe-salen compound (figure 29d) [70,71], which suggest formation of a similar iron complex. The poor solubility can be a property of the complex as sparing solubility is reported for the Fe-Salen complex [72]. It may also indicate a form of polymer formation. The metal can act as a Lewis acid and/or template which directs towards polymer formation (1.4.1 Design). Coordination of metal ions can still occur in polymers, for instance similar to a complex illustrated in figure 30 found by Mushtaq *et al.* [73].

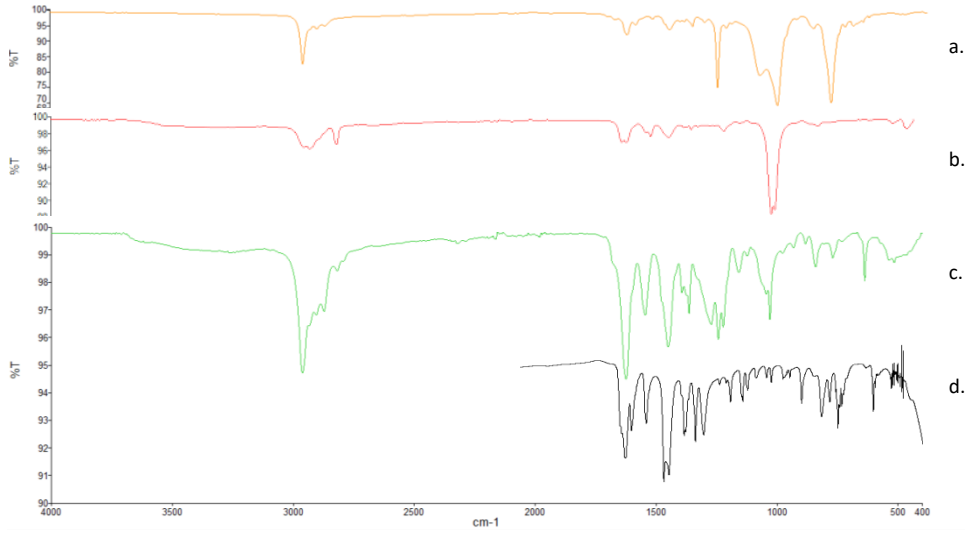

Figure 29: *IR spectra of (a)* ***C2****. (b) Residue of $FeCl_3$ complexation. (c) Residue of $Fe(OTf)_2 \cdot 2$ MeCN complexation. (d) Fe-Salen.*

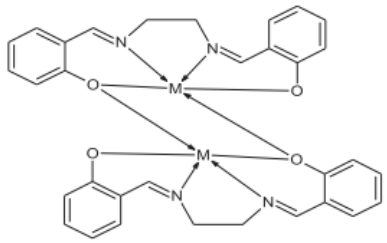

Figure 30: *Similar structure to metal ions coordinated in polymers.*

To summarize, no direct evidence of an iron complex is found for all experiments. However, lack of rebuttal suggests a reaction occurred and possibly an insoluble iron complex is formed similar to Fe-Salen. Unfortunately, no further conclusions can be drawn.

Co: 6 eq of copper(II)acetate (pink solution) is added to a yellow suspension of **C2** where after it immediately turns to dark brown/green suspension. The color change indicates that a reaction has occurred. The solubility of the formed solid in CD_2CL_2 and MeCN is minor to none. No peaks are observed of new compounds. In addition, ESI-MS shows multiple compounds, but no clear peaks above the mass of **C2**. Some peak could be recognized just above noise levels (see experimental). Therefore, it is suggested that a cobalt complex could have formed, but no direct evidence is found.

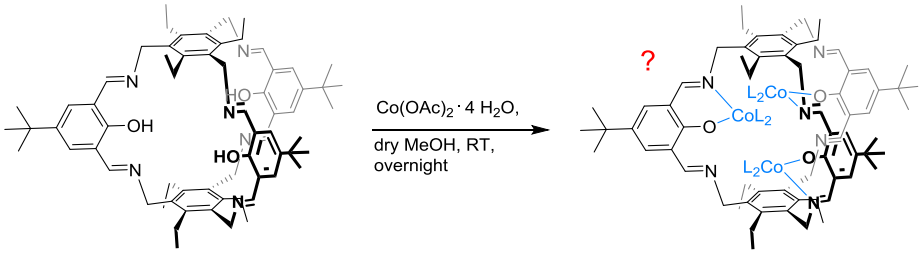

Scheme 23: *Coordination of cobalt ions in* ***C2****.*

Cu: Various reaction conditions are tested for copper coordination: copper salts ($Cu(OAc)_2$, $CuCl_2$, CuCl), temperatures (RT, 60°C) and ratios (cage:Cu = 1:3 or 1:6). An overview of the reactions is provided by scheme 24. All reactants are added as solutions except CuCl which is added as solid due to insolubility in MeOH. Combination of reactants turns all mixtures in different shades of green, which are stirred overnight. More precipitate forms, which is separated with canula filtration. Solubility proves to be a problem for the residues as well as for the filtrates. Filtrates seem to partly solve in CD_2CL_2, d4-MeCN and d4-MeOH.

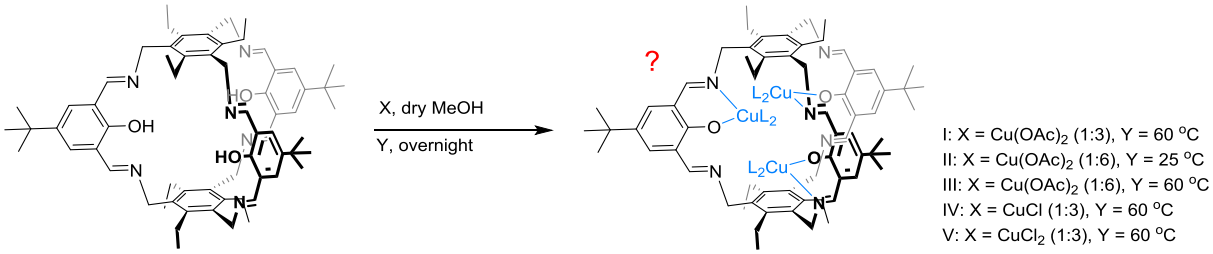

Entry	Metal salt (x)	T (°C)	Ratio (cage : metal source : base)	Outcome
1	$Cu(OAc)_2$	60	1 : 3 : 0	Insoluble solids, **C2**, NEt_3, paramagnetic species
2	$Cu(OAc)_2$	25	1 : 6 : 0	Insoluble solids, NEt_3
3	$Cu(OAc)_2$	60	1 : 6 : 0	Insoluble solids, NEt_3
4	CuCl	60	1 : 3 : 9.3	Insoluble solids, **C2**, NEt_3
5	$CuCl_2$	60	1 : 3 : 9.3	Insoluble solids, **C2**, NEt_3

Scheme 24: *Coordination of copper ions in* ***C2****.*

^{1}H-NMR is used to analyze the filtrates [9]. Three broad peaks are observed in all spectra (12.59, 2.57 and -0.39 ppm). It corresponds to paramagnetic copper acetate, which is unreacted starting material. or acetate bounded to a copper-cage-complex. No large shift is seen in the NMR, which if often found upon coordination. All other peaks can be explained from solvents [10]. Paramagnetic NMR for entry **1** reveals six new minor peaks at 31.97, 31.47, 23.52, 22.45, 20,95 and 19.88 ppm. Under these reaction conditions it is possible to form a soluble paramagnetic compound, which might be a copper-cage-complex. The other routes (scheme 24) might not form this compound(s) or something prevents the visibility in NMR such as further complexation, which results in an insoluble complex.

For entry **1**, ESI-MS shows some remaining empty cage and many additional peaks between 1200 - 1400 m/z, which show no recognizable isotope patterns. Unfortunately, no matching formula is found yet. The peak of 1383.7036 m/z seems to have an overlapping pattern of one compound of Δ =

[9] Note: insoluble compound are invisible for ^{1}H-NMR.
[10] Except for one minor impurity in entry **2**: 2 singlets: 1.01 ppm and 8.80 ppm.

1.0 m/z and another of Δ = 0.5 m/z. This corresponds with a mono protonated species ($M + H^+$) and a double protonated species with a twice as large mass ($2M + 2H^+$). The combination of the [2+3] and [4+6] cage is most probable, but cluster formation is also possible (see Zn coordination, p. 44). ESI-MS shows for entry **2**-**5** no peaks above the mass of **C2**, with corresponds with the NMR data.

IR is used to gain additional information on the filtrates and residues. The spectra of the reactions are shown in figure 31. Upon comparison, a clear change can be seen between the different reactions and the empty cage (figure 32). This suggest that a reaction has occurred. The main difference is seen in the intensity of bands. The imine bond **E** is still present in all spectra, but the peaks labeled **K**, **L**, **M** and **N** seem to be not simply recognizable or have disappeared completely. The spectra show many other peaks, which can be assigned with literature [74] (see appendix D).The overall low intensity can be caused by a low concentration of compound or a very thin sample (see formula 2). The last is most probable as all samples consists of very fine sheets, which are crushed to thin pallets.

In all samples a distinct peak is seen between 1630.67 and 1598.53 cm^{-1} (**E**), which is in the range of an imine (1690-1520 cm^{-1}) [74]. Without III. (unclear top) the average imine wavelength is 1625.46 cm^{-1} (± 2.08), which is lower than the empty cage with a peak of 1629.90 cm^{-1}. Shifted peak positions can indicate metal coordination [75], however the difference seems not significant enough. Still, similar small differences are observed by Sagir *et al.* [73] for complexation of imines from salen to copper. No clear Cu-O peak is not found in these spectra, which might be due to the range. Lower wave numbers should be measured for this.

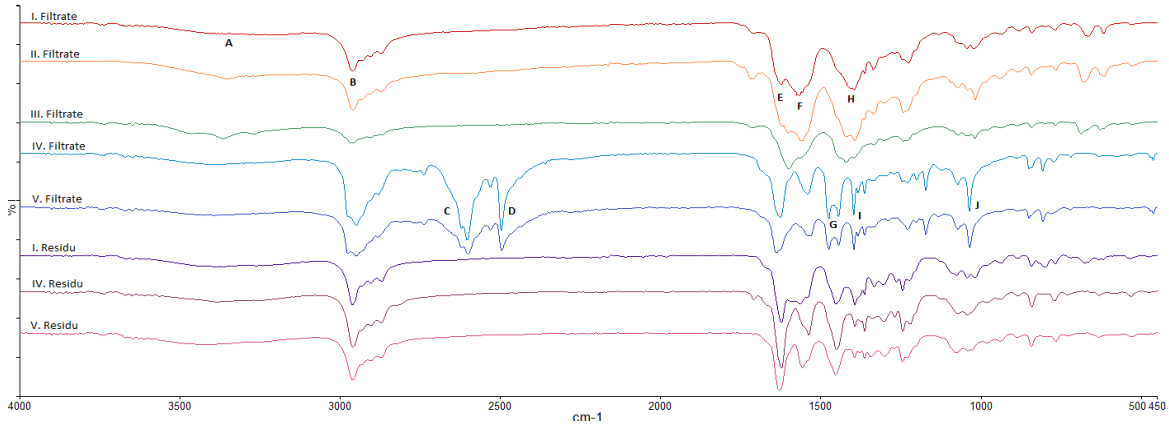

Figure 31: *Infrared spectra of copper coordination attempts.*

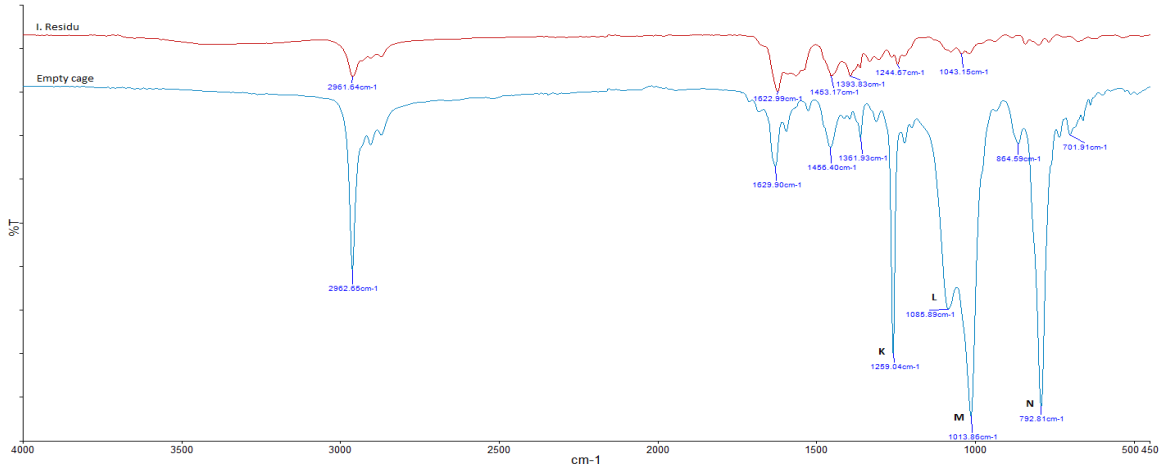

Figure 32: *Infrared spectra of copper coordination attempt compared to **C2**.*

Concluding, different ways of copper coordination are attempted. IR indicates a reaction occurred in all attempts. A slight shift in imine peak is seen which might indicate coordination. Only in the filtrate of reaction I is clear paramagnetic signals seen and high masses detected in ESI-MS. In the other reactions resulted into insoluble products, which still might be desired copper complexes.

Zn: An overview of zinc coordination I provided by scheme 25. Entry **1** reaction is executed with a mixture of cage, $ZnCl_2$ and NEt_3 (1:3:9.3) is heated to 60 degrees and stirred overnight. A yellow solid remains after evaporation, which does reasonably dissolve in CD_2CL_2. The ^{1}H-NMR shows many peaks positioned around the original cage peaks. This suggests the same protons as in **C2** have slightly different environments; A possible reason can be that multiple isomers have formed. Over time a phase separation is seen in the NMR tube. Orange amorphous solid depositions on the sides and a yellow liquid remains. This process is proven to be irreversible by motion or heat. Due to this disturbance, quality carbon NMR could not be obtained. However, ESI-MS shows three main peaks above the mass of **C2**, all with an interesting pattern (such as in figure 33). The pattern is explained by two overlaying signals: normal [2+3] cage and [4+6] cage. The main peak at 1357.3143 m/z is explained by a cage with three deprotonated OH-groups, 3xZn, 3xCl and 3xH_2O groups and its [4+6] cage. A structure or this result is proposed in figure 33. All zinc atoms have all an oxidation state of two with a coordination of two X-ligands and two L-ligands. Water and chloride are both not large in size. Therefore, they are all expected to fit in the cavity. Lastly, no crystals are obtained yet to confirm the structure(s).

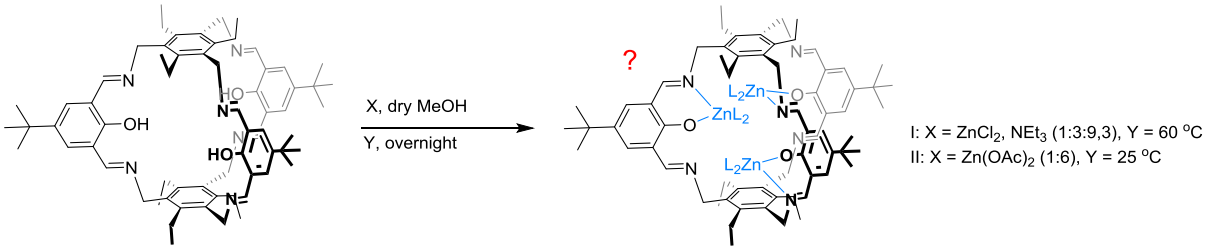

Entry	Metal salt (x)	T (Y) (°C)	Ratio (cage : metal source : base)	Outcome
1	$ZnCl_2$	60 °C	1 : 3 : 9.3	Zinc-cage-complexes with 3-5 metal ions
2	$Zn(OAc)_2$	25 °C	1 : 6 : 0	Zinc-cage-complexes with 2 metal ions

Scheme 25: *Coordination of zinc ions in **C2**.*

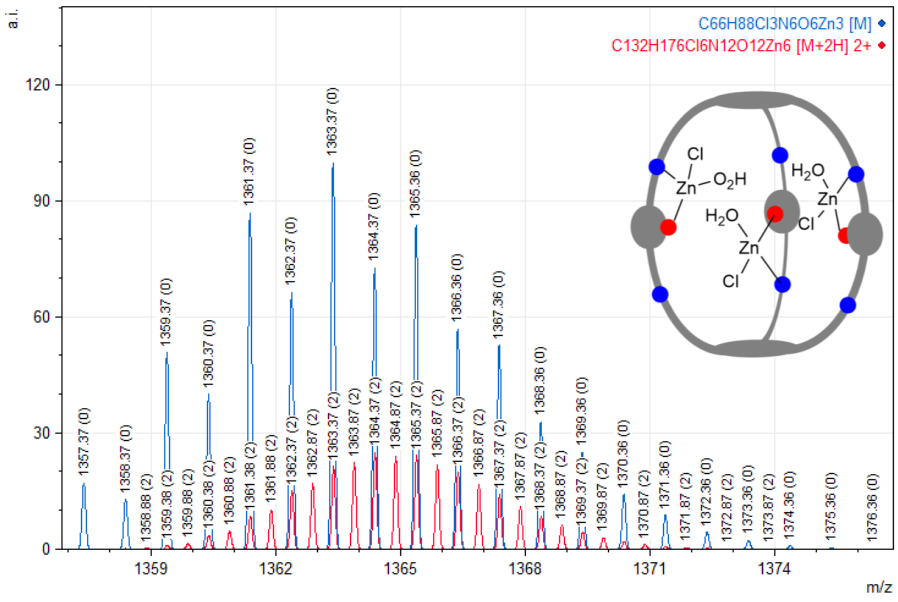

Figure 33: *ESI-MS stimulation of zinc coordination attempt with zinc chloride. Calculated model from mMas v.5.*

Reaction of $Zn(OAc)_2$ with **C2** over the course of four days' results in a yellow suspension (entry **2**). The following canula filtration yields an insoluble residue and a yellow filtrate. NMR of the filtrate shows again many peaks located around the original cage positions. Probably multiple compounds are present which are very similar to each other e.g. isomers. ESI-MS shows many peaks with all patterns of zinc-coordination. The main peaks have an isotope pattern corresponding with two zinc atoms. Unfortunately, the mass could not be matched to a structure yet. Upon further inspection, the cage appears to have some polymerization occurring, which could explain the insoluble solid in the reaction (figure 20a). It may even be responsible for the many peaks. Oligomers would give slightly different environments and could probably still coordinate zinc. Probably in a similar manner as it is illustrated in figure 30. It should be mentioned that some free **C2** is also found in the mixture, which could also give rise to the Zn-compounds found with ESI-MS. Therefore, no clear conclusions can be made on the nature of the Zn-compounds. Nevertheless, we can still conclude that zinc ions can coordinate with both methods.

5.2.4. CATALYSIS OF C2

As previously described, **C2** is likely to coordinate iron ions. Catalytic properties of this combination are tested by synthesizing an iron complex in situ. $Fe(acac)_3$ is added to **C2** and subsequently, the reactants are added to the mixture. The sulfoxidation of thioanisole is tested, shown in scheme 26 [76]. This straightforward reaction uses cheap hydrogen peroxide to oxidize sulfides such as thioanisole. The reaction mixtures are analyzed with (quantitative) NMR and the results are shown in scheme 26. The results appear peculiar. No clear relation can be seen between different entries. More important, more starting material is converted than products are seen (conversion >> yield) where no significant byproducts are seen. This can be partly explained by a weighting error in the internal standard. This error is solved for the entries 8, 9, 14 and 15. However, the numbers are still off. Other explanations could be error due to heterogeneity, filtration or method [11]. The conversion and yield are not reliable and will not be further analyzed. The results will be treated as preliminary results and only the ratio of starting material and product will be used.

Some toluic acid is added in entry 1 and 2. This gives higher sulfoxidation yields according to literature. However, the cage will probably undergo hydrolysis over time. No significant difference is seen in the ratio product: start material. Therefore, it is not advised to add acid to the mixture.

Entry 8, 9, 14 and 15 are done as last and seem to deviate from the other data. Without these points a clear relationship between entries with or without cage and $Fe(acac)_3$ can be seen. With the ration P:SM to be around 1 : 2.4 with the cage and 1 : 15,0 without the cage. Therefore, it appears that the combination helps the reaction. However, we should be very careful in this manner, because of the strange last entries.

To conclude, **C2** might have a catalytic contribution to sulfoxidation. However, more experiments are needed to statistically confirm this. Errors in this method might give a false positive.

[11] Quantitative NMR has till 10% uncertainty.

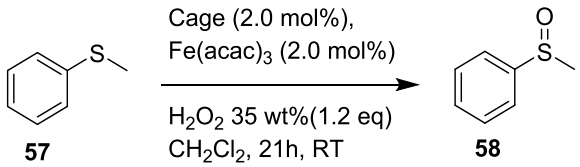

Entry	Description	Ratio P:SM	Conversion (%)	Yield (%)
1	Cage, $Fe(acac)_3$, reactants, toluic acid [1]	1 : 2.7	-	-
2	Cage, $Fe(acac)_3$, reactants, toluic acid [2]	1 : 2.4	63	16
3	Cage, $Fe(acac)_3$, reactants [1]	1 : 1.6	-	-
4	Cage, $Fe(acac)_3$, reactants [2]	1 : 3.0	68	11
5	Cage, $Fe(acac)_3$, reactants [3]	1 : 2.1	53	22
6	$Fe(acac)_3$, reactants [2]	0 : 1	54	0
7	$Fe(acac)_3$, reactants [3]	0 : 1	54	0
8	$Fe(acac)_3$, reactants [3]	1 : 4.8	40	13
9	$Fe(acac)_3$, reactants [3]	1 : 4.8	43	12
10	Cage, reactants [2]	1 : 11.8	15	7
11	Reactants [1]	1 : 24.4	-	-
12	Reactants [2]	1 : 12.0	34	5
13	Reactants [2]	1 : 11.6	26	6
14	Reactants [2]	1 : 0.5	75	51
15	Reactants [2]	1 : 0.2	90	62

Scheme 26: *Proposed reaction for sulfoxidation of thioanisole and table of results of catalytic testing with in situ iron-cage complex(es).* [1] *H-NMR tube, no internal standard, 16h.* [2] *Flask with 1,4-dimethoxybenzene as internal standard, 21h.* [3] *Filtered though silica, 21 h.*

5.3. C1: AMINE CAGE

5.3.1. SYNTHESIS OF C1

The synthesis of **C1** starts with an imine condensation similar as for **C2**. In contrast, it is followed by a reduction with $NaBH_4$ (scheme 27). The imine bonds are reduced to amine bonds. The product is not susceptible to water by reduction of the imine bonds as the bonds are not longer reversible. Therefore, no polymerization is expected and any reactions can be carried out in water containing solvents [12]. The observed fluorescence does not exist after reduction due to the decrease in conjugated system. In addition, imines and amines bind differently to metal ions. It is not known what the influence will be.

[12] if other reactants are not influenced by water

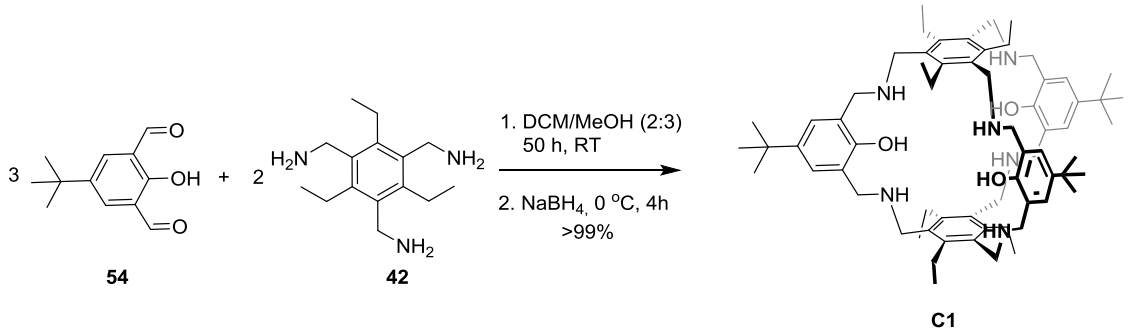

Scheme 27: *Synthesis of* ***C1****.*

The ^{1}H-NMR spectrum and ^{13}C-NMR spectrum are clean and can be fully assigned to **C1** (See appendix E). The distinct broad peak around 12 ppm disappeared due to the removal of the intramolecular H-bond. In addition, the clear imine vibration is disappeared in the IR spectrum, which lies in the line of expectations. ESI-MS nicely shows the mono-, di- and tricationic species of **C1**. Small traces of the **C2** are still seen in ESI-MS, however, in such small amount that it is not seen in NMR.

DFT can add insight in the structure of **C1**. The optimized structure is shown in figure 34. In contrast to the **C2**, this structure is more distorted. The reason could hide in amine bonds. The bond angles in the imines of **C2** are flat, which creates a completely flat linker. The amines of **C1** contain tetrahedron bond angles, which could twist the cage together to minimize energy. Therefore, the top and bottom do not overlap in the top view.

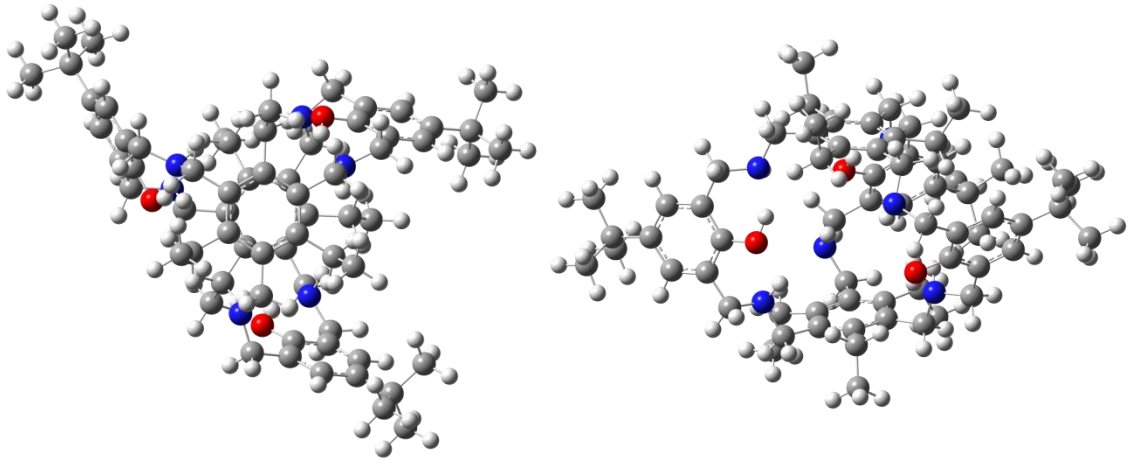

Figure 34: *DFT optimizations of C1. a) Top view of C1. b) Side view of C1.*

Similar as for **C2** the linkers are positioned in a fixed angle, but the direction is random. One of two orientations provide an opened side as is shown for figure 34. Stacking would be possible for both orientations, which could provide solubility issues. However, the lack in polymerization will most likely give more manageable reaction mixtures.

Crystallization of **C1** appears to be difficult. After many attempts a crystal is grown by diffusion crystallization of hexane and CH_2CL_2 followed by slow evaporation. The crystal consists of stacked ultra platelets (figure 35a). Unfortunately, the crystals are very facile and contain defects. Therefore, only a preliminary structure is obtained. The data will be discussed, despite, the rough solution

structure. Please keep in mind it is a preliminary structure, for instance numbers could be slightly off in reality.

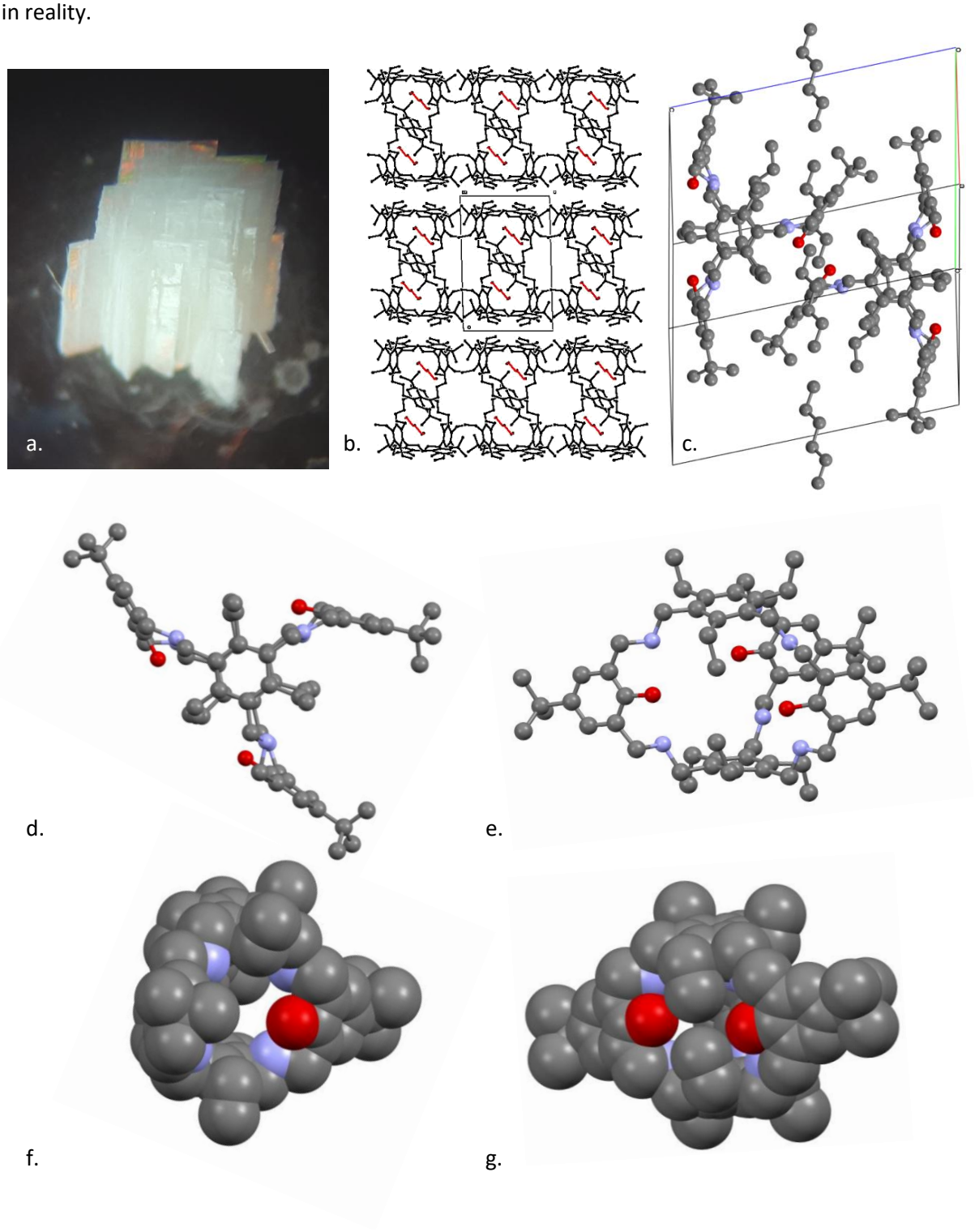

Figure 35: *Preliminary x-ray data. (a) Crystal.(b) Stacking of unit cells. (c) Unit cell with hexane molecules. (d) top view of crystal structure. (e) side view of crystal structure. (f) space filled model with open sites shown. (g) space filled model with closed side shown.*

An unit cell consist of two molecules **C1** and two hexane molecules (figure 35b-c). One hexane is orientated in the cavity and side pocket, the other in between cages. An additional solvent might be present, but could not be identified. The linkers of C**1** make up one nearly flat side, which is aligned in the intersections of the unit cells, and the other linker stacks with its analogue in the unit cell (figure 35c). An individual **C1** molecule is shown in figure 35d-e. The structures show many similarities to the DFT calculated structure. In fact, the angles of the linkers overlap. However, two differences can be noted in the comparison between the crystal data and DFT. In contrast to DFT, the top and bottom align fairly well. The angles correspond quite well to the VSEPR theory for both structures; therefore, the cause should be elsewhere. The structures might be close in energy and both can exist. The structure found in the crystal is more prone to stack and therefore form crystals. The structure could slightly differ in solution. Another difference is found in the positioning of the ethyl groups. They are expected to rotate away from the centre due to steric hindrance, however, this applies only for 2 out of 3 ethyl groups in the crystal structure. One out of three ethyl groups are directed towards the centre, which completely closes one of the entries of **C1**. A space filling model shows this phenomenon well, as shown in figure 35f-g. A well-defined cavity with two free entries is seen in 38e whereas 38f clearly shows one entry is closed by ethyl groups. In addition, the specific rotation of the phenyl groups results in the smallest distance between the oxygen atoms with 6.31 Å. The closed entry may result in lower metal coordination or lower catalysis speed; however, it is not expected to completely shut down these processes, they might rotate in solution.

The dimensions of C1 can be expressed on the basis of the distances between oxygen atoms, which are for the crystal structure: 7.76, 7.18 and 6.31 Å [13]. In comparison with DFT are these slightly larger values, this could still originate from the rough structure. The height ranges from 7.35 - 8.05 Å. The bonds reflect normal lengths. For instance, the CH_2-NH bond length is 1.50 - 1.55 Å which is in line with the average length of 1.47 Å. Therefore, reduction was successful as an average iminebond is much shorter with 1.28 Å.

In conclusion, **C1** could be synthesized via reductive amination and is completely analyzed. DFT shows a similar structure to **C2**, in which the phenol groups are placed in the interior and the linker are positioned in a fixed angle. This is confirmed by preliminary x-ray data. In addition, the crystal shows one of three entries is closed by ethyl groups.

5.3.2. COMPLEXATION OF C1

C1 has comparable dimensions, groups and symmetry as **C2,** therefore similar coordination of metals is expected. Zinc seems to be the most straightforward coordination for **C2**. Hence, coordination of zinc is first attempted for **C1**.

Zn: First, zinc coordination is attempted with **C1** and $Zn(OAc)_2 \cdot 2\ H_2O$ in MeOH (1:6). Many peaks are seen in the ^{1}H-NMR, mainly positioned around the chemical shifts of **C1**. As previously described, small changes in the cage are the origin. Different isomers of asymmetric zinc coordination could give an explanation of the many peaks. More difference in chemical shift can be the result of a different environment such as Zn coordination, which will lead to a broader region of peaks NMR. Especially the region 4.5-3.5 ppm contains many peaks, which corresponds with the CH_2-groups next to the

[13] Note: preliminary data can be slightly off.

amine. This could be a hint of nitrogen coordination to Zn. ESI-MS shows six peaks (one large, two medium and 3 small). All patterns correspond to two incorporated zinc ions. It seems difficult to match the masses for the peaks though the many possibilities for high masses. Unfortunately, no success yet.

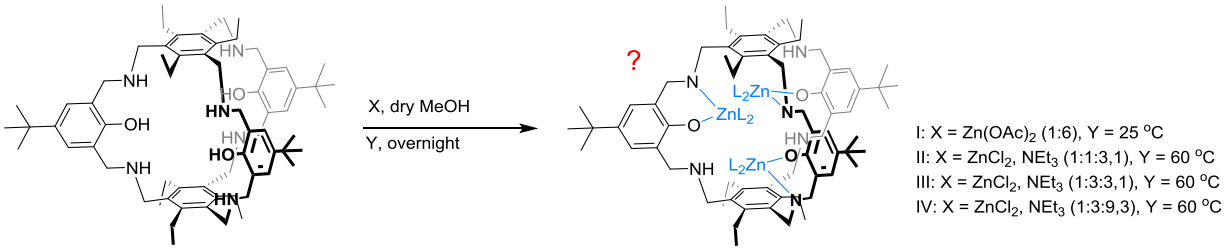

Entry	Metal salt (x)	T (Y) (°C)	Ratio (cage : metal source : base)	Outcome
1	$Zn(OAc)_2$	25 °C	1 : 6 : 0	Zinc-cage-complexes with 2 metal ions
2	$ZnCl_2$	60 °C	1 : 1 : 3.1	**C1**, Zinc-cage-complexes with 3-5 metal ions
3	$ZnCl_2$	60 °C	1 : 3 : 3.1	Zinc-cage-complexes with 3-5 metal ions
4	$ZnCl_2$	60 °C	1 : 3 : 9.3	Zinc-cage-complexes with 3-5 metal ions

Scheme 28: *Attempts on zinc coordination in* ***C1****.*

Zinc coordination is also attempted with $ZnCl_2$ and NEt_3. An advantage of this method is the possibility to tune the ratio cage : zinc source : base. Different ratios are tested (1:1:3, 1:3:3 and 1:3:9) and all result in the same compound(s). Some empty cage can be seen in the reaction with one equivalent of zinc salt, which implies it is favored to have more than one zinc atom coordinated to a cage. Again, ^{1}H-NMR spectra show many peaks between 4.5-3.5 ppm as seen for $Zn(OAc)_2$. as well as multiple peaks around 7.2 ppm. In contrast to the $Zn(OAc)_2$, a clear gap can be seen in the region. ESI-MS show three main peaks with three equivalent of zinc. It shows many more peaks in case of addition one equivalent of zinc salt, due to an uncompleted reaction. All spectra have the same major peak at 1383.44 m/z. The peak overlaps with another peak at a slightly higher mass (8 m/z), which differs in intensity for different experiments. The peak shows an isotope pattern of 3-5 zincs, which are very close to each other. Unfortunately, no structure can be established. A jobs plot could be made to determine exactly how many zinc atoms are coordinated inside a cage.

Still, it is shown zinc can coordinate in the cage when using $ZnCl_2$ and NEt_3. The amount of coordinated zinc increased from the $Zn(OAc)_2$ experiment. This could be due to the counter ion of choice. Acetate is much bigger than chloride. Therefore, more than two acetate molecules might not fit within the cage.

6. Conclusions

Three cage compounds were synthesized and synthetic plans were made with the help of retrosynthetic analysis.

6.1 Cage A

Building block **16** was successfully synthesized from **11** in a 5-step synthesis with an overall yield of 45%. **16** is not known in literature yet. Its analogue building block, **7**, could not be obtained; the last reaction failed probably due to reactivity or solubility issues. In addition, building block **20** was obtained in multiple two-step reactions. The best results were provided by nucleophilic substitution with NaN_3 followed by a Staudinger reduction (overall yield = 44%).

Imine condensation was achieved in multiple model systems. The reaction is water sensitive; therefore, direct reduction often leads to higher yields. Unfortunately, imine condensation with building block **16** has resulted into insoluble solids, which were difficult to analyze. The solids are possibly stacked macrocycles or insoluble oligomers.

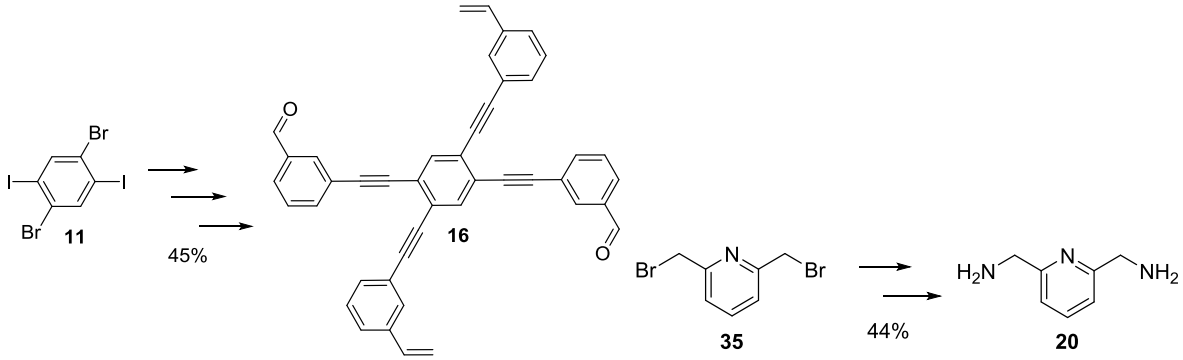

Figure 36: *Synthesis of (a)* ***16*** *and (b)* ***20****.*

6.2 Cage B

Building block **43** was obtained in a 3-step synthesis with an overall yield of 65%. Side product **50** was formed during Gabriel Synthesis, which could be useful for research of other heterosequenced cages. A mechanism for formation of **50** was proposed.

Homosequenced cages **53** and the tribromide analogue are obtained after mixing of **43** and **51** followed by addition of either **24** or **54** (figure 37c). We can conclude that reductive amination was successful in contrast to the proposed S_N2 reaction.

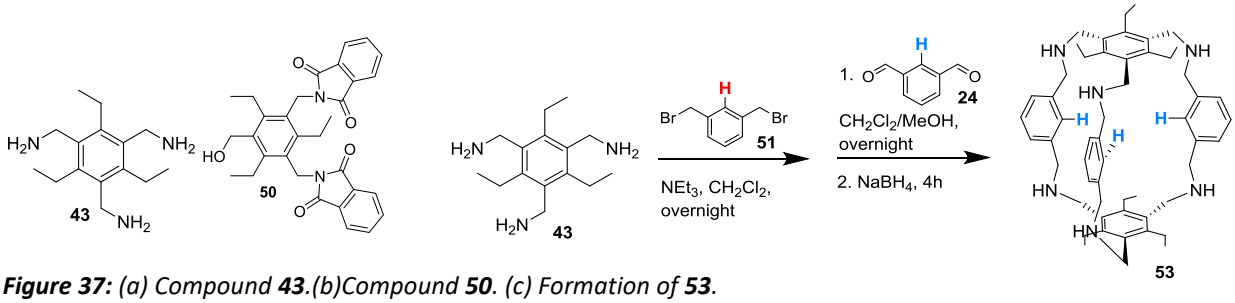

Figure 37: *(a) Compound* ***43****.(b)Compound* ***50****. (c) Formation of* ***53****.*

6.3 CAGE C

Homosequenced cage **C2** was synthesized via imine condensation in a quantitative yield. The reaction is sensitive as different results were obtained, with the same reaction conditions. Poorly soluble solids were often formed, which could originate as stacked cages, [4+6]-cages, COFs or polymers. No insoluble solids are formed after drying over molsieves for 3 days.

C2 is not reported in literature before and was therefore completely analyzed. DFT calculations of **C2** show a shape-persistent structure with a cavity of approximately 5.83 Å. The linkers are positioned in a fixed angle of 57° in a random direction (figure 38b-c).

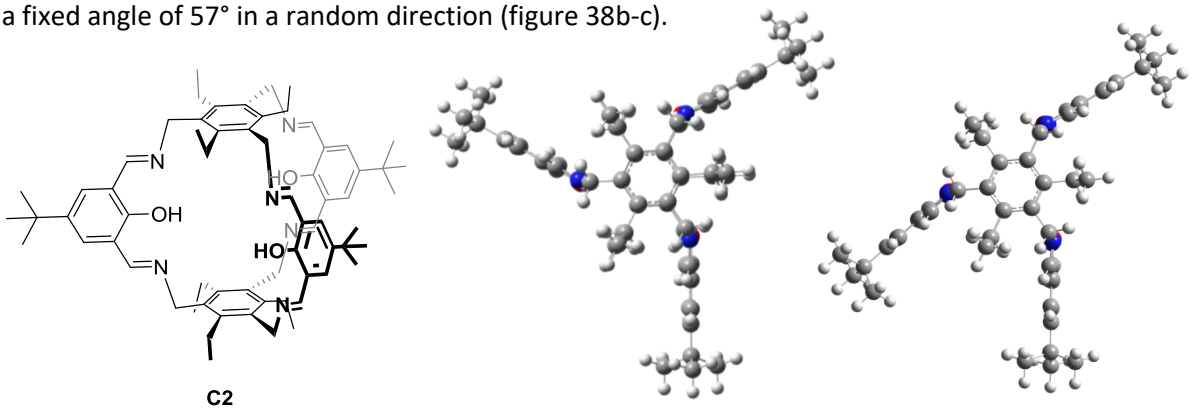

Figure 38: *(a)* ***C2****. (b) top view of DFT optimizations of* ***C2****.*

Compound **C2** showed fluorescence after addition of acid, which is studied with UV-VIS and fluorescence spectrometry. Increasing acid concentration lead to an increase in absorption around 360 nm and a bathochromic shift. Three species were observed, which are either **2+S/1+S/0S** or **1+S/0S/1-S** (scheme 29). Extinction and emission were also determined for the found species. Finally, the measured effect by protonation could be reversed with base as NEt_3.

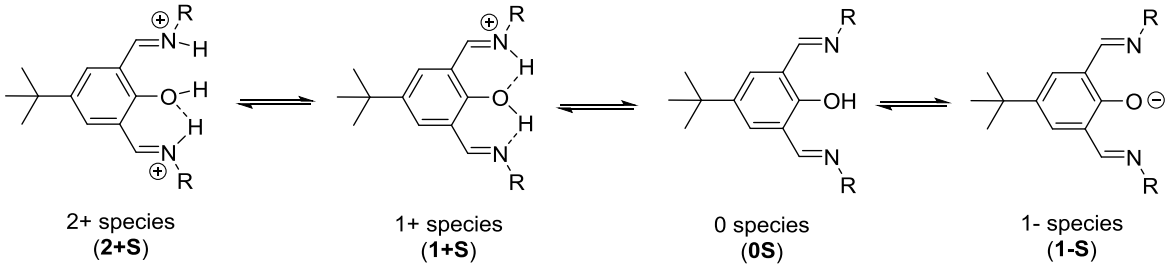

Scheme 29: *Species that could have been found in UV-VIS-spectroscopy.*

Iron complexation of **C2** and $Fe(OTf)_2 \cdot 2MeCN$ could have been successful as the IR of the product(s) and Fe-Salen have many similarities. Insolubility made further analysis impossible [14]. Also, coordination with $Cu(OAc)_2$ was promising as paramagnetic compounds were observed in ^{1}H-NMR when 3 equivalents were used. In addition, ESI-MS showed peaks above the mass of **C2**, which hints to complexation. More equivalents tend to result in completely insoluble compounds. Zinc-cage-complexes can be synthesized with $ZnCl_2$ or $Zn(OAc)_2 \cdot 2\ H_2O$; evidence is provided by NMR in combination with ESI-MS. One mass in ESI-MS could be matched to the zinc-cage-complex shown below, in which three zinc ions were coordinated. Many coordination experiments led to poorly

[14] Currently, no other analysis techniques are available for solid analysis.

soluble solids and limited analysis. No (in)direct evidence for coordination of **C2** with $FeCl_3$, $Co(OAc)_2 \cdot 4H_2O$ or $CuCl_x$ was found. Therefore, no conclusion can be drawn for these experiments.

Catalytic activity could be tested with in situ complexation of **C2** and $Fe(acac)_3$. Preliminary results suggest a catalytic active compound is formed, however, further research is needed to confirm this.

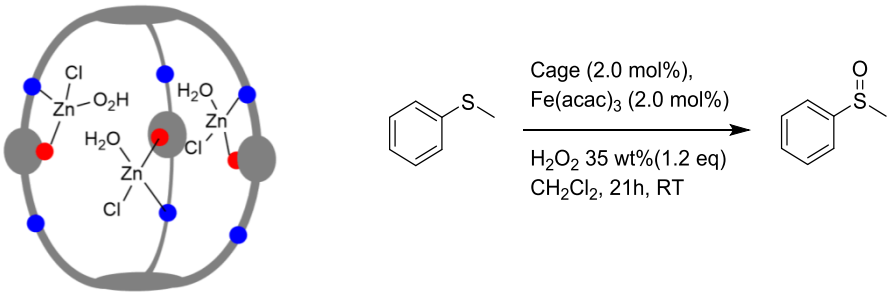

Figure 39: *(a) proposed zinc-cage-complex. (b) proposed catalytic reaction.*

Reduction of **C2** resulted in **C1**, again a new compound, not found in literature. Reduction was executed with $NaBH_4$ and was again quantitative. Crystals could be grown via diffusion of hexane/ CH_2CL_2 followed by slow evaporation. The crystals led to a preliminary crystal structure, which shows many similarities to the calculated structure by DFT. In contrast, 1 out of 3 ethyl groups point towards **C1**, which blocks one of the entries. The other two entries are available for interaction.

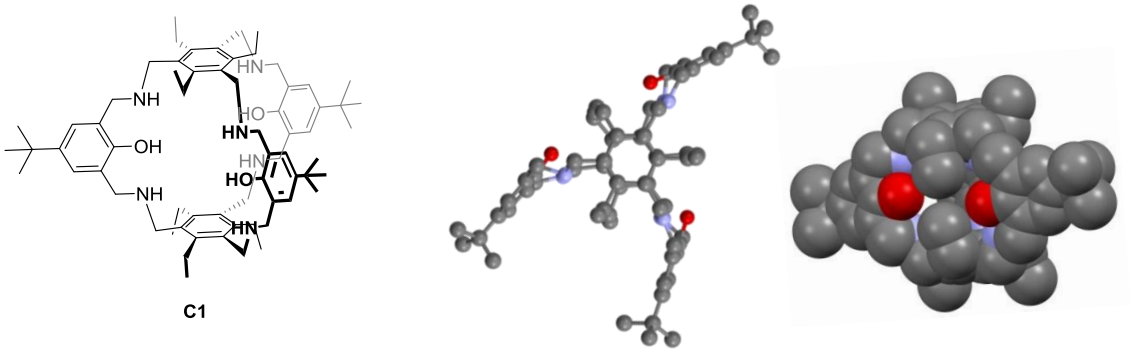

Figure 40: *(a)* ***C1****. (b) top view crystal structure. (c) Closed entrée shown in space filled model.*

Zn coordination was successful for **C1**. Coordination with $ZnCl_2$ led to coordination of 3-5 zinc-ions whereas $Zn(OAc)_2 \cdot 2\ H_2O$ leads to coordination of two zinc-ions. The structures of the complexes are not known.

To summarize, the three new designs that were investigated in this study, are a promising expansion to the field. They provide better understanding of these systems and open doors to new applications.

7. OUTLOOK

In this chapter are some ideas, which could improve the current results presented. In addition, a brief elaboration on possible applications of the cages is presented. The chapter will first focus on some general comments and is followed by specific remarks for each cage.

7.1 SOLUBILITY AND SYNTHESIS IN GENERAL

The poor solubility of compounds is a general issue in this work, which complicates analysis. Therefore, many compounds could not be identified. Analysis with additional techniques can elucidate their identify. Firstly, MALDI-TOF could be used for mass analysis. ESI-MS is in this work used as mass analysis technique. However, it is less sensitive for molecule masses above 1 kD as it has difficulty producing molecule ions. MALDI-TOF is far more sensitive for higher masses. It is commonly used for analysis of macromolecules and polymers. Mass could identify any formed clusters, [4+6]- cages and polymers. In addition, analysis of complexation would be improved. It could display compounds, which were hidden before. Secondly, size-exclusion chromatography (SEC) could be used. This technique provides a size distribution of mixtures of large molecules. It could provide a size separation of the compounds seen with DOSY-NMR and could shed light on any formed side products (e.g. see section 5.2.1). Note that it should the compounds should be soluble and tolerate the required conditions, e.g. air sensitive compound could not be analyzed with SEC. Finally, ^{13}C-MAS NMR is a variety of NMR operates with solid state compounds. In general, solid state NMR results in very broad signals due to orientation-dependent interactions. By spinning the sample with an angle of 54.74° are these interactions averaged and sharper signals are obtained. It could provide structural information of insoluble solids comparable as solution NMR does [27].

The gained knowledge on the solids could facilitate specific modifications based on their identity. A Change in reaction conditions could increase solubility if the desired products are insoluble, e.g. DMF could be used as solvent [15]. Other identities of the solids such as COFs or [4+6] cages could be an interesting side tracks to study, but will not be included in this outlook. However, polymers are undesired and their formation should be prevented as much as possible. The synthesis could be adapted to diminish polymerization. A low water content is proven to be essential for cage formation; drying agents favor cage formation. Other examples are synthesis under highly diluted conditions or slow addition of reactants. In our research was highly diluted conditions a standard with some exceptions. The use of a syringe pump is tested for **A** but could also be applied for further research in **B** and **C**. Besides, the use of templates could be considered as they can favor cage synthesis instead of polymerization (*See 1.4.1 Design*). A template must be matched to the diameter and functional groups of the cage. Moore *et al.* [77] demonstrated that the choice of functional groups can also be based on the template. Some templates will be mentioned for the specific cages. Lastly, building blocks could be simplified to study the coupling reaction before introducing complexity, which provides the possibility to create targeted solutions.

7.2 CAGE A

Besides the general remarks mentioned in 7.1, some specific ideas could benefit synthesis of cage **A**. Formation of **31** could be repeated in another solvent than DMF, which enables analysis and

[15] Note: DMF is difficult to remove, which is disadvantageous for analysis.

conclusions. In addition, solubility can be increased for the synthesis of cage **A** with introduction of alkyl chains. An example is provided in scheme 30. Hexyl groups are introduced on compound **12** to decrease the solubility issue. Therefore, the following reaction to form building **7'** might be successful in contrast to previous attempts. The alkyl groups also assist in later phases of synthesis by increasing solubility (in this case, formation of **31'** and cage **A'**).

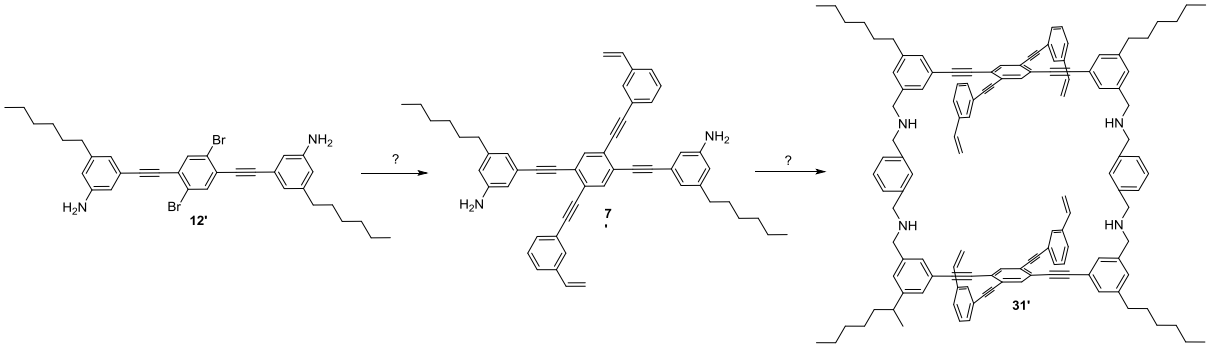

Scheme 30: *Introduction of alkyl chains to increase the solubility of compounds **12', 7'** and **31'**.*

The design of cage **A** as described in route II should be critically examined as it might be hindered due to a mismatch in bite angles. The cage is likely to have a distorted geometry (figure 41a).The stability of the cage is decreased, which might lead to collapse or prevent formation. The design could be modified to have better matching bite angles, and stimulate formation. Another cage design is proposed in figure 41b. The size of linkers is varied to better match the bite angles. The diaminophenol building block is commercially available (R = H or CH_3) or could be synthesized in a two-step synthesis shown in scheme 31 [78]. The inexpensive **59** is converted to **60** in a nitration reaction with 70% yield. Reduction with activated carbon leads to the desired building block **61**.

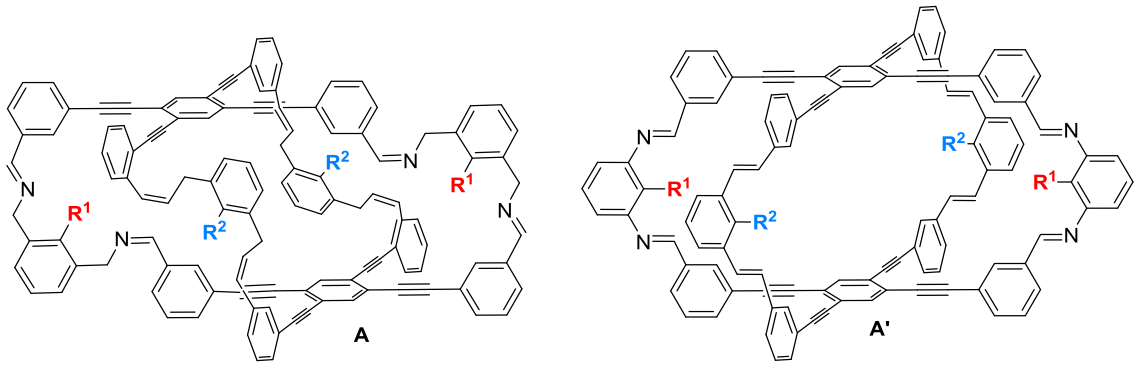

Figure 41: *(a) Representation of cage A (route II). (b) Modified cage design.*

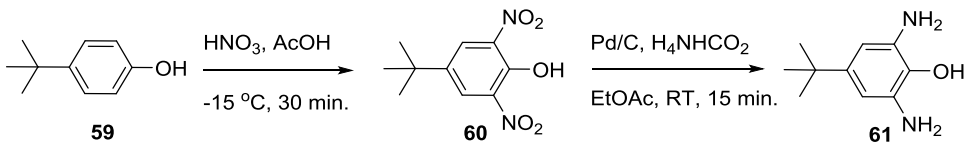

Scheme 31: *Synthesis scheme of **61**.*

Olefin building blocks should be synthesized if imine condensation succeeds (**9** and **18**). Building block **9** (R^2 = H) can be made from **24** and methyltriphenylphosphonium bromide via a Wittig reaction in a 75% yield [79] (scheme 32). The phenol analogue of **9** is also known in literature. The synthesis of building block **18** (R^2 = OH) is described in scheme 33. Esterification of **62** with an allyl chloride

generates **63**. The reaction mixture is heated to enable a Claisen rearrangement. **64** isomerizes to **18** to reform the aromaticity. The product can be formed in an overall yield of 68% as described by Lu *et al.* [80].

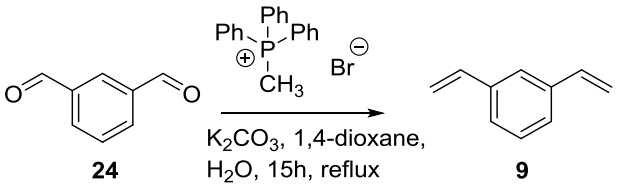

Scheme 32: *Formation of **9** via a Wittig reaction.*

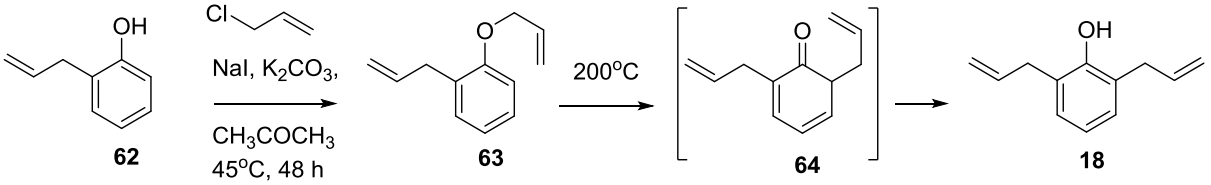

Scheme 33: *Formation of **18** via esterification and Claisen rearrangement.*

Cage **A** provides a large cavity and is therefore useful for various applications. For example, cage **A** could be exploited for recognition of large guests molecules, incorporation of nanoparticles [81] or coordination of multiple metal ions to enable co-operating catalytic centers. Interaction with guests molecules could be studied with DOSY-NMR as is described by Frisch et al. [82].

7.3 CAGE B

A few specific changes can be made for cage **B** to enable successful synthesis. First, S_N2 reactions should be examined in depth to make precise changes which could enable S_N2 reactions. For instance, dialkylation might cause a problem [66]. It should be investigated if it occurs and how to prevent it. In addition, cesium ions could be used as templates to pre-organize the reactants to facilitate a S_N2 reaction [14].

The synthesis or design of cage **B** could be altered to avoid S_N2 reactions. Side product **50** could be used to offer an alternative synthesis. The retrosynthetic analysis is shown in scheme 34. The first half is similar to the previous retrosynthesis on cage **B**. The amines in compound **41** are changed to phtalimides which act as protection group. Another FGI and C/N disconnection leads to building block **65** and **66**. A final FGI derives **50**. Translation of the retrosynthesis provides multiple reaction step synthesis. First, a basic oxidation of **50** followed by two reductive aminations. The phtalimide group can be removed by hydrazine. Note that the phtalimides are required to prevent intermolecular imine formation between molecules of **65**. This new synthesis plan could yield the desired heterosequenced cage **B**, although it requires numerous reaction steps. This synthesis route offers selectivity by stepwise exposure of the reactive groups while still using a single couplings reaction.

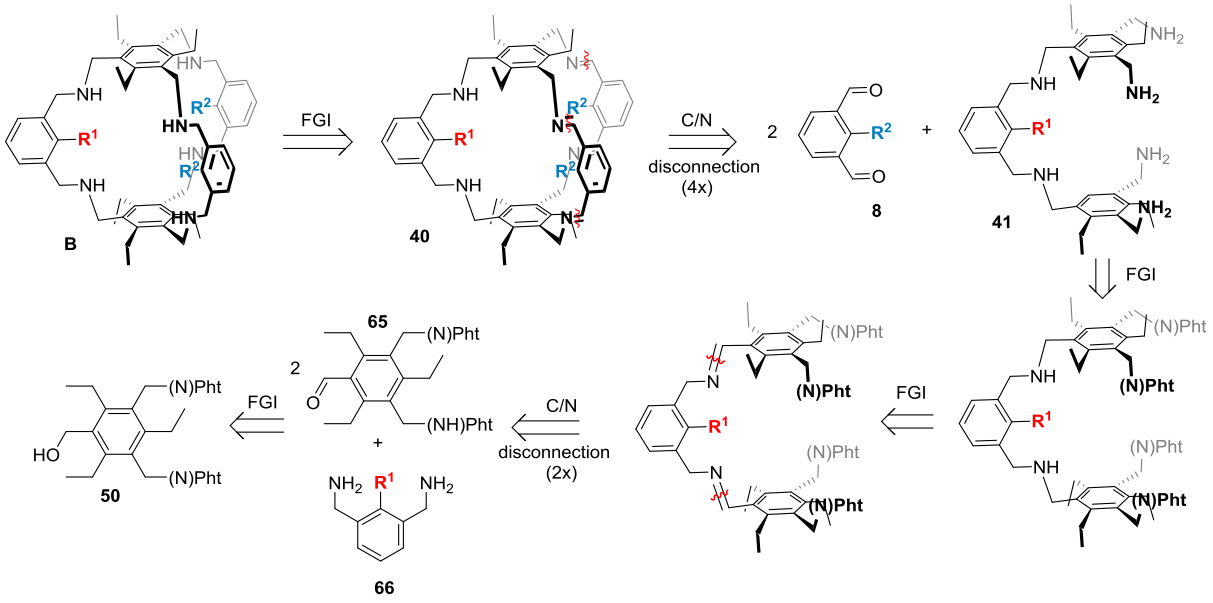

Scheme 34: *Alternative retrosynthesis for cage B.*

Other couplings reactions could also be used. We will only focus on coupling reactions involving amines, as then building block **43** could still be used. At first, amide formation could be used as initial reaction. Building block **43** could still be used as only the linker is exchanged to an acid or acid chloride. Any remaining acid should be completely removed as imine bonds are highly acid sensitive. The Strecker reaction could be another possibility in which an amine, imine and protected cyanide[16] form a new bond (scheme 35) [9,83]. Again **43** could still be used. The cyano group might provide additional interaction for metal ions or guests. In addition, chirality is created during the reaction which might allow chiral catalysis in a later phase.

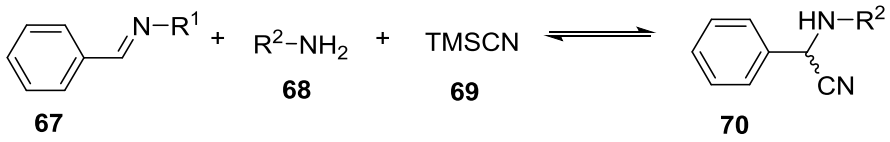

Scheme 35: *The schematic representation of a Strecker reaction.*

Cages similar as **B** have been found to be effective ion receptors. They show that both, H-donor and H-acceptor properties are achievable. The interior is provides mainly H-bond acceptor interactions, which enables cation recognition, whereas the protonated cage provides a H-bond donor environment ideal for anions [65,84]. Regulation of pH is essential for strong cage-guest interaction; a buffer might be beneficial. Successful synthesis of **B** opens the door to investigate specific ion interactions and other applications.

7.4 Cage C

The synthesis should be further optimized to prevent insoluble solids, especially for cage **C2**. The length of the imine condensation should be examined in addition to the general remark discussed before. Longer reaction times lead to inefficient synthesis and possibly more side products. An

[16] Note: TMSCN is highly toxic and should be handled with care.

attempt was made to follow the reaction with TLC. However, no clear conclusions could be drawn yet as insoluble compound will not show on TLC. Furthermore, **C2** might degrade due to the silica. 2D-TLC could test the amount of degradation as it makes the process visible.

Crystallization of cage **C2** or **C1** is proven to be difficult. Co-crystallization could facilitate crystal growth. The compound should contain hydrogen bond acceptors for interaction with phenols linkers. Some candidates could be triphenylphosphine oxide (TPPO), sulfoxides as DMSO or picrate. Picrate matches best in geometry, however the compound should be carefully handled as it is slightly explosive.

Numerous experiments are carried out on coordination chemistry of cages **C2** and **C1**. More data is required to prove metal ion coordination for all base metal ions in **C2** and elucidate the structures. Variations could be made in base (e.g. KHMDS [85], BnK [86] or KH [55]) or coordination method (e.g. use of $M(Mesityl)_x$ or $M(Alkyl)_x$ [55]. Furthermore, coordination chemistry on **C1** should be expanded as this reduced compound is more flexible and therefore soluble [87] than **C2**. The metal complexes of **C1** are also expected to be better soluble. Coordination is proven for our zinc systems. However, the complexes formed with $ZnCl_2$ do not have a defined amount of coordinated zinc ions (range of 3-5 ions). The quantity can be determined by the use of a JOBs plot or ICP-AES.

Catalysis with **C2** or **C1** is not proven up to now. Preliminary catalytic results of **C2** with $Fe(acac)_3$ should be confirmed. Thioanisole, is relative large due to its phenyl group. Smaller substrates might be easier to get in the interior as larger substrates might be distanced from the interior. Investigating the range of substrate could find size selectivity. The tested reaction, sulfoxidation, can take place without the catalyst which complicate the analysis. Other reactions could be tested such as epoxidation of cis-4-octene described by Bruijnincx and Klein Gebbink *et al.* [88] and C-H activation described by White *et al.* [89].

Fluorescence of **C2** is found by serendipity. It might be used in an application as chemosensor. Mukherjee *et al.* [90] describes a cage of similar size as cage **C** with could detect the explosive pyric acid. The sensor can be based on fluorescence on interaction or quenching of fluorescence on interaction. A chemosensor should be very selective to be of good quality. **C2** could be investigated with titration of specific molecules as explosives and drugs such as TNT or amphetamine. The difficulty for **C2** is the reaction with acid. Therefore, the pH should be carefully regulated possibly by a buffer. Quenching of fluorescence could be tested for low pH's and increase of fluorescence for high pHs.

8. EXPERIMENTAL SECTION

General

All chemicals were used as received unless stated otherwise. All reactions with possibly moisture sensitive compounds were carried out under a N_2 atmosphere, using glovebox and/or schlenkline-techniques. In addition, all moisture sensitive reagents and products were stored under a N_2 atmosphere. Solvents for air- or moisture sensitive reactions were dried by an MBRAUN MB SPS-79 system. The solvents were degassed by bubbling N_2 through solution for 30 min and eventual stored over molecular sieves (4Å) in the MB200B MBRAUN glovebox. The solvents MeOH and CH_2Cl_2 were further dried over CaH_2, degassed and distilled before use. NMR solvent CD_2Cl_2 was degassed by the freeze-pump-thaw procedure and dried over molsieves. All moisture sensitive NMR-samples were prepared under a N_2 atmosphere and transferred in a Young-type NMR tube for NMR analysis. All NMR spectra were recorded at 298 K on either an Agilent 400 MHz or a Varian 400MHz NMR spectrometer. Mass samples were prepared with CH_2Cl_2, MeCN and/or FA. Mass analysis was performed on a Waters LCT Premier XE KE317 Micromass Technologies spectrometer. Attenuated Total Reflectance (ATR) IR-spectroscopy was recorded on a Perkin Elmer Spectrum One FT-IR spectrometer. UV-VIS samples were made with CH_2Cl_2 and recorded at a Lambda 950 UV-VIS spectrometer. Photoluminescence measurements were performed with an Edinburgh Instruments FLS920 fluorescence spectrometer equipped with a 450 W Xenon lamp. Excitation and emission spectra were recorded using a double excitation monochromator with a grating blazed at 500 nm and a Hamamatsu R928 photomultiplier tube was used for detection. An excitation and emission slit width of 1.0 nm were used. Quantitative NMR was executed with Agilent 400 MHz with a relaxation time of 0.1 s and acquisition time = 0.1 s. DFT calculations were performed with Gaussian 09 with the B3LYP functional.

Synthesis of 1,4-dibromo-2,5-diiodobenzene (11)

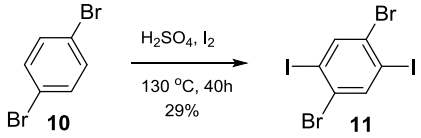

Synthesis is done according to literature [60]. 1,4-dibromobenzene **10** (9.82 g, 41.63 mmol) is added to sulfuric acid (125 mL). The mixture is stirred and heated to 60 °C under N_2 atmosphere. Iodine (23.14 g, 91.15 mmol) is added in small portions. The mixture is further heated to 130 °C. After two nights the mixture is cooled to room temperature and poured into ice water. Dichloromethane is used to extract (3 x 120 mL). The organic layer is washed with 2M NaOH-solution (2 x 75 mL). The solution is dried over $MgSO_4$ and evaporated. To the pinkish solvent is 150 mL 2M NaOH-solution added, mixed and filtrated. The white residue is dried under reduced pressure. The filtrate is also evaporated, yellow solid stays behind this is purified with recrystallization (Methanol/ CH_2CL_2, 1:1). Yield = 29% (5,86 g, 12,0 mmol). ^{1}H NMR (400 MHz, CD_2Cl_2, 25°C): δ/ppm 8.05 (s, 2H, Ar-H).

Synthesis of 3,3'-((2,5-dibromo-1,4-phenylene)bis(ethyne-2,1-diyl))dianiline (12)

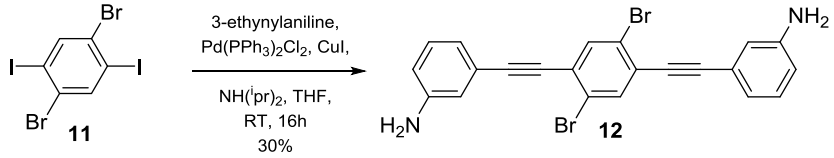

Synthesis is again based on similar literature [60,91]. **11** (0.487 g, 0.995 mmol) is dissolved in THF (5 mL) under N_2 atmosphere. Degassed $NH(^{i}pr)_2$ (3 mL), CuI (7.9 mg, 0.041 mmol), $PdCl_2(PPh_3)_2$ (6.7 mg, 0.00954 mmol) and 3-ethynylanaline (2,05 mL, 1.98 mmol) are added while stirring. A change from yellow solution to brown suspension is seen immediately after addition. The reaction mixture stirred over night. Subsequently, demiwater is added (6 mL). Extraction is done with EtOH (4 mL). The water layer is extracted with EtOH (2x 6 mL), dried over $MgSO_4$ and evaporated under reduced pressure. An extraction is done with eluent (40% PE, 60% EA, 1% NEt_3). The obtained brownish solid is poorly soluble. Yield = 30% (149.9 mg, 0.3 mmol). ^{1}H-NMR (400 Hz, CD_2Cl_2, 25°C): δ/ppm 7.80 (s, 1H, Ar-H), 7.17 (t, 2H, Ar-H, ^{3}J=7.84 Hz), 6.96 (d, 2H, Ar-H, ^{3}J =7.67 Hz), 6.89 (s, 2H, Ar-H), 6.73 (s, 2H, Ar-H, ^{3}J = 8.32 Hz), 3.82 (bs, 4H, NH_2). ^{13}C-NMR (400 Hz, CD_2Cl_2, 25°C): δ/ppm 146.84, 135.96, 129.38, 126.35, 123.59, 122.72, 121.68, 117.40, 116.00, 109.99, 96.94, 85.97 IR: 3467.74 cm^{-1}, 3375.13 cm^{-1}, 2209.75 cm^{-1}, 1616.85 cm^{-1}, 1595.19 cm^{-1}, 1574.98 cm^{-1}, 1494.55 cm^{-1}, 1441.39 cm^{-1}, 1356.51 cm^{-1}, 1305.14 cm^{-1}, 1054.71 cm^{-1}, 856.45 cm^{-1}, 775.21 cm^{-1}, 683.99 cm^{-1}. Exact mass ESI-MS: $C_{22}H_{14}Br_2N_2H$ calculated: 464.9602, found: 466.9581. $C_{22}H_{14}Br_2N_2H + CH_3CN$ calculated: 505.9868, found: 505.9863. $C_{22}H_{14}Br_2N_2H + CH_3CN + H_2O$ calculated: 523.9973, found: 523.9977.

Synthesis of 1-ethynyl-3-vinylbenzene (15)

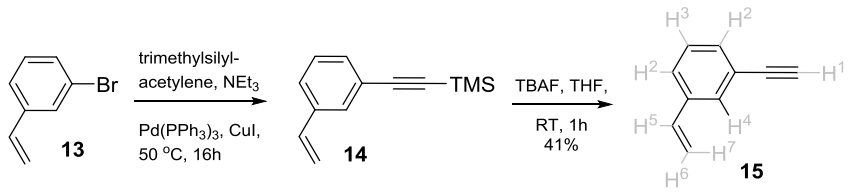

Synthesis is based on similar synthesis [92]. 3-bromostyrene **13** (1.56 mL, 11.98 mmol), trimethylsilylacetylene (3.92 mL, 27.74 mmol) and NEt_3 (50 mL) are added to a schlenk-flask under N_2 atmosphere. $PdCl_2(PPh_3)_2$ (0.842 g, 1.20 mmol) is added, shielded from light and heated to 50 °C. CuI (0.171 g, 0.897 mmol) is added to the mixture and left stirring overnight. After cooling down to RT is the mixture is filtrated with celite, washed with CH_2Cl_2 (150 mL) and evacuated. The mixture was solved again in THF (200 mL), TBAF (20 mL, 1 M) is added and mixture is stirred for 50 min. Next, THF is evaporated. Mixture is solved in CH_2Cl_2 (150 mL) and washed with water (3x 50 mL). The mixture is dried over $MgSO_4$ and evaporated. The black oil is columned with pentane (R_F = 0.67) , some CH_2Cl_2 was needed to bring it on the column. The **15** was obtained with a yield of 41% (625.1 mg, 4.88 mmol).^{1}H-NMR (400 Hz, CD_2Cl_2, 25°C): δ/ppm 7.54 (s, 1H, H^4), 7.39 (d, 2H, $^{3}J_{HH}$=7.32 Hz, H^2), 7.28 (t, 1H, ^{3}J=9.06, H^3), 6.68 (dd, 1H,, $^{3}J_{HH}$= 10.90 Hz, $^{3}J_{HH}$ = 17.67 Hz, H^5), 5.77 (d, 1H, $^{3}J_{HH}$ =17.61 Hz, H^6 or H^7), 5.29 (d, 1H, $^{3}J_{HH}$ =10.83 Hz, H^6 or H^7), 3.07 (s, 1H, H^1). ^{13}C-NMR (400 Hz, CD_2Cl_2, 25°C): δ/ppm 137.71, 135.90, 131.32, 129.87, 128.49, 126.63, 122.31, 114.84, 83.48.

Attempted Sonogashira to form 7: attempt 1

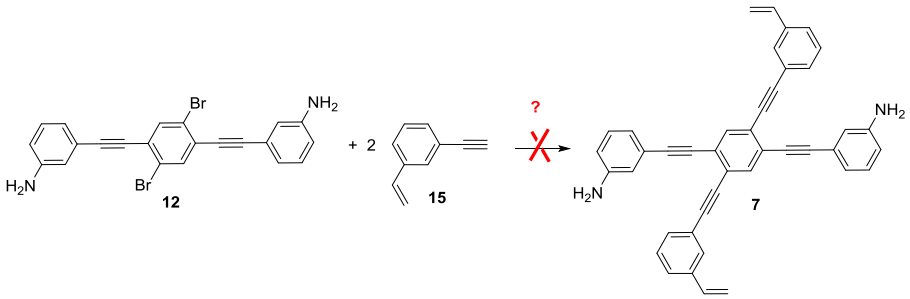

15 (102.4 mg, 0.516 mmol), **12** (68.3 mg, 0.147 mmol), $PdCl_2(PPh_3)_2$ (17.9 mg, 0.0255 mmol), CuI (54.9 mg, 0.288 mmol), NEt_3 (0,42 mL) and dry toluene (0,84 mL) are added to a schlenk under N_2 atmosphere. The reaction mixture is heated to 50 °C and left overnight. Subsequently, demiwater is added (6 mL) and EtOH (3x 6 mL) is used to extract. The mixture is dried over $MgSO_4$ and evaporated. Mixture is washed with pentane. The NMR spectra contains lots of peaks, most of them seem to correspond to start material. No new product seems to be formed.

Attempted Sonogashira to form 7: attempt 2

15 (85.5 mg, 0.426 mmol), **12** (71.4 mg, 0.153 mmol), dry toluene (5 mL), CuI (51.2 mg, 0.269 mmol), $Pd(PPh_3)_4$ (31.7 mg, 0.0274 mmol) and $NH(^{i}pr)_2$ (4.2 mL) are added to a schlenk under N_2 atmosphere and the reaction mixture is heated at 50 °C overnight. Demiwater is added (6 mL) and EtOH (3x 6 mL) is used to extract. The mixture is dried over $MgSO_4$ and solvent is reduced under reduced pressure. Same observations are seem with NMR.

Synthesis of N,N'-(1,3-phenylenebis(methylene))bis(1-phenylmethaneamine) (22)

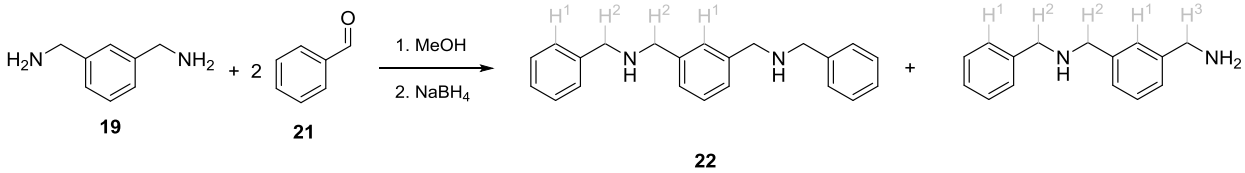

Benzaldehyde **21** is filtered over basic alumina. *m*-Xylylenediamine **19** (70.2 mg, 0.515 mmol) and **21** (106.5 mg, 1.00 mmol) are solved in dry MeOH and stirred for 17 h. The mixture is cooled in an ice bath. Subsequently, $NaBH_4$ is added (230.3 mg, 6.09 mmol), which resulted in gas formation. The ice bath is removed and mixture is stirred for an hour. An excess of demiwater is added dropwise. Extraction is done with CH_2CL_2 (3 x 50mL). Solvent is evaporated, slightly yellow solid remains (160 mg). Monosubstituted (M) and disubstituted (D) product (**22**) is found. ^{1}H-NMR (400 Hz, CD_2Cl_2, 25°C): δ/ppm 7.34 (m, 11.47H, H^1), 4.68 (s, 2.10H, H^2), 3.81 (s, 4.43H, H^3). ^{1}H-NMR (400 Hz, $CDCl_3$, 25°C): δ/ppm 7.44 (m, 9.15H, H^1), 4.70 (s, 2H, H^2), 3.82 (d, 3.15 H, $^{3}J_{HH}$ =10.44 Hz, H^3). ^{13}C-NMR (400 Hz, $CDCl_3$, 25°C): δ/ppm 141.09, 140.23, 140.02, 128.52, 128.46, 128.24, 128.05, 127.55, 127.05, 126.95, 65.14 (M), 53.14, 53.03. ESI-MS (CH_2CL_2/FA): m/z 227.1464 (M+H), 317.1921 (D+H), 633.3832 (2D+H). IR (Film): cm^{-1} 3085.87 (CH st), 3061.77 (CH st), 3027.48 (ar CH st), 2841.76 (NH st), 1452.30 (ar C-C), 1023.94 (CN st), 732.10 (ar C-H δ oop, *o*-di-substituted), 695.19 (ar C-H δ oop, mono-substituted) Experiment with borated $NaBH_4$ yielded in the imine version. ^{1}H-NMR (400 Hz, $CDCl_3$,

25°C): δ/ppm 8.40 (s, 2H, Ar-CH=N), 7.79 (d, 4H, $^3J_{HH}$ =6.12 Hz, Ar-H), 7.43 (m, 6H, Ar-H), 7.23 (m, 2H, Ar-H), 4.83 (s, 4H, N-CH_2-Ar). ESI-MS (CH_2CL_2/FA): 313.2343 m/z.

Synthesis of 1,1'-(pyridine-2,6-diyl)bis(N-benzylmethanamine) (23)

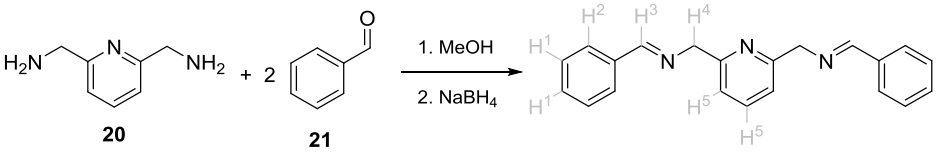

Compound **21** (37.6 mg, 0.35 mmol) is solved in dry CH_2CL_2 (11.65 mL) and MeOH (0.5 mL). Compound **20** (14.3 mg, 0.10 mmol) is added and stirred for 41.5 h. The mixture is cooled to 0 °C where after $NaBH_4$. Demiwater is added after an hour of stirring. The organic layer is evaporated and a brown oil is collected (98 mg). Analysis reveals a mixture of imine analogue of **23** and **21** (1:9). ^{1}H-NMR (400 Hz, $CDCl_3$, 25°C): δ/ppm 8.48 (s, 2H, H^3), 7.81 (m, 4H, $^3J_{HH}$ =7.53 Hz, H^2), 7.44 (t, 6H, $^3J_{HH}$ =5.08 Hz, H^1), 7.32 (m, 3H, $^3J_{HH}$ =7.62 Hz, H^5), 4.98 (s, 4H, H^4). ESI-MS (CH_2CL_2/FA): 314.1595 m/z (M+H), 627.3159 (2M+H). IR (Film): cm^{-1} 3060.93, 3028.31, 2819.77, 2735.13, 1699.50, 1644.58, 1574.86, 1453.66, 1202.77, 744.90, 688.76.

Synthesis of 3,7,11,15-tetraaza-1,5,9,13(1,3)-tetrabenzenacyclohexadecaphane (25)

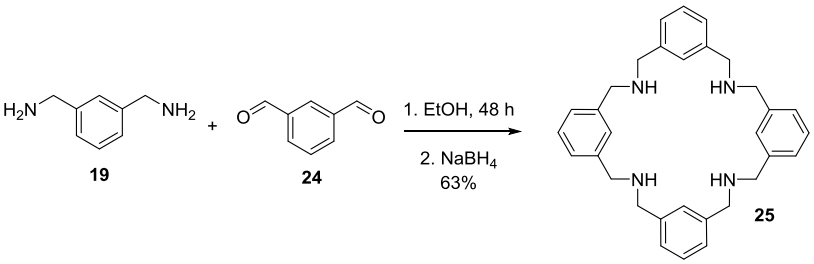

Synthesis according to literature [62]. Compound **19** (38.1 mg, 0.28 mmol) is dissolved in dry MeOH (5.3 mL). **24** (33.7 mg, 0.25 mmol) is dissolved dissolves in MeOH (5.3 mL). Both solutions are places in syringes and added to a flask under N_2 with MeOH (5.3 mL) with a speed of 0.13 mL/h and is additionally stirred for 48 hours. White solid forms over time. Dry toluene (10.6 mL) and THF (10.6 mL) are added. $NaBH_4$ (54.3 mg, 1.44 mmol) is added at 0 °C and stirred for 3 h. An excess of water is added dropwise. Mixture is extracted with CH_2CL_2 (3x50mL). Organic layer is washed with brine solution and dried with $MgSO_4$. Solvents are evaporated after filtration. White crystals quench out of solution. Yield = 63% (75 mg, 0.16 mmol). ^{1}H-NMR (400 Hz, CD_2Cl_2, 25°C): δ/ppm 7.25 (m, 16H, Ar-H), 3.79 (s, 16H, Ar-CH_2-N). ^{13}C-NMR (400 Hz, CD_2Cl_2, 25°C): δ/ppm 140.65, 128.09, 127.76, 126.80. ESI-MS (CH_2CL_2/FA): 239.1482 m/z ([1+1]+H), 477.2972 m/z ([2+2]+H)

Synthesis of building block 16

Building block **16** is synthesized by Dr. M. Otte in the *Organic Chemistry and Catalysis* research group at Utrecht University. Synthesis is discussed at p. 23.

Synthesis of pyridine-2,6-diyldimethanamine (20)

Via Gabriel synthesis attempt 1

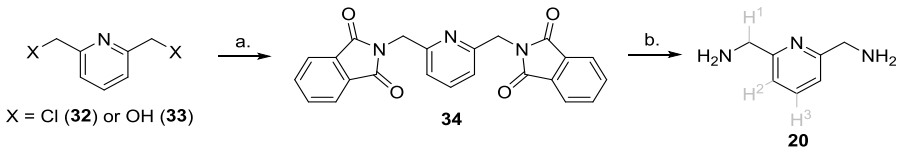

X = Cl (**32**) or OH (**33**) **34** **20**

The synthesis is based on literature [93]. Compound **32** (1.06 g, 6.0 mmol), phtalimide K salt (2.25 g, 12.16 mmol), K_2CO_3 (253.5 mg, 1,83 mmol) and DMF (24 mL) are heated to 140 ˚C in a schlenk flask. The mixture is stirred for 5 hours. The mixture is cooled to RT and stored in freezer overnight. Mixture is filtrated. The white residue is solved in 100 mL demiwater and extracted with CH_2CL_2. Organic layer is evaporated and white solid (2.36 g) is collected. Solid does not dissolve in DMSO or $CDCl_3$. Therefore, no analysis is done.

EtOH (35.5 mL) and $N_2H_4 \cdot H_2O$ (0,58 mL, 17,0 mmol) are added to the white solid (if pure: 2.36 g, 5,94 mmol). The mixture is refluxed for 14 hours. Where after, 50 mL of EtOH is added. Concentrated HCl is added (3.55 mL) and refluxed for 2h. The mixture is cooled to RT and filtered. The filtrate is evaporated, white solid remains. Subsequently, hot water (40 mL) is added to the mixture and filtrated. White solid is obtained (281 mg). **20** seems to be present. However, quite some impurities are seen and the concentration is low. Recrystallization is done (acetone : water = 1:1). Although in lesser concentration, impurities are still present. The total yield is 34% is the solid is assumed dry. ^{1}H-NMR (400 Hz, D_2O, 25°C): δ/ppm 7.92 (t, 1H, $^3J_{HH}$=7.92 Hz, H^3), 7.45 (d, 2H, $^3J_{HH}$=7.58 Hz, H^2), 4.40 (s, 4H, H^1).

Via Gabriel synthesis attempt 2

A similar synthesis is executed as the previous Gabriel synthesis [94]. **33** (817.9 mg, 5.88 mmol) and PPh_3 (3.16 g, 12,0 mmol) are solved in dry THF and cooled to 0 °C. Phtalimide (1.80 g, 12.2 mmol) is added followed by DEAD (2 mL, 12.7 mmol) drop wise. The ice bath is removed and the mixture is stirred for 21.5 h. A yellow suspension is formed. Solvents is evaporated, washed with CH_2CL_2 (50 mL). 2.35 g of white solid is obtained. The product is used without purification. Yield = 59% (1.40 g, 3.53 mmol). ^{1}H-NMR (400 Hz, $CDCl_3$, 25°C): δ/ppm 7.74 (m, 4H, phtalimide Ar-H), 7.70 (m, 4H, phtalimide Ar-H), 7.12 (d, 2H, $^3J_{HH}$=7.71 Hz, H^2), 4.93 (s, 4H, H^1).

All solid is suspended in EtOH (56.5 mL) and water (2.9 mL). Mixture is refluxed for 3.5 h. Solid slowly dissolves and later white solid precipitates again. Mixture is filtered. Filtrate is evaporated, and dissolved in $CHCl_3$. A pink solid is formed. Mixture is again filtered. The evaporated residue gives a pinkish oil (759.4 mg, product but impure). The first residue is dissolves in 40% KOH in water (50 mL). Extraction with CH_2CL_2 (2x50mL). Organic layer is evaporated. Yellow solid is formed. **20** is present, but large impurity present (product : derivative of DEAD = 2:1), which could not be separated so far. Yield = 9% (43.8 mg, 0.319 mmol) ^{1}H-NMR (400 Hz, DMSO, 25°C): δ/ppm 7.67 (t, 1H, $^3J_{HH}$=7.81 Hz, H^3), 7.23 (d, 2H, ^{3}J=7.56 Hz, H^2), 3.74 (s, 4H, H^1).

via azide compound attempt 1

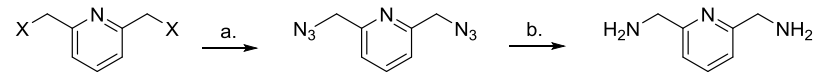

X = Cl (**32**) or Br (**35**) **36** **20**

Synthesis of **36** is done according to a literature procedure [95]. 18-crown-6 (148 mg, 6.80 mmol), tetrabutylammonium bromide (170.0 mg, 0.53 mmol) and **32** (885.0 mg, 5.03 mmol) are used. Yield = 75% (709 mg, 3.75 mmol). ^{1}H NMR (400 MHz, $CDCl_3$, 25°C): δ/ppm 7.75 (t, $^3J_{HH}$ = 7.7 Hz, 1H, H^3), 7.30 (d, $^3J_{HH}$ = 7.7 Hz, 2H, H^2), 4.48 (s, 4H, H^1). ^{13}C NMR (101 MHz, $CDCl_3$, 25°C): δ/ppm 155.86 (N-**C**=C-C), 138.01 (N-C=C-**C**), 121.07 (N-C=**C**-C), 55.38 (CH_2).

The reduction of **36** is also based on literature [63]. A static hydrogen atmosphere is achieved by freezing a EtOH solution of **36** with liquid nitrogen, remove air with vacuum, fill with H_2 and let warm up to RT. It is calculated 8,5 mmol H_2 is present in the reaction. An orange oil is obtained (621.1 mg). The oil solves poorly when a NMR sample is made with $CDCl_3$ or CD_2Cl_2. Yield = 47% (243.5 mg, 1.775 mmol). ^{1}H-NMR (400 Hz, $CDCl_3$, 25°C): δ/ppm 7.60 (t, 1H, $^3J_{HH}$ =7.65 Hz, H^3), 7.13 (d, 2H, $^3J_{HH}$ =7.65 Hz, H^2), 3.96 (s, 4H, H^1). ^{1}H-NMR (400 Hz, D_2O, 25°C): δ/ppm 7.98 (t, 1H, $^3J_{HH}$ =7.61 Hz, H^3), 7.47 (d, 2H, $^3J_{HH}$ =7.90 Hz, H^2), 4.07 (s, 4H, H^1).

Via azide compound attempt 2

The *s*ynthesis is described by Raymond *et al.* [96]. An yellow oil is obtained. Yield = 93% (334.1 mg, 1.77 mmol). ^{1}H NMR (400 MHz, $CDCl_3$, 25°C): δ/ppm 7.76 (t, $^3J_{HH}$ = 9.0, 6.8 Hz, 1H, H^3), 7.31 (d, $^3J_{HH}$ = 7.7 Hz, 2H, H^2), 4.49 (s, 4H, H^1).

Staudinger reduction of **36** with PPh_3 and water is based on literature [97]. NMR data does not match the values from the article, but matches the previous experiment. Yield = 47% (114.0 mg, 0.83 mmol). ^{1}H-NMR (400 Hz, $CDCl_3$, 25°C): δ/ppm 7.61 (t, 1H, $^3J_{HH}$ =7.64 Hz, H^3), 7.13 (d, 2H, $^3J_{HH}$ =7.54 Hz, H^2), 3.96 (s, 4H, H^1).

Synthesis of (2,4,6-triethylbenzene-1,3,5-triyl)trimethanamine (43).

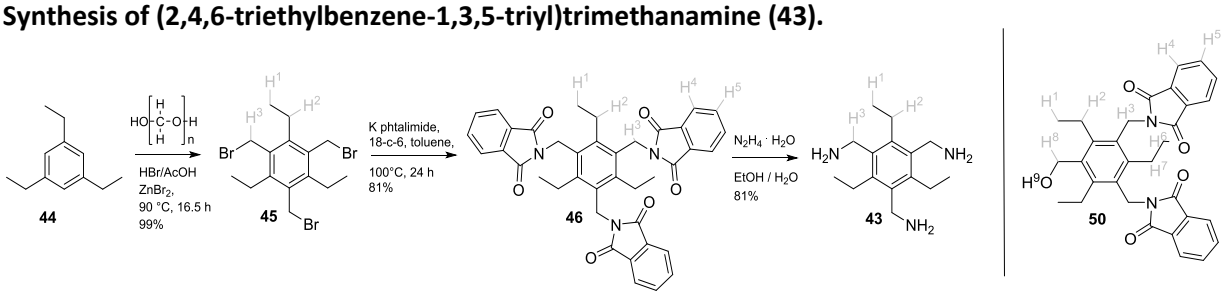

44 **45** **46** **43** **50**

The synthesis of **45** is done according to literature [98]. Yield = 99% (13.06 g, 29.6 mmol). ^{1}H NMR (400 MHz, $CDCl_3$, 25°C): δ/ppm 4.58 (s, 6H, H^3), 2.94 (q, $^3J_{HH}$ = 7.6 Hz, 6H, H^2), 1.34 (t, $^3J_{HH}$ = 7.6 Hz, 9H, H^1). ^{13}C NMR (101 MHz, $CDCl_3$, 25°C) δ/ppm 144.98 (Ar), 132.63 (Ar), 28.53 (**C**H_2-Br), 22.73 (**C**H_2-CH_3), 15.60 (CH_2-**C**H_3).

Synthesis of **46** is also done according to literature [99]. Purification with column chromatography with acetone:CH_2Cl_2 = 1:20 (R_F = 0.67). Yield = 81% (15.38 g, 24.0 mmol). ^{1}H NMR (400 MHz, $CDCl_3$, 25°C): δ/ppm 7.80 (dd, $^3J_{HH}$ = 5.4, 3.0 Hz, 6H, H^4 or H^5), 7.68 (dd, $^3J_{HH}$ = 5.5, 3.0 Hz, 6H, H^4 or H^5), 4.94 (s, 6H, H^3), 3.10 (q, $^3J_{HH}$ = 7.5 Hz, 6H, H^2), 0.96 (t, $^3J_{HH}$ = 7.5 Hz, 9H, H^1). Compound **50** is found as side product

(15-20%). Separation with column chromatography with acetone:CH_2Cl_2 = 1:20 (R_F = 0.23). ^{1}H NMR (400 MHz, $CDCl_3$, 25°C): δ/ppm 7.74 (dd, $^3J_{HH}$ = 5.4, 2.6, 1.4 Hz, 4H, phtalimide Ar-**H**), 7.65 (dd, $^3J_{HH}$ = 5.5, 3.1 Hz, 4H, H^4 or H^5), 4.91 (s, 4H, H^3), 4.72 (d, $^3J_{HH}$ = 4.0 Hz, 2H, H^8), 3.12 (q, $^3J_{HH}$ = 7.5 Hz, 2H, H^7), 2.95 (q, $^3J_{HH}$ = 7.5 Hz, 4H, H^2), 1.38 (t, $^3J_{HH}$ = 4.0 Hz, 1H, H^9),1.08 (t, $^3J_{HH}$ = 7.5 Hz, 6H, H^6), 0.95 (t, $^3J_{HH}$ = 7.5 Hz, 9H, H^1). ^{13}C NMR (101 MHz, $CDCl_3$, 25°C): δ/ppm 168.21 (**C**=O), 145.73 (**C**-CH_2-OH), 144.68, 134.73, 133.94, 131.91, 129.52, 123.17, 58.92 (**C**H_2-OH), 37.37 (**C**-N(Pht)), 23.34 (Ar-**C**H_2-CH_3), 22.89 (Ar-**C**H_2-CH_3), 16.32 (Ar-CH_2-**C**H_3), 15.82 (Ar-CH_2-**C**H_3).

Synthesis **43** done according to literature [99]. Yield = 81% (4.86 g, 19.5 mmol). ^{1}H NMR (400 MHz, $CDCl_3$, 25°C): δ/ppm 3.87 (s, 6H, H^3), 2.82 (q, $^3J_{HH}$ = 7.5 Hz, 6H, H^2), 1.23 (t, $^3J_{HH}$ = 7.5 Hz, 9H, H^1).

Synthesis of cage B X=H, Y=H

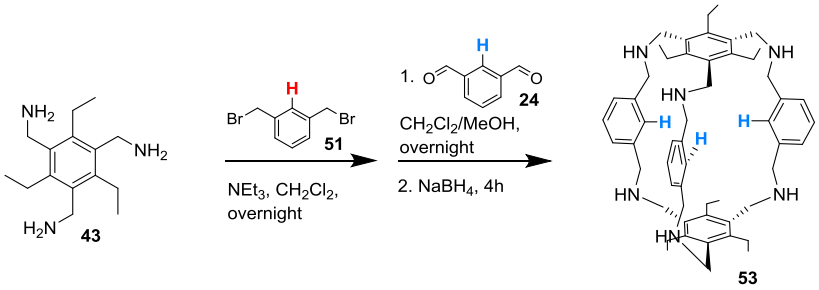

51 (52.9 mg, 0.20 mmol) in CH_2CL_2 (0.5 mL) is added to **43** (109.9 mg, 0.44 mmol) and NEt_3 (0.6 mL) in CH_2CL_2 (2.5 mL) and is stirred overnight. **24** (56.8 mg, 0.42 mmol) in CH_2CL_2 (1.0 mL) is added and mixture is again stirred overnight. $NaBH_4$ (186.8 mg, 4.94 mmol) is added at 0 °C. After two hours, the mixture is quenched with an excess of demiwater. Extraction with CH_2CL_2 (3x50mL) is done. After evaporation a off white solid remains (227.9 mg). Analysis revealed **53** is synthesized, but not completely pure, yield could not be determined. ^{1}H-NMR (400 Hz, $CDCl_3$, 25°C): δ/ppm 7.32 (s, 3H, Ar-H), 7.19 (d, 3H, Ar-H), 7.09 (d, 6H, Ar-H), 3.95 (s, 12H, Ar-CH_2-N), 3.81 (s, 12H, Ar-CH_2-N), 2.52 (q, 12H, Ar-CH_2-CH_3), 1.12 (t, 18H, CH_3). ESI-MS (CH_2CL_2/FA): 403.2995 m/z (M+2H), 805.5995 m/z (M+H)

Synthesis of cage B X=H, Y=Br

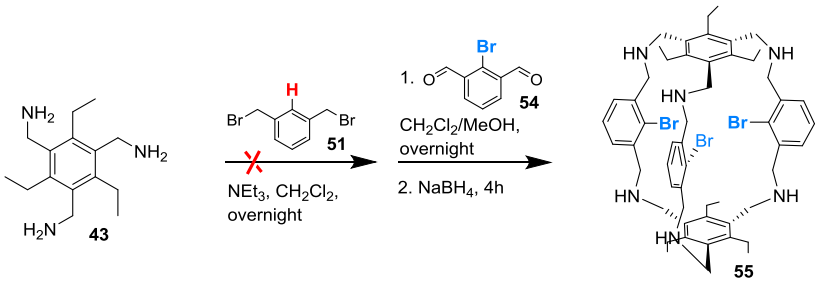

43 (110.2 mg, 0.44 mmol) is solved in CH_2CL_2 (5mL). NEt_3 is added. Solution is **51** (53.2 mg, 0.20 mmol) and NEt_3 (0.6 mL) in CH_2CL_2 (5 mL) is slowly added and stirred over the weekend. 2-**54** (89.3 mg, 0.42 mmol) is dissolves in MeOH (2 mL) and CH_2CL_2 (3 mL) and added drop wise. Mixture is left stirring overnight. $NaBH_4$ (196.8 mg, 5.20 mmol) is added at 0 °C. After three hours, the mixture is quenched with an excess of demiwater (20 mL). Brine (5 mL) is added. Extraction with CH_2CL_2 (3x50mL) is done. After evaporation, a white solid remains (351.2 mg). Analysis reveals tribromide

cage **55** is formed. ^{1}H-NMR (400 Hz, $CDCl_3$, 25°C): δ/ppm 7.24 (d, Ar-H), 7.17 (t/q, Ar-H), 3.81 (s, Ar-CH_2-N), 3.76 (s, Ar-CH_2-N), 2.79 (d, Ar-CH_2-CH_3), 2.56 (d, Ar-CH_2-CH_3). 1.19 (t, CH_3), 1.11 (t, CH_3), 1.05 (t, CH_3). ESI-MS (CH_2CL_2/FA): 520.1645 m/z (M+2H), 1039.3212 m/z (M+H)

Synthesis of C2

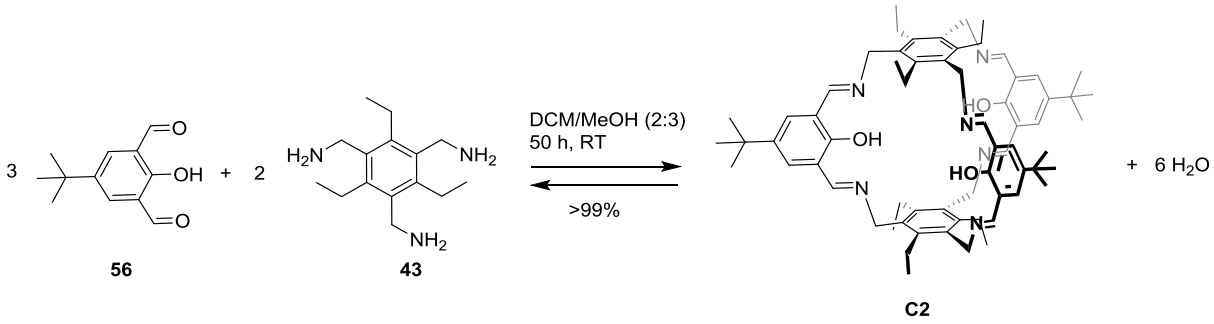

56 **43** **C2**

43 (249.0 mg, 1.00 mmol) is dissolved in dry CH_2CL_2 (20mL) and MeOH (30 mL). **56** (308.3 mg, 1.49 mmol) is added to the mixture is stirred for 50 h. The color turns slightly darker. Solvent is evaporated and yellow solid remains. Yield is quantitative (505 mg, 0.50 mmol). Some trapped water is not taken into account. ^{1}H-NMR (400 Hz, $CDCl_3$, 25°C): δ/ppm 8.41 (s, 6H, CH_2-CH=N), 7.69 (s, 6H, Ar-H), 4.91 (s, 12H, Ar-CH_2-N), 2.51 (q, 12H, $^{3}J_{HH}$ = 7.4 Hz, Ar-CH_2-CH_3), 1.33 (s, 27H, tBu), 1.17 (t, 18H, $^{3}J_{HH}$ = 7.5 Hz, CH_3). ^{13}C-NMR (400 Hz, $CDCl_3$, 25°C): δ/ppm 160.09 (Ar-C=N), 158.40 (Ar(C)-OH), 143.40 (Ar(C)-^{t}Bu), 140.71 (Ar(C)-CH_2N), 132.71 (Ar(C)-CH_2CH_3), 128.45 (Ar(C)), 121.25 (Ar(C)-CHN), 55.45 (Ar-C-N), 34.12 (Ar-**C**$(CH_3)_3$) 31.34 (C-C(**C**$H_3)_3$, 23.10 (Ar-**C**H_2-CH_3), 15.77 (Ar-CH_2-**C**H_3). ESI-MS (CH_2CL_2/FA): 337.2271 m/z ($[M+3H]^{3+}$), 505.3415 m/z ($[M+2H]^{2+}$), 1009.6683 m/z ($[M+H]^{+}$). IR (cm^{-1}) 2962.63 (s), 2905.31 (m), 1631.11 (m), 1456.45 (m), 1259.12 (s), 1085.11 (s), 1014.38 (s), 793.14 (s). UV-VIS (nm): 285.91, 347.02, 464.27.

An excess of formic acid is added. ^{1}H-NMR (400 Hz, $CDCl_3$, 25°C): δ/ppm 7.82 (s, 6H, CH_2-CH=N), 7.75 (s, 6H, Ar-H), 5.02 (s, 12H, Ar-CH_2-N), 2.69 (q, 12H, $^{3}J_{HH}$ = 7.4 Hz, Ar-CH_2-CH_3), 1.27 (s, 27H, tBu), 1.11 (t, 18H, $^{3}J_{HH}$ = 7.4 Hz, CH_3). UV-VIS (nm): 289, 335, 450.

Preparation samples for optical properties measurements of C2

C2 (15.0 mg, 0.0149 mmol) is dissolved in CH_2Cl_2 (10 mL), which is 40x diluted to obtain a good absorption (M=3.7175 · 10^{-5}). 2.5 mL is used for each measurement. FA (60.5 mg, 1.31 mmol) is dissolved in CH2Cl2 (7.05 mL). One equivalent is equal to 0.05 mL of solution. 0 to 600 eq is measured. A large difference is seen (see data). Solution is diluted 10x to include 10 to 90 equivalents measurements. All samples are mixed with a pipette. NEt_3 (31.2 mg, 0.308 mmol) is dissolved in CH_2Cl_2 (1.65 mL). 100 eq is equal to 0.05 mL. To the 600 eq sample is 0 to 600 eq base added. While adding base the color turns from yellow to colorless, where the dissolved cage had already a yellow color. Results are shown in *5.2.2 Optical properties of **C2***.

Coordinationexperiment of C2 and $FeCl_3$

C2 (50.0 mg, 0.050 mmol), $FeCl_3$ (25.6 mg, 0.16 mmol), NEt_3 (47.1 mg, 0.47 mmol) and MeOH (20 mL) are heated to 60 °C and stirred for 18h. Dark brown/green suspension is separated with canula filtration. Filtrate is evaporated, solves poorly in common organic solvents. Does not solve in common organic solvents with slight solubility in trichlorobenzene as exception. IR (cm^{-1}): 2934.74 (m), 2822.85 (m), 1650.80 (m), 1531.43 (m), 1460.71 (m), 1034.98 (s), 478.31 (m).

Coordinationexperiment of C2 and $Fe(OTf)_2 \cdot 2MeCN$

C2 (52.4 mg, 0.052 mmol), $Fe(OTf)_2 \cdot 2$ MeCN (21.9 mg, 0,05 mmol or 65.55 mg, 0,15 mmol), NEt_3 (47.2 mg, 0.47 mmol) and MeOH (15 mL) are heated to 60 °C and stirred for 18h. Dark brown suspension is separated with canula filtration. Filtrate is evaporated, solves poorly in common organic solvents. Does not solve in common organic solvents with slight solubility in trichlorobenzene as exception. IR is made of residue. IR (cm^{-1}): 2960.88 (s), 1625.28 (s) 1545.86 (m), 1449.86 (s), 1363.86 (m), 1273.67 (m), 1243.26 (s), 1222.77 (m), 1029.65 (m), 638.19 (m), 523.72 (b).

Coordinationexperiment of C2 and $Co(OAc)_2 \cdot 4\ H_2O$

C2 (49.2 mg, 0.049 mmol), is dissolved in 10 mL dry MeOH (10 mL) resulting in a bright yellow suspention. $Co(OAc)_2 \cdot 4\ H_2O$ (75.5 mg, 0.303 mmol) is solved in dry MeOH (10 mL), which gives a bright pink color. Addition of the $Co(OAc)_2 \cdot 4\ H_2O$ solution results in a brown/green suspension. The mixture is stirred for 18h. The mixture is evaporated. The solid does not solve in common organic solvents. Analysis cannot be done with NMR. ESI-MS (CD_3CN) gives around 50 peaks, only major are gives: m/z 233.2012, 374.3620, 389.2937, 727.2137, 822.1634, 836.1762, 909.1935. IR (cm^{-1}): 2961.59 (m), 1557.07 (m), 1635.30 (s), 1409.48 (s), 1336.85 (m), 1223.91 (m), 1021.69 (m), 665.94 (m), 615.01.

Coordinationexperiment of C2 and $Cu(OAc)_2$

The experiments are based on literature [100]**. C2** (47.3 mg, 0.047 mmol), is dissolved in 10 mL dry MeOH (10 mL) resulting in a bright yellow suspention. $Cu(OAc)_2$ (54.6 mg, 0.301 mmol) is solved in dry MeOH (10 mL), which gives a bright blue color. Addition of the $Cu(OAc)_2$ solution results in a green suspension. Additional MeOH (10 mL) is added. The mixture is stirred for 20h. The mixture is separated with canula filtration and the filtrate is evaporated. Reaction is also executed on 60 °C and with 3 instead of 6 equivalent $Cu(OAc)_2$. Only relevant data will be shown below.

RT, 1:6; ^{1}H-NMR (400 Hz, MeCN-d4, 25°C): δ/ppm 12.60 (bs), 2.56 (bs), -0.38 (bs). IR(cm^{-1}): 3370.56 (b), 2960.42 (m), 1713.10 (m), 1574.84 (s), 1580.51 (s), 1410.87 (s), 1384.17 (m), 1241.95 (m), 1027.92 (m), 680.05 (m), 621.10 (m).

60 °C, 1:6; IR filtrate (cm^{-1}): 3366.76 (m), 2964.64 (m), 1598.82 (s), 1421.21 (s).

60 °C, 1:3; Paramagnetisch ^{1}H-NMR (400 Hz, MeCN-d4, 25°C, range -500-500, relaxation delay = 0.1 s, acquisition time = 0.1 s): δ/ppm 23.57, 22.37, 20.95, 19.91. ESI-MS (CD_3CN): m/z 389.3155, 602.3556, 1009.7244, 1254.7487, 1286.7678, 1324.7104, 1385.7214. IR filtrate (cm^{-1}):2962.41 (m), 1567.77 (s), 1394.61 (s), 1044.65 (m). IR residue (cm^{-1}): 2961.64 (m), 1622.99 (s), 1453.17 (m), 1393.83 (m), 1244.67 (m), 1043.15 (m).

Coordinationexperiment of C2 and CuCl2

Experiment is based on literature [101]. **C2** (29.7 mg, 0.029 mmol), is dissolved in 20 mL dry MeOH (20 mL) resulting in a bright yellow suspension. $CuCl_2$ (12.1 mg, 0.09 mmol) is solved in dry MeOH (5 mL), which gives a light green color. Addition of the $CuCl_2$ solution results in a dark green suspension. NEt_3 (0.279 mmol) is added. The mixture is heated to 60 °C and stirred for 18h. The mixture is separated with canula filtration and the filtrate is evaporated. IR filtrate (cm^{-1}): 2949.93 (s), 2601.48 (s), 2495.94

(s), 1638.67 (s), 1474.63 (s), 1396.96 (s), 1172.08 (m), 1035.74 (s). IR residue (cm^{-1}): 2961.81 (s), 1630.67 (s), 1557.80 (m), 1454.62 (s), 1078.21 (m).

Coordinationexperiment of C2 and CuCl

C2 (30.0 mg, 0.030 mmol), is dissolved in 20 mL dry MeOH (20 mL) resulting in a bright yellow suspension. CuCl (9.4 mg, 0.09 mmol) and NEt_3 (0.279 mmol) are added to the mixture. The mixture is heated to 60 °C and stirred for 18h. The mixture is separated with canula filtration and the filtrate is evaporated. IR filtrate (cm^{-1}): 2949.95 (s), 2603.94 (s), 2497.67 (s), 1626.92 (s), 1540.09 (m), 1475.11 (s), 1397.24 (s), 1172.54 (m), 1036.60 (s). IR residue (cm^{-1}): 2960.53 (s), 1622.35 (s), 1538.38 (m), 1451.45 (s), 1363.07 (m), 1243.94 (m), 1041.64 (m).

Coordinationexperiment of C2 and $Zn(OAc)_2 \cdot 2H_2O$

Possibly polymerized cage (50.9 mg, 0.05 mmol if pure), $Zn(OAc)_2 \cdot 2H_2O$ (60.4 mg, 0.33 mmol) and dry MeOH (20 mL) are stirred for 65 h at RT. Mixture is concentrated and dry CH_2CL_2 (40 mL) is added. Stirred for 22 h. Yellow solid is separated with canula filtration. Filtrate is evaporated, yellow solid remains. ^{1}H-NMR (400 Hz, $CDCl_3$, 25°C): δ/ppm 8.58 (m, CH_2-CH=N), 7.76 (m, Ar-H), 5.02 (m, Ar-CH_2-N), 2.77 (m, Ar-CH_2-CH_3), 1.37 (m, tBu), 1.27 (m, CH_3). ESI-MS (CH_2CL_2): m/z 669.1898, 1183.3846, 1328.3821, 1341.4772, 1368.4801, 1449.4205, 1491.4365, 1553.4025, 1601.4630

Coordinationexperiment of C2 and $ZnCl_2$

C2 (52.0 mg, 0.050 mmol), $ZnCl_2$ (20.5 mg, 0.15 mmol), NEt_3 (47.0 mg, 0.465 mmol) and dry MeOH (30 mL) are heated to 60 °C and stirred for 18h. Mixture is evaporated and yellow solid remains. Solid quenches out of solution in NMR tube after a while, therefore no ^{13}C-NMR can be taken. ^{1}H-NMR (400 Hz, CD_2Cl_2, 25°C): δ/ppm 8.43 (m, CH_2-CH=N), 7.69 (m, Ar-H), 5.00 (m, Ar-CH_2-N), 2.67 (m, Ar-CH_2-CH_3), 1.38 (m, tBu), 1.16 (m, CH_3). ESI-MS (CH_2CL_2): m/z 1339.3342, 1357.3020, 1496.3964.

Catalysis testing of C2

C2 (20.2 mg, 0.02 mmol) is weighted. Solution of $Fe(acac)_3$ (7.1 mg, 0.02 mmol) in CH_2CL_2 (0.7 mL) is added and mixture is stirred for 15 min. Toluic acid (1.0 mg, 0.073 mmol) is dissolved in CH_2CL_2 and added to the mixture. Thioanisole (0.12 mL, 1.00 mmol) and 35wt% H_2O_2 (0.10 mL, 1.20 mmol) are also added to the suspension and stirred for 21h. All solvent is evaporated and solved in a solution of 1,4-dimethoxybenzene (5.9 mg, 0.043 mmol) in $CDCl_3$(1.2 mL). Notes: Variations of the experiment are made by elimination of toluic acid, C2 and/or $Fe(acac)_3$. First experiments are done in CD_2CL_2 in a NMR-tube. Last experiments are filtered through a silica filter to remove iron for GC. Unfortunately, some iron remains present in the mixtures, probably in the form of $Fe(acac)_3$. Methyl(phenyl)sulfane: ^{1}H-NMR (400 Hz, $CDCl_3$, 25°C): δ/ppm 7.35-7.26 (m, 4H), 7.16 (tt, $^3J_{HH}$ =6.2, 1.8, 1H) 2.49 (s, 3H). (Methylsulfinyl)benzene: ^{1}H-NMR (400 Hz, $CDCl_3$, 25°C): δ/ppm 7.72-7.65 (m, 2H), 7.62-7.51 (m, 3H), 2.73 (s, 3H).

Synthesis of C1

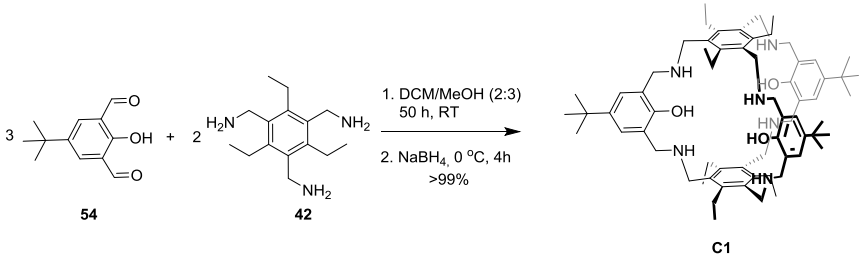

43 (254.3 mg, 1.02 mmol) is dissolved in dry CH_2CL_2 (20mL) and MeOH (30 mL). **54** (309.6 mg, 1.50 mmol) is added to the mixture is stirred for 50 h. The color turns slightly darker. The mixture is cooled with an ice bath, $NaBH_4$ (252.7 mg, 6.68 mmol) is added and stirred for 4 h. Mixture is quenched with demiwater. Extraction with CH_2CL_2 (3x50mL) is done. Solvent is evaporated and white solid remains. Yield is quantitative (509 mg, 0,498 mmol). Some trapped water is not taken into account. ^{1}H-NMR (400 Hz, $CDCl_3$, 25°C): δ/ppm 6.98 (s, 6H, Ar-H), 3.83 (s, 12H, Ar-CH_2-N), 3.75 (s, 12H, Ar-CH_2-N), 2.73 (q, 12H, $^3J_{HH}$ = 7.4 Hz, Ar-CH_2-CH_3), 1.29 (s, 27H, tBu), 1.22 (t, 18H, $^3J_{HH}$ = 7.5 Hz, CH_3). ^{13}C-NMR (400 Hz, $CDCl_3$, 25°C): δ/ppm 153.21 (Ar(C)-OH), 142.59 (Ar(C)-CH_2CH_3), 141.19 (Ar(C)-^{t}Bu), 133.64 (Ar(C)-CH_2N), 125.29 (Ar(C)), 125.19 (Ar(C)-CH_2N), 53.35 (Ar-C-N), 47.85 (Ar-C-N), 33.91 (Ar-**C**$(CH_3)_3$) 31.61 (C- C(**C**$H_3)_3$, 22.90 (Ar-**C**H_2-CH_3), 16.89 (Ar-CH_2-**C**H_3). ESI-MS (CH_2CL_2/FA): 341.2542 m/z ($[M+3H]^{3+}$), 511.3835 m/z ($[M+2H]^{2+}$), 1021.7803 m/z ($[M+H]^+$). IR (cm^{-1}) 2956.70 (s), 2868.25 (s), 1609.25, 1482.73 (s), 1451.70 (m), 1492.80, 1361.45 (m), 1299.35, 1259.90, 1213.75 (m), 1073.04 (m), 997.85, 875.47 (m), 820.21, 730.46 (m).

Coordinationexperiment of C1 and $Zn(OAc)_2$

C1 (98.2 mg, 0.096 mmol) is dissolved in dry MeOH (5 mL). $Zn(OAc)_2 \cdot 2\ H_2O$ (139.2 mg, 0.63 mmol) is dissolved in MeOH (5 mL) and added to the cage solution, a light-yellow solution occurs. The mixture is stirred overnight on RT. Solvent is evaporated and the solid is washed with hexane (10 mL). ^{1}H-NMR (400 Hz, CD_2Cl_2, 25°C): δ/ppm 8.18 (s), 7.28-7.01 (m), 4.82-3.21 (m), 2.96 (m), 2.80 (m), 2.01 (s), 1.28 (s), 1.06 (t), 0.96 (t), 0.84 (s),0.71 (t). ^{13}C-NMR (400 Hz, CD_2Cl_2, 25°C): δ/ppm 186.05, 180.07, 179.94, 164.94, 161.57, 159.14, 156.05, 153.72, 147.72, 146.75, 146.03, 144.97, 144.10, 141.52, 138.87, 134.12, 132.83, 130.99, 129.63, 129.11, 128.10, 127.24, 127.02, 125.89, 125.49, 122.79, 122.58, 120.08, 117.74, 65.61, 48.80, 46.96, 45.81, 45.31, 44.04, 33.92, 33.85, 33.78, 33.64, 31.46, 31.30, 31.18, 23.24, 22.75, 21.57, 17.01, 16.37, 16.01, 15.82, 15.36, 15.05, 13.83, 0.72. ESI-MS (CH_2CL_2): m/z 1297.6182, 1311.6254, 1323.6415, 1357.6259, 1449.1459.

Coordinationexperiment of C1 and $ZnCl_2$

C1 (50.9 mg, 0.050 mmol), $ZnCl_2$ (0.05 mmol or 0.15 mmol), NEt_3 (0.155 mmol or 0.465 mmol) and dry MeOH (15 mL) are heated to 60 °C and stirred for 18h. Solvent is evaporated, a light yellow remains. ^{1}H-NMR (400 Hz, CD_2Cl_2, 25°C): δ/ppm 7.21 (m), 7.06 (m), 4.95-2.55 (m), 0.89 (t), 0.83 (m). ESI-MS (CH_2CL_2): m/z 470.1732, 510.1790, 578.2977, 1021.7540, 1377.4276, 1385.4540,

ACKNOWLEDGEMENTS

First, I would like to thank **Prof. Dr. Bert Klein Gebbink** for allowing me to do a project at OCC and stepping in as supervisor during the last months. I am grateful for the critical input and multiple new insights your provided during the work discussions. Then, I would like to thank **Dr. Marc-Etienne Moret** for the advice and input during work discussions and for being my second supervisor. Your door was always open if I had questions, which is highly appreciated.

I would like to thank **Dr. Matthias Otte** for his daily supervision. Thank you for your time, discussions about organic chemistry and guidance during lab work. I enjoyed the time in the lab and our conversations about the important matters in life such as movies, politics and the latest news.

Thank you **Johan**, **Henk** and **Jord** for the technical support during my stay. I valued that I could ask anything and the nice coffee breaks. The same holds for **Adri**.

In addition, I would like to thank **Léon** for the DFT calculations and, in combination with **Dide**, for answering questions when Matthias was unavailable

Thanks to **CMI** for the possibility to measure photoluminescence of **C2**.

I would like to thank the whole **OCC group** for the nice time I had and the open environment. I enjoyed the coffee breaks, UMC lunches, etc. I like to specially mention the members of the "Secret meeting group" - **Martine**, **Desmond** and **Tom** - , the members of the "Fumehood social group" - **Richard** and **Marc -** , **Cecilia**, **Laura** and **Laurens**.

Finally, I would like to thank my family and friend for their support with particularly mentioning **Nico**.

REFERENCES

[1] J. Lehn, *Science* **2002**, *295*, 2400–2403.

[2] R. W. Saalfrank, H. Maid, A. Scheurer, *Angew. Chem. Int. Ed.* **2008**, *47*, 8795–8824.

[3] J.-M. Lehn, *Angew. Chem. Int. Ed.* **1990**, *29*, 1304–1319.

[4] M. Albrecht, *Naturwissenschaften* **2007**, *94*, 951–966.

[5] C. Seel, F. Vogtle, *Angew. Chem. Int. Ed.* **1992**, *31*, 528–549.

[6] E. Mattia, S. Otto, *Nat. Nanotechnol.* **2015**, *10*, 111–119.

[7] S. I. Stupp, L. C. Palmer, *Chem. Mater.* **2014**, *26*, 507–518.

[8] M. J. Wiester, P. A. Ulmann, C. A. Mirkin, *Angew. Chem. Int. Ed.* **2011**, *50*, 114–137.

[9] Y. Jin, C. Yu, R. J. Denman, W. Zhang, *Chem. Soc. Rev.* **2013**, *42*, 6634–6654.

[10] A. D. Jenkins, P. Kratochvíl, R. F. T. Stepto, U. W. Suter, *Pure Appl. Chem.* **1996**, *68*, 2287–2311.

[11] A. S. Shetty, J. Zhang, J. S. Moore, *J. Am. Chem. Soc.* **1996**, *118*, 1019–1027.

[12] M. B. Dewal, M. W. Lufaso, A. D. Hughes, S. A. Samuel, P. Pellechia, L. S. Shimizu, *Chem. Mater.* **2006**, *18*, 4855–4864.

[13] D. Zhao, J. S. Moore, *J. Org. Chem.* **2002**, *67*, 3548–3554.

[14] G. Zhang, M. Mastalerz, *Chem. Soc. Rev.* **2014**, *43*, 1934–1947.

[15] S. Höger, *Chemistry* **2004**, *10*, 1320–1329.

[16] M. Iyoda, J. Yamakawa, M. J. Rahman, *Angew. Chem. Int. Ed.* **2011**, *50*, 10522–10553.

[17] A. B. Vliegenthart, F. a. L. Welling, M. Roemelt, R. J. M. Klein Gebbink, M. Otte, *Org. Lett.* **2015**, *17*, 4172–4175.

[18] X. Feng, X. Ding, D. Jiang, *Chem. Soc. Rev.* **2012**, *41*, 6010–6022.

[19] S.-Y. Ding, W. Wang, *Chem. Soc. Rev.* **2013**, *42*, 548–568.

[20] Z. Lin, J. Sun, B. Efremovska, R. Warmuth, *Chem. - A Eur. J.* **2012**, *18*, 12864–12872.

[21] G. Alibrandi, V. Amendola, G. Bergamaschi, L. Fabbrizzi, M. Licchelli, *Org. Biomol. Chem.* **2015**, *13*, 3510–3524.

[22] M. Arunachalam, I. Ravikumar, P. Ghosh, *J. Org. Chem.* **2008**, *73*, 9144–9147.

[23] C. Schouwey, R. Scopelliti, K. Severin, *Chem. - A Eur. J.* **2013**, *19*, 6274–6281.

[24] T. Tozawa, J. T. a Jones, S. I. Swamy, S. Jiang, D. J. Adams, S. Shakespeare, R. Clowes, D. Bradshaw, T. Hasell, S. Y. Chong, et al., *Nat. Mater.* **2009**, *8*, 973–978.

[25] J. R. Holst, A. Trewin, A. I. Cooper, *Nat. Chem.* **2010**, *2*, 915–920.

[26] J. Tian, P. K. Thallapally, S. J. Dalgarno, P. B. McGrail, J. L. Atwood, *Angew. Chem. Int. Ed.* **2009**, *48*, 5492–5495.

[27] M. W. Schneider, H.-J. Siegfried Hauswald, R. Stoll, M. Mastalerz, *Chem. Commun.* **2012**, *48*, 9861–9863.

[28] S. Enthaler, K. Junge, M. Beller, *Angew. Chem. Int. Ed.* **2008**, *47*, 3317–3321.

[29] M. Yoshizawa, J. K. Klosterman, M. Fujita, *Angew. Chem. Int. Ed.* **2009**, *48*, 3418–3438.

[30] M. Otte, *ACS Catal.* **2016**, *6*, 6491–6510.

[31] B. Chatelet, V. Dufaud, J. P. Dutasta, A. Martinez, *J. Org. Chem.* **2014**, *79*, 8684–8688.

[32] B. Chatelet, L. Joucla, J. P. Dutasta, A. Martinez, V. Dufaud, *Chem. - A Eur. J.* **2014**, *20*, 8571–8574.

[33] D. M. Ermert, L. J. Murray, *Dalt. Trans.* **2016**, *78*, 701–722.

[34] L. J. Murray, W. W. Weare, J. Shearer, A. D. Mitchell, K. A. Abboud, *J. Am. Chem. Soc.* **2014**, *136*, 13502–13505.

[35] D. M. Ermert, J. B. Gordon, K. A. Abboud, L. J. Murray, *Inorg. Chem.* **2015**, *54*, 9282–9289.

[36] Y. Lee, F. T. Sloane, G. Blondin, K. A. Abboud, R. García-Serres, L. J. Murray, *Angew. Chem. Int. Ed.* **2015**, *54*, 1499–1503.

[37] Y. Lee, K. J. Anderton, F. T. Sloane, D. M. Ermert, K. A. Abboud, R. García-Serres, L. J. Murray, *J. Am. Chem. Soc.* **2015**, *137*, 10610–10617.

[38] D. M. Ermert, I. Ghiviriga, V. J. Catalano, J. Shearer, L. J. Murray, *Angew. Chem. Int. Ed.* **2015**, *54*, 7047–7050.

[39] M. Mastalerz, *Angew. Chem. Int. Ed.* **2010**, *49*, 5042–5053.

[40] Y. Jin, Q. Wang, P. Taynton, W. Zhang, *Acc. Chem. Res.* **2014**, *47*, 1575–1586.

[41] S. Klotzbach, F. Beuerle, *Angew. Chem. Int. Ed.* **2015**, *54*, 10356 –10360.

[42] J. Janczak, D. Prochowicz, J. Lewiński, D. Fairen-Jimenez, T. Bereta, J. Lisowski, *Chem. - A Eur. J.* **2016**, *22*, 598–609.

[43] F. Diederich, P. J. Stang, *Templated Organic Synthesis*, Wiley-VCH Verlag GmbH, Weinheim, **2000**.

[44] T. Fiehn, R. Goddard, R. W. Seidel, S. Kubik, *Chem. - A Eur. J.* **2010**, *16*, 7241–7255.

[45] M. W. Schneider, I. M. Oppel, A. Griffin, M. Mastalerz, *Angew. Chem. Int. Ed.* **2013**, *52*, 3611–3615.

[46] O. Francesconi, A. Ienco, G. Moneti, C. Nativi, S. Roelens, *Angew. Chem. Int. Ed.* **2006**, *45*, 6693–6696.

[47] G. Ambrosi, P. Dapporto, M. Formica, V. Fusi, L. Giorgi, A. Guerri, M. Micheloni, P. Paoli, R. Pontellini, P. Rossi, *Inorg. Chem.* **2006**, *45*, 304–314.

[48] S. L. Schreiber, *Science* **2000**, *287*, 1964–1969.

[49] K. D. Okochi, G. S. Han, I. M. Aldridge, Y. Liu, W. Zhang, *Org. Lett.* **2013**, *15*, 4296–4299.

[50] K. D. Okochi, Y. Jin, W. Zhang, *Chem. Commun.* **2013**, *49*, 4418–4420.

[51] P. Skowronek, B. Warżajtis, U. Rychlewska, J. Gawroński, *Chem. Commun.* **2013**, *49*, 2524–2526.

[52] P. Pfeiffer, E. Breith, E. Lübbe, T. Tsumaki, *Justus Liebigs Ann. Chem.* **1933**, *503*, 84–130.

[53] A. Decortes, A. M. Castilla, A. W. Kleij, *Angew. Chem. Int. Ed.* **2010**, *49*, 9822–9837.

[54] C. Baleiza, *Chem. Rev.* **2006**, *106*, 3987–4043.

[55] P. G. Cozzi, *Chem. Soc. Rev.* **2004**, *33*, 410–421.

[56] K. C. Gupta, A. K. Sutar, *Coord. Chem. Rev.* **2008**, *252*, 1420–1450.

[57] S. Shaw, J. D. White, *Synthesis* **2016**, *48*, 2768–2780.

[58] N. S. Venkataramanan, G. Kuppuraj, S. Rajagopal, *Coord. Chem. Rev.* **2005**, *249*, 1249–1268.

[59] D. E. F. Hisashi Ōkawa, Hideki Furutachi, *Coord. Chem. Rev.* **1998**, *174*, 51–75.

[60] M. Modjewski, S. V. Lindeman, R. Rathore, *Org. Lett.* **2009**, *11*, 4656–4659.

[61] T. E. Müller, M. Beller, *Chem. Rev.* **1998**, *98*, 675–704.

[62] P. Rajakumar, R. Padmanabhan, *Tetrahedron Lett.* **2010**, *51*, 1059–1063.

[63] S. Ouizem, D. Rosario-Amorin, D. A. Dickie, R. T. Paine, A. de Bettencourt-Dias, B. P. Hay, J. Podair, L. H. Delmau, *Dalt. Trans.* **2014**, *43*, 8368–8386.

[64] O. Francesconi, M. Gentili, S. Roelens, *J. Org. Chem.* **2012**, *77*, 7548–7554.

[65] P. Mateus, R. Delgado, P. Brandão, S. Carvalho, V. Félix, *Org. Biomol. Chem.* **2009**, *7*, 4661–4673.

[66] A. F. Abdel-Magid, K. G. Carson, B. D. Harris, C. A. Maryanoff, R. D. Shah, *J. Org. Chem.* **1996**, *61*, 3849–3862.

[67] H. Ding, Y. Yang, B. Li, F. Pan, G. Zhu, M. Zeller, D. Yuan, C. Wang, *Chem. Commun.* **2015**, *51*, 1976–1979.

[68] Z. Rozwadowski, T. Dziembowska, G. Schroeder, B. Brzezinski, *J. Mol. Struct.* **1998**, *444*, 221–225.

[69] G. L. Guillet, J. B. Gordon, G. N. Di Francesco, M. W. Calkins, E. Čižmár, K. A. Abboud, M. W. Meisel, R. García-Serres, L. J. Murray, *Inorg. Chem.* **2015**, *54*, 2691–2704.

[70] K. J. Gallagher, R. Webster, *Chem. Commun.* **2014**, *50*, 12109–12111.

[71] SDBS, "Spectral Database for Organic Compounds," can be found under http://sdbs.db.aist.go.jp/sdbs/cgi-bin/direct_frame_disp.cgi?sdbsno=41080, **n.d.**

[72] R. N. Mukherjee, a J. Abrahamson, G. S. Patterson, T. D. P. Stack, R. H. Holm, *Inorg. Chem.* **1988**, *27*, 2137–2144.

[73] M. Pervaiz, M. Yousaf, M. Sagir, M. Mushtaq, M. Y. Naz, S. Ullah, R. Mushtaq, in *Synth. React. Inorganic, Met. Nano-Metal Chem.*, **2013**, pp. 546–552.

[74] E. Pretsch, P. Bühlmann, M. Badertscher, *Structure Determination of Organic Compounds - Tables of Spectral Data*, Springer-Verlag Berlin, Heidelberg, **2009**.

[75] S. Mukherjee, T. Weyhermüller, E. Bothe, K. Wieghardt, P. Chaudhuri, *Eur. J. Inorg. Chem.* **2003**, 863–875.

[76] J. Legros, C. Bolm, *Angew. Chem. Int. Ed.* **2004**, *43*, 4225–4228.

[77] D. Zhao, J. S. Moore, *Chem. Commun.* **2003**, 807–818.

[78] J. Rojo, J. Lehn, G. Baum, D. Fenske, O. Waldmann, P. Müller, *Structure* **1999**, 517–522.

[79] R. Gauler, N. Risch, *European J. Org. Chem.* **1998**, *1998*, 1193–1200.

[80] J. P. Shi, D. L. Wu, Y. Ding, D. H. Wu, H. W. Hu, G. Y. Lu, *Tetrahedron* **2012**, *68*, 2770–2777.

[81] B. Mondal, K. Acharyya, P. Howlader, P. S. Mukherjee, *J. Am. Chem. Soc.* **2016**, *138*, 1709–1716.

[82] Y. Cohen, L. Avram, L. Frish, *Angew. Chem. Int. Ed.* **2005**, *44*, 520–554.

[83] P. Vongvilai, O. Ramström, *J. Am. Chem. Soc.* **2009**, *131*, 14419–14425.

[84] S. Kubik, in *TripleC*, **2013**, pp. 13–35.

[85] G. L. Guillet, F. T. Sloane, M. F. Dumont, K. A. Abboud, L. J. Murray, *Dalt. Trans.* **2012**, *41*, 7866–7869.

[86] G. L. Guillet, F. T. Sloane, D. M. Ermert, M. W. Calkins, M. K. Peprah, E. S. Knowles, E. Čižmár, K. A. Abboud, M. W. Meisel, L. J. Murray, *Chem. Commun.* **2013**, *49*, 6635–6637.

[87] M. Mastalerz, *Chem. Commun.* **2008**, 4756–4758.

[88] P. Spannring, V. Yazerski, P. C. A. Bruijnincx, B. M. Weckhuysen, R. J. M. Klein Gebbink, *Chem. - A Eur. J.* **2013**, *19*, 15012–15018.

[89] M. S. Chen, M. C. White, *Science* **2010**, *327*, 566–572.

[90] K. Acharyya, P. S. Mukherjee, *Chem. Commun.* **2014**, *50*, 15788–15791.

[91] M. C. Martos-Maldonado, I. Quesada-Soriano, J. M. Casas-Solvas, L. García-Fuentes, A. Vargas-Berenguel, *European J. Org. Chem.* **2012**, 2560–2571.

[92] J. D. Megiatto, Jr., D. I. Schuster, *New J. Chem.* **2010**, *34*, 276–286.

[93] G. Lee, M. Oka, H. Takemura, Y. Miyahara, N. Shimizu, T. Inazu, *J. Org. Chem.* **1996**, *61*, 8304–8306.

[94] N. Komine, R. W. Buell, C. H. Chen, A. K. Hui, M. Pink, K. G. Caulton, *Inorg. Chem.* **2014**, *53*, 1361–1369.

[95] W. S. Brotherton, P. M. Guha, H. Phan, R. J. Clark, M. Shatruk, L. Zhu, *Dalt. Trans.* **2011**, *40*, 3655–3665.

[96] X. You, Z. Wei, *Inorganica Chim. Acta* **2014**, *423*, 332–339.

[97] M. Sawicki, D. Lecerclé, G. Grillon, B. Le Gall, A. L. Sérandour, J. L. Poncy, T. Bailly, R. Burgada, M. Lecouvey, V. Challeix, et al., *Eur. J. Med. Chem.* **2008**, *43*, 2768–2777.

[98] A. Vacca, C. Nativi, M. Cacciarini, R. Pergoli, S. Roelens, *J. Am. Chem. Soc.* **2004**, *126*, 16456–16465.

[99] M. Mazik, A. Hartmann, P. G. Jones, *European J. Org. Chem.* **2010**, *3*, 458–463.

[100] J. U. Ahmad, M. T. Räisänen, M. Kemell, M. J. Heikkilä, M. Leskelä, T. Repo, *Appl. Catal. A Gen.* **2012**, *449*, 153–162.

[101] S. E. Balaghi, E. Safaei, M. Rafiee, M. H. Kowsari, *Polyhedron* **2012**, *47*, 94–103.

[102] D. Luo, X. P. Zhou, D. Li, *Angew. Chem. Int. Ed.* **2015**, *54*, 6190–6195.

APPENDICES

APPENDIX A

^{1}H-NMR spectrum of **12** (400 Hz, CD_2Cl_2, 25°C)

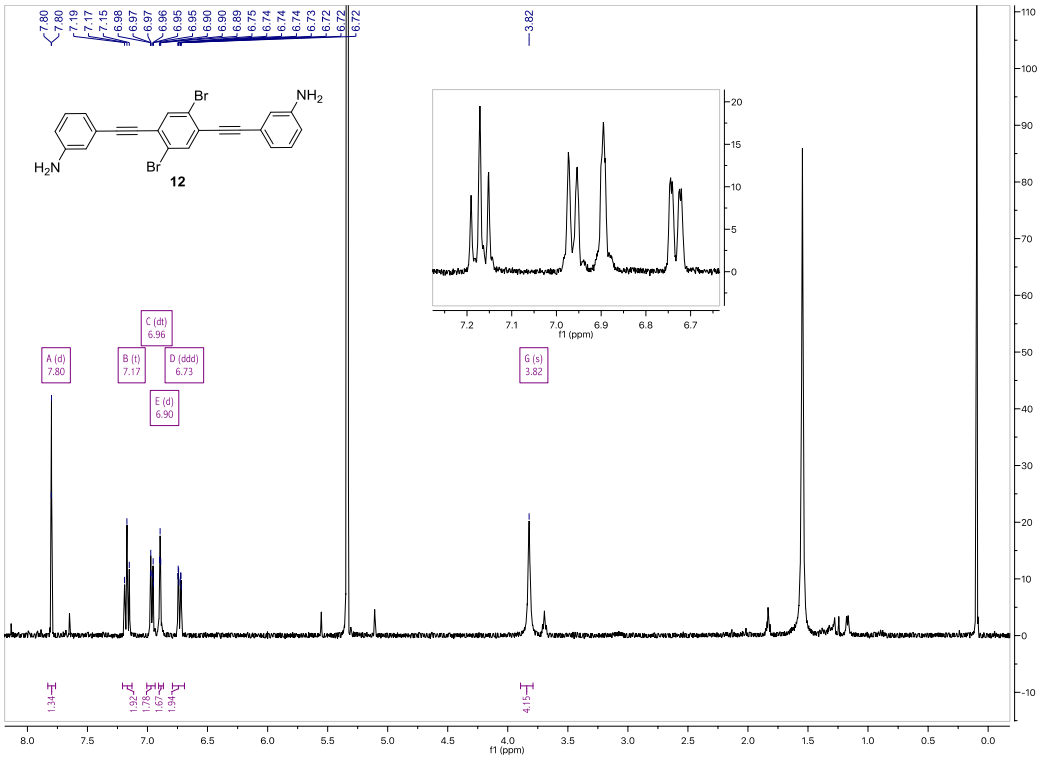

^{13}C NMR spectrum of **12** (100 Hz, CD_2Cl_2, 25°C)

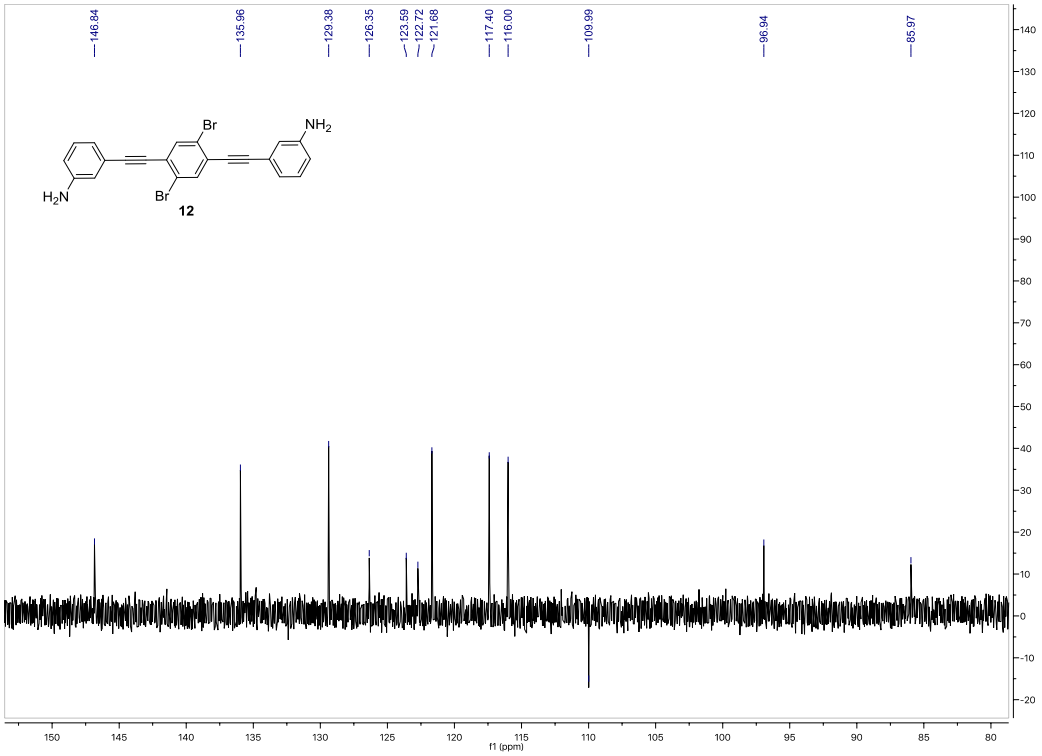

^{1}H-NMR SPECTRUM OF **15** (400 Hz, CD_2CL_2, 25°C)

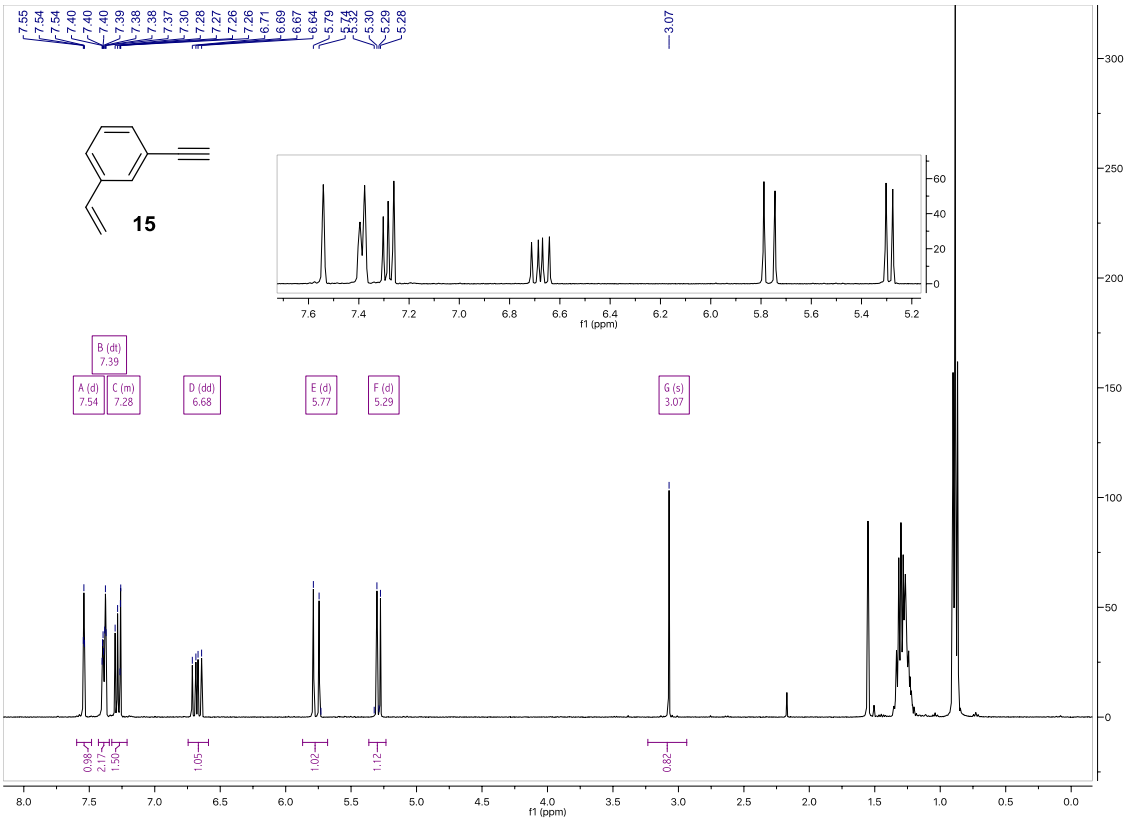

^{13}C-NMR SPECTRUM OF **15** (100 Hz, CD_2CL_2, 25°C)

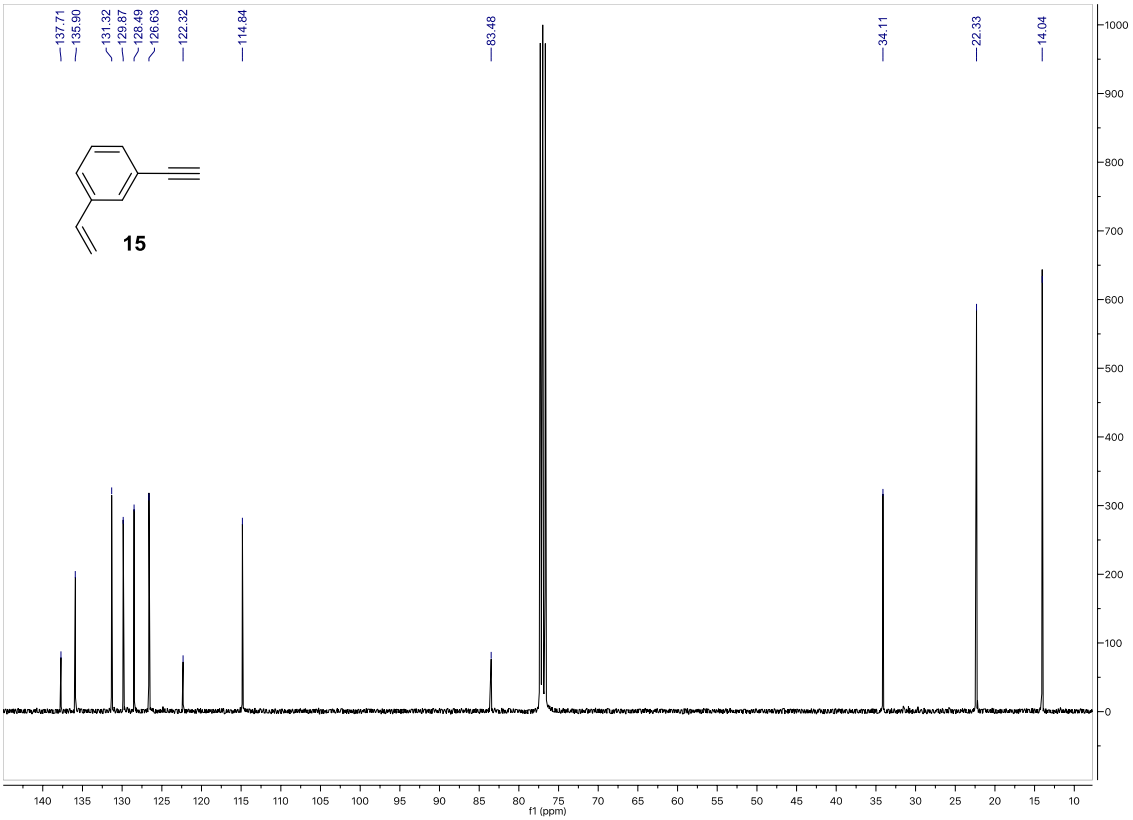

APPENDIX B

^{1}H-NMR spectrum of imine analogue of **22** (400 Hz, CD_2Cl_2, 25°C)

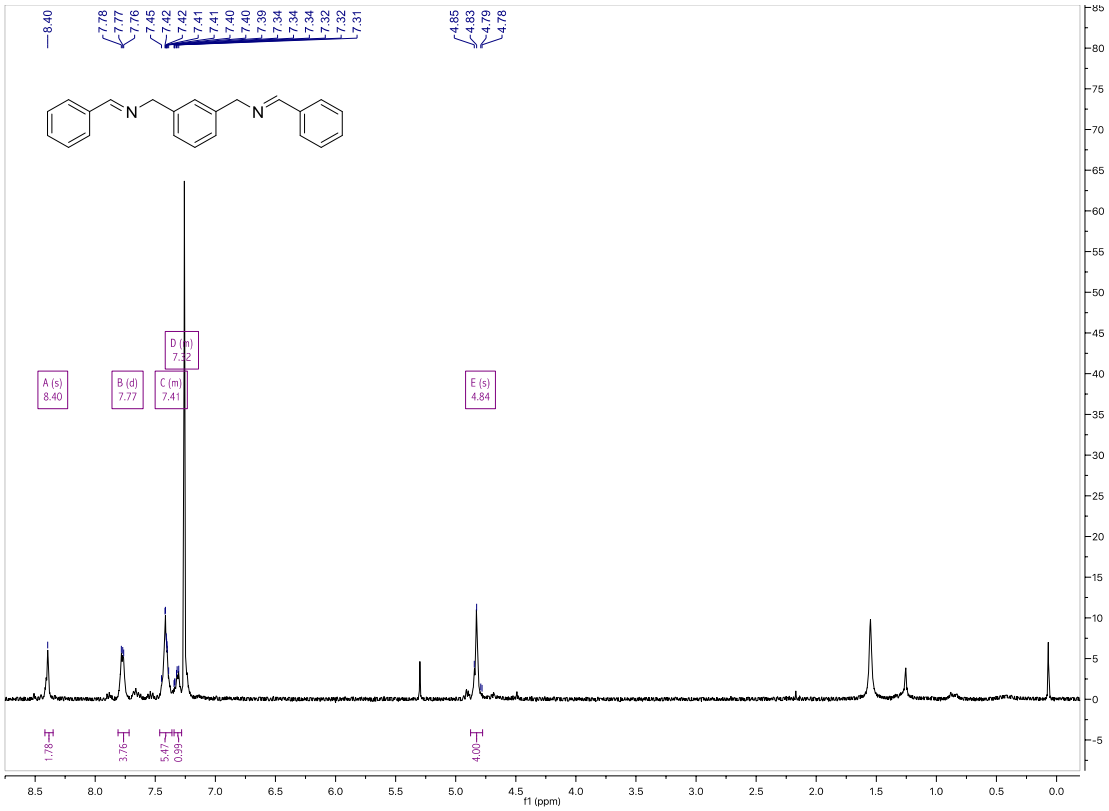

^{1}H-NMR spectrum of **22** and the monosubstituted analogue (400 Hz, CD_2Cl_2, 25°C)

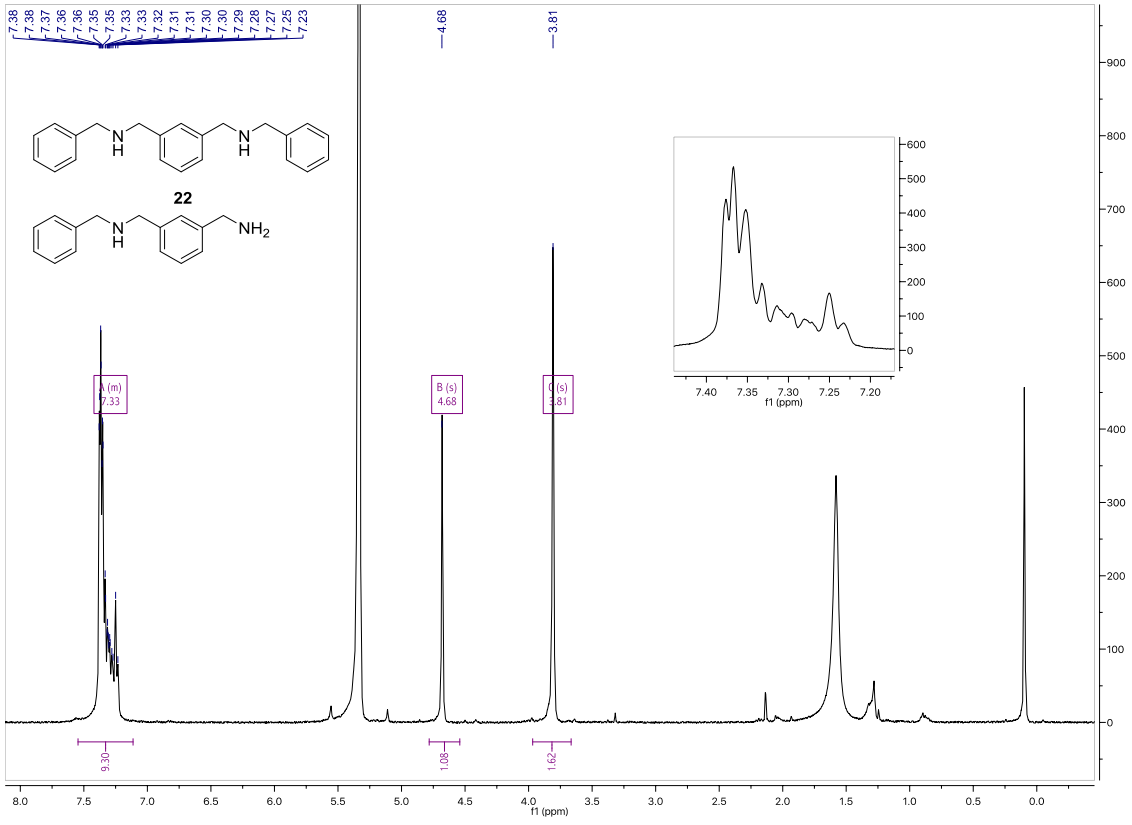

^{1}H-NMR spectrum of **22** and the monosubstituted analogue (400 Hz, $CDCl_3$, 25°C)

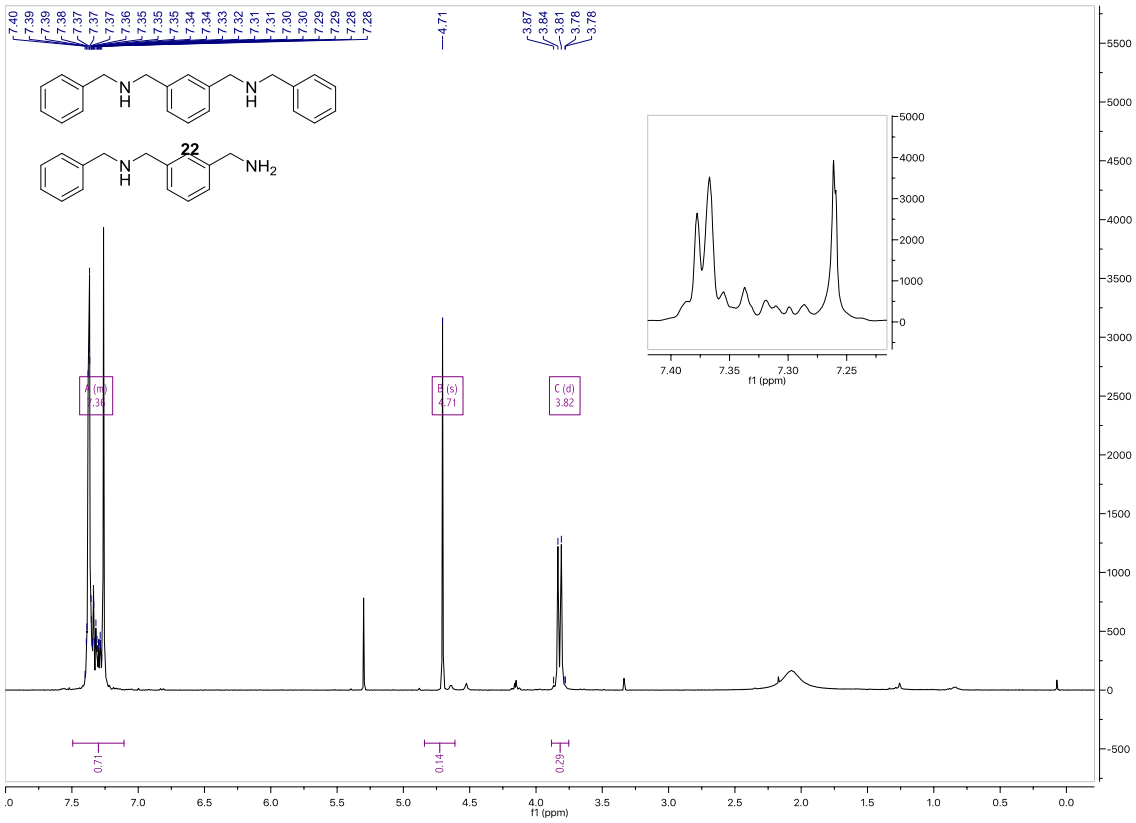

^{13}C-NMR spectrum of **22** and the monosubstituted analogue (100 Hz, $CDCl_3$, 25°C)

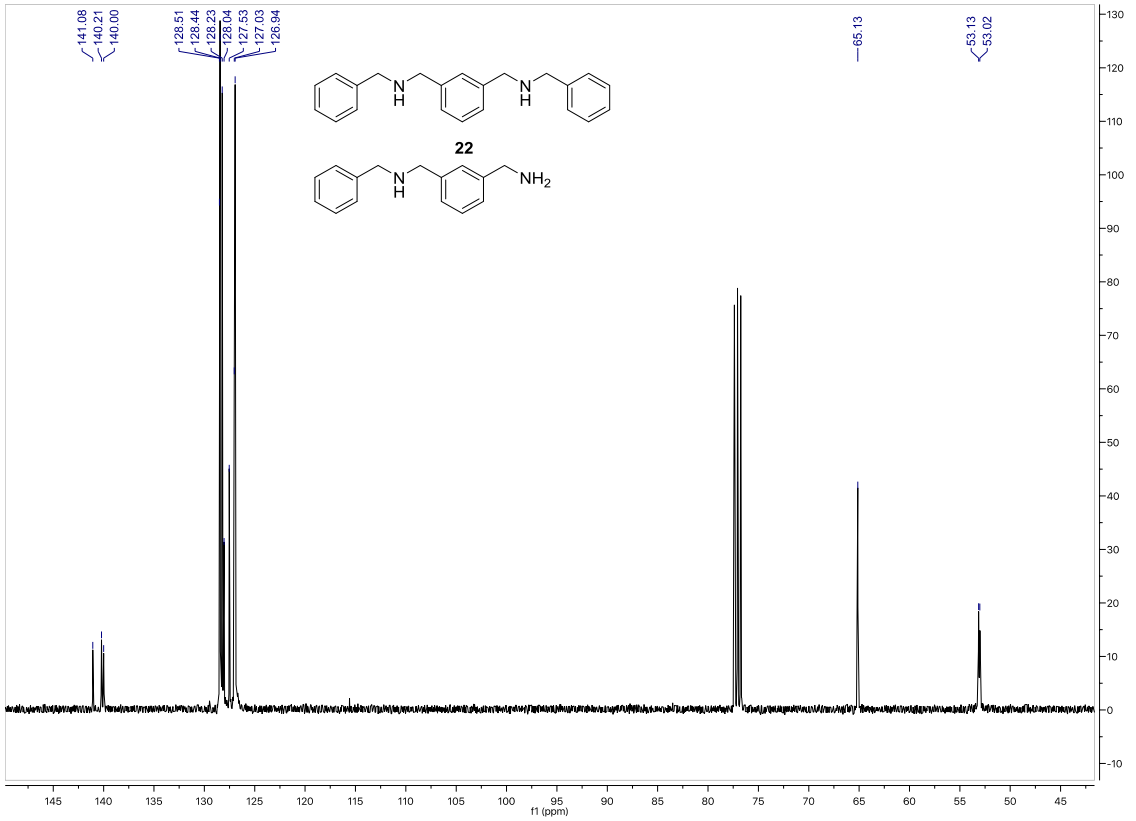

^{1}H-NMR spectrum of imine analogue of **23** (400 Hz, $CDCl_3$, 25°C)

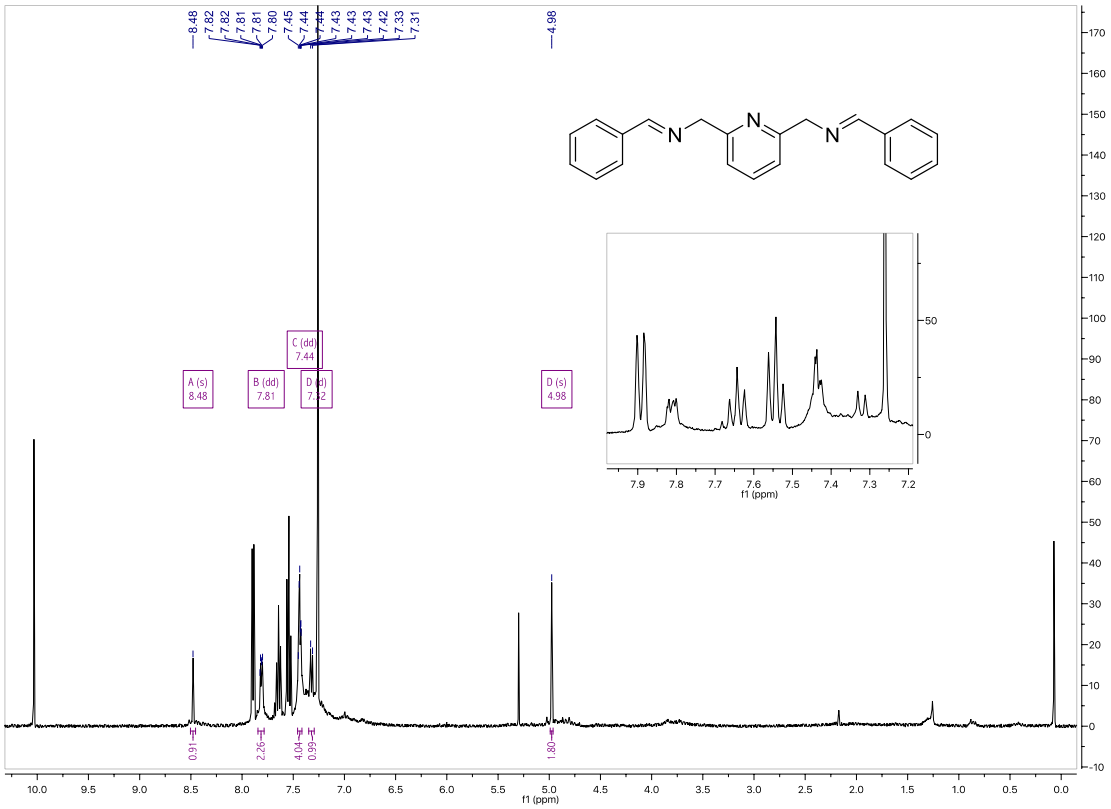

APPENDIX C

Synthesizes of **20**: ^{1}H-NMR (a) Gabriel Synthesis attempt 1, D_2O. (b) Gabriel Synthesis attempt 2, d6-DMSO. (c) Azide Synthesis attempt 1, $CDCl_3$. (d) Azide Synthesis attempt 2, $CDCl_3$. (e) Purchased **20**, $CDCl_3$.

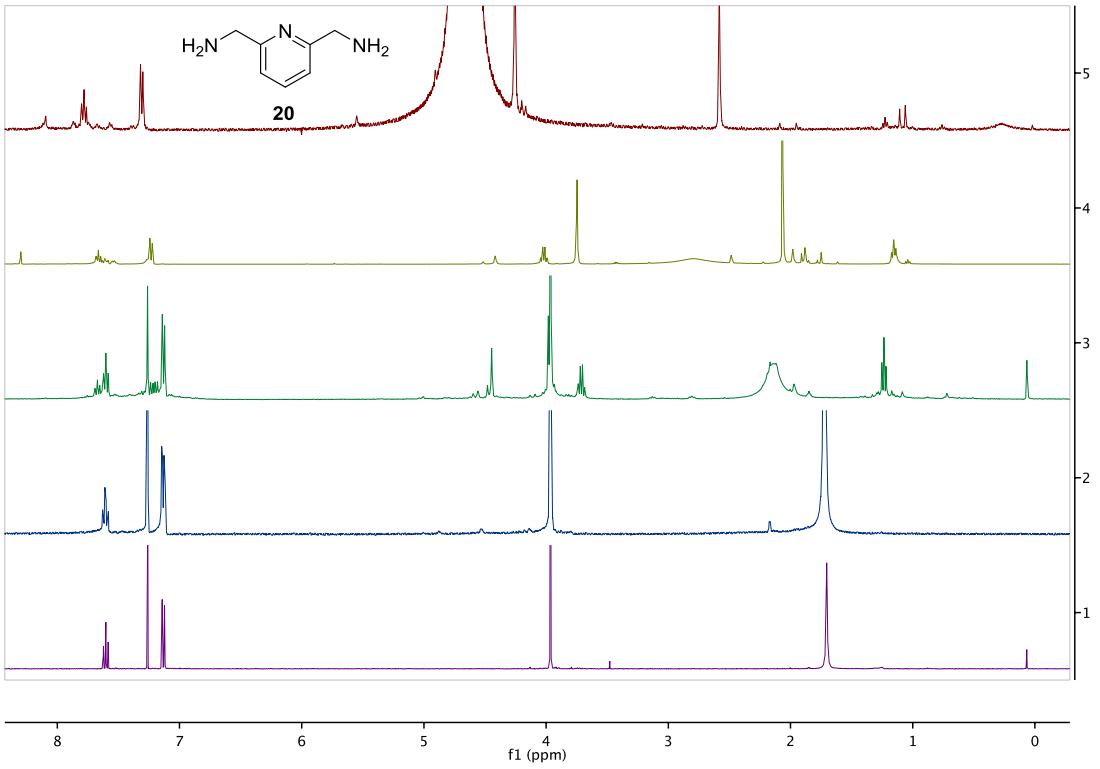

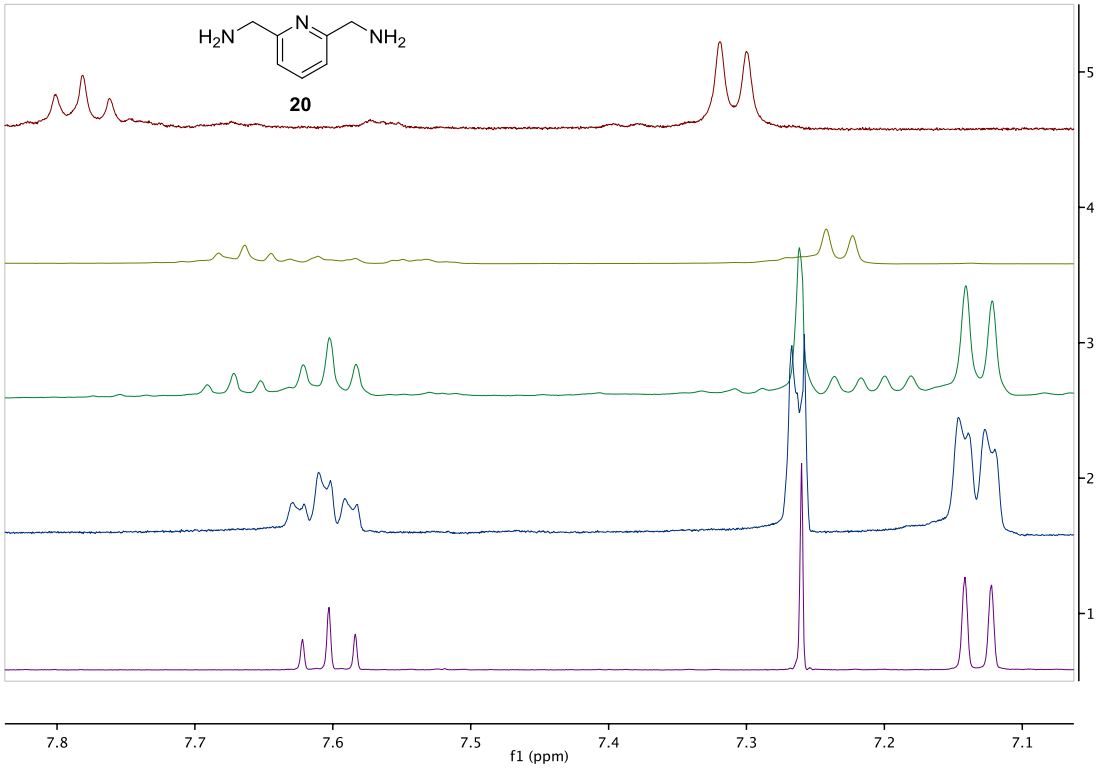

APPENDIX D

^{1}H-NMR spectrum of **50** (400 Hz, $CDCl_3$, 25°C)

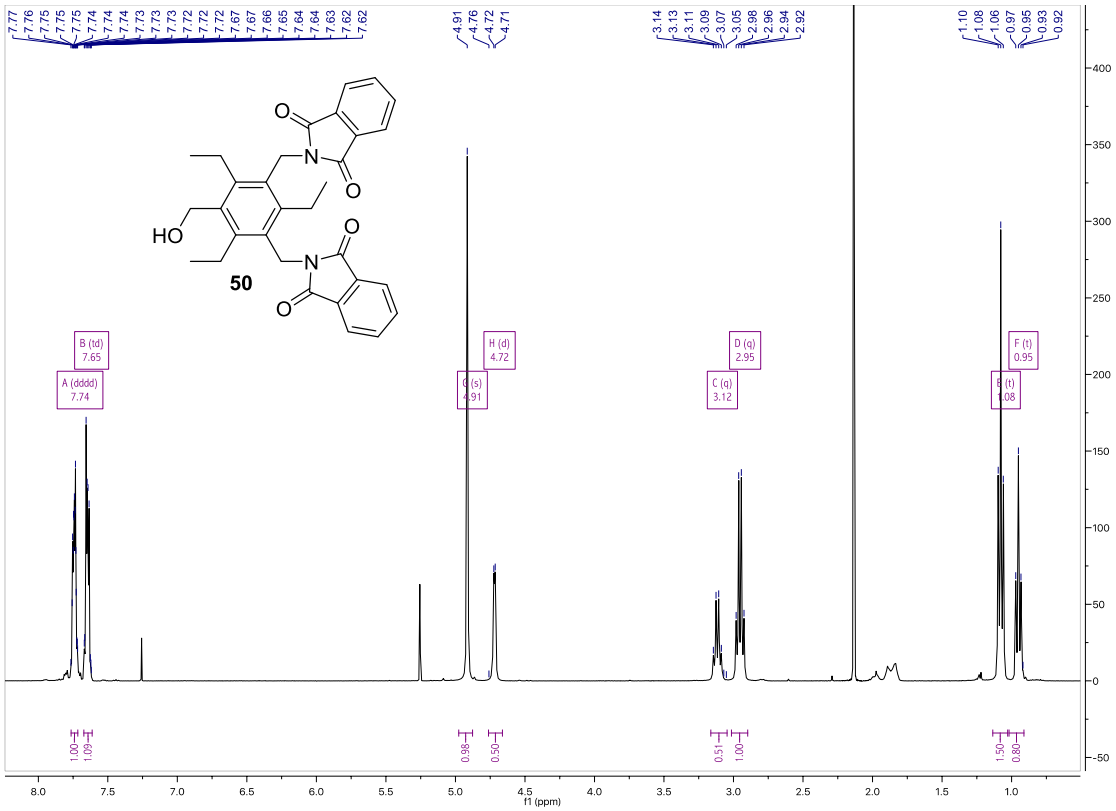

^{13}C-NMR spectrum of **50** (100 Hz, $CDCl_3$, 25°C)

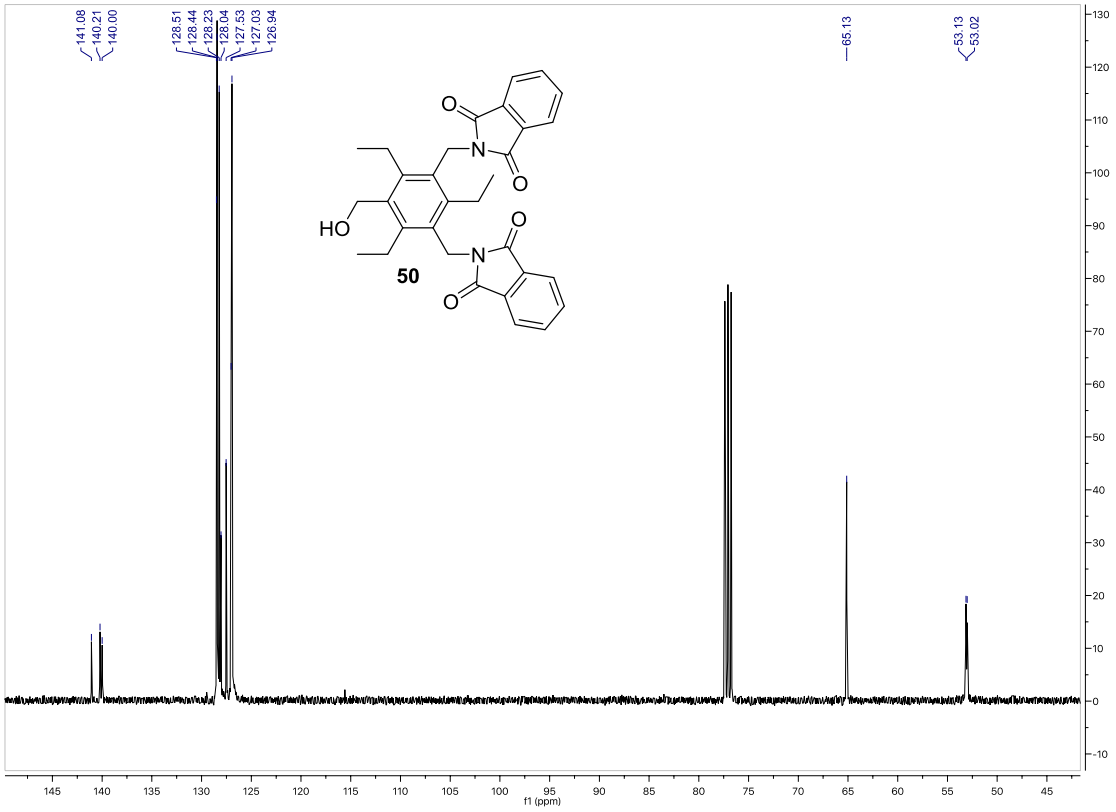

APPENDIX E

^{1}H-NMR spectrum of **53** (400 Hz, $CDCl_3$, 25°C)

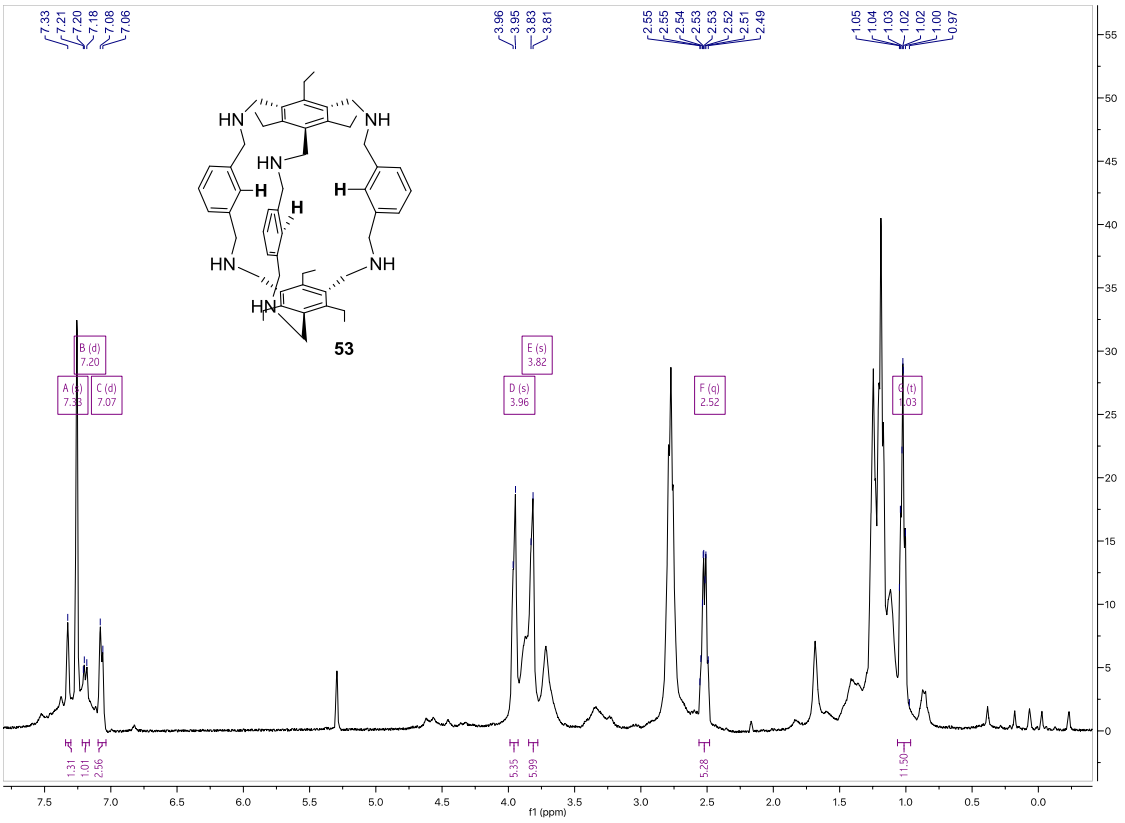

^{1}H-NMR spectrum of tribromide analogue of cage B **55** (400 Hz, $CDCl_3$, 25°C)

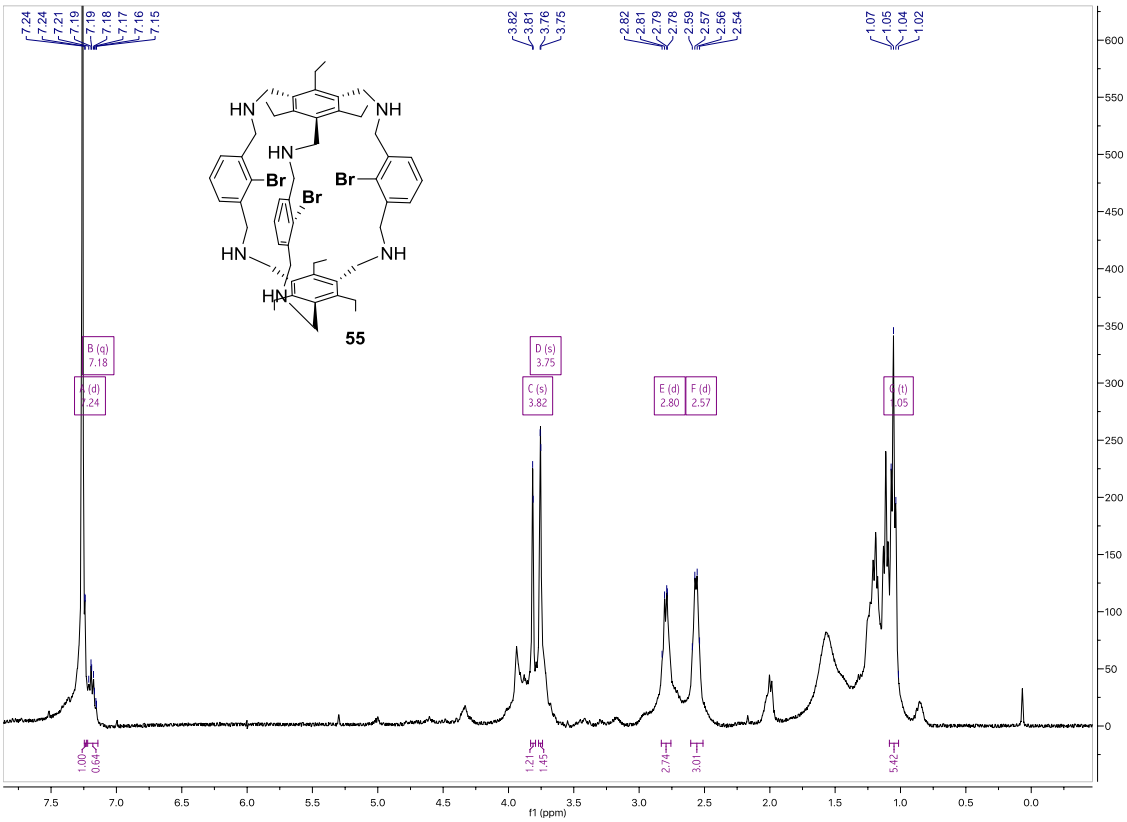

APPENDIX F

^{1}H-NMR spectrum of **C2** (400 Hz, $CDCl_3$, 25°C)

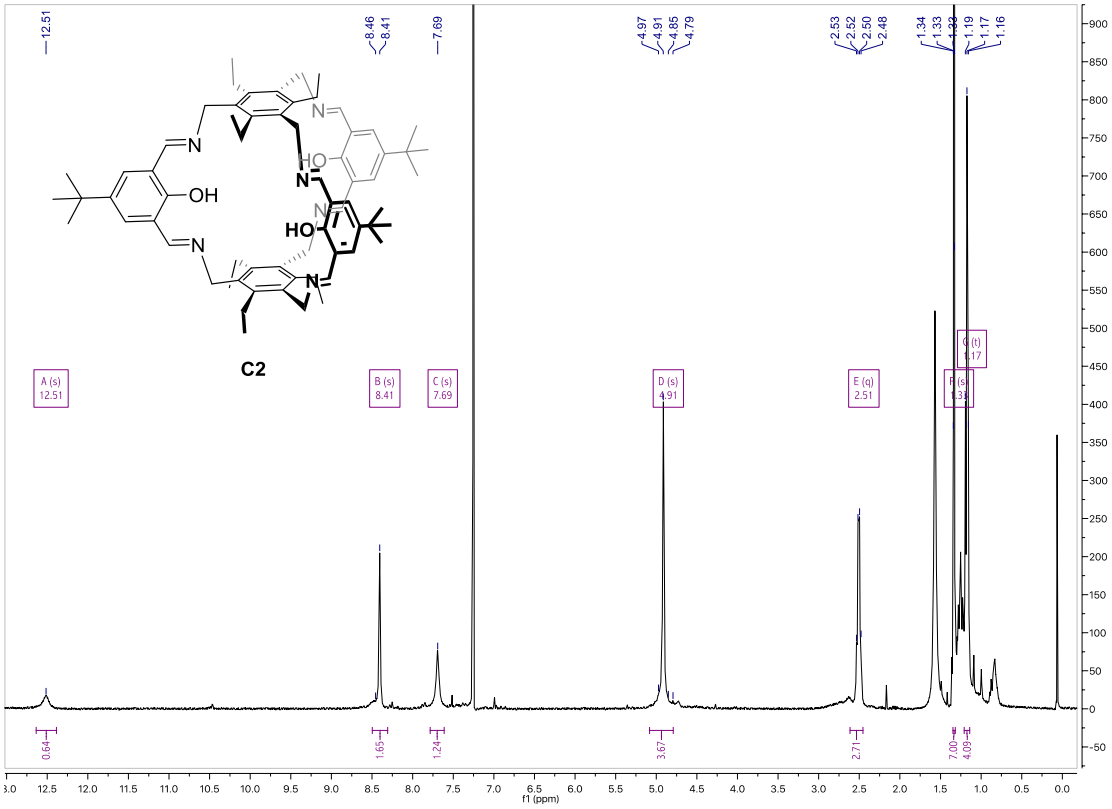

^{13}C-NMR spectrum of **C2** (100 Hz, $CDCl_3$, 25°C)

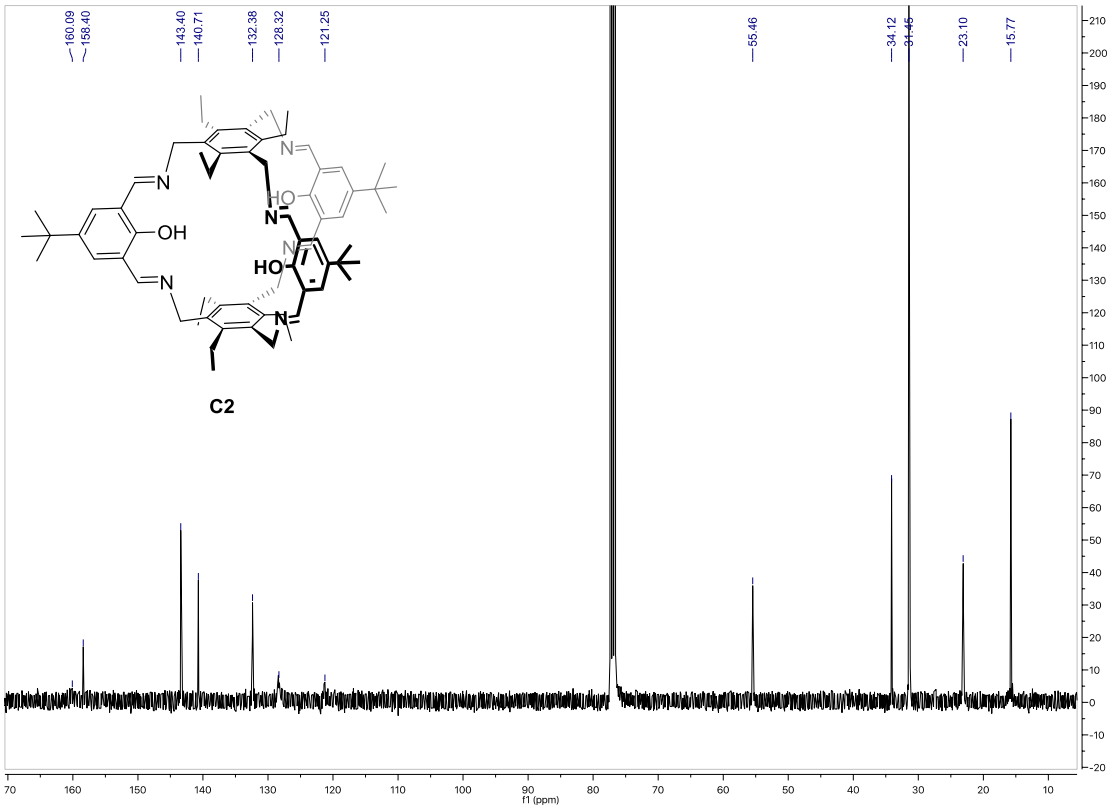

DOSY-NMR of synthesis of **C2**, 1 compound (400 Hz, $CDCl_3$, 25°C)

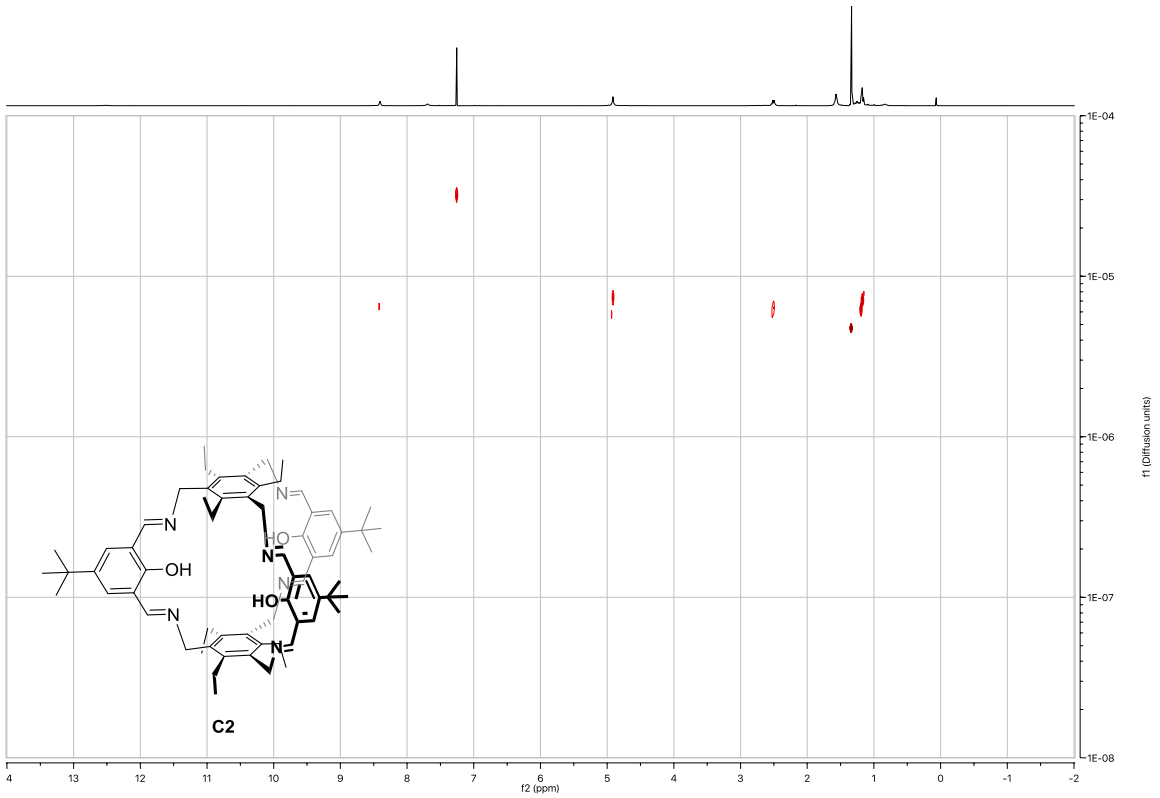

DOSY-NMR of synthesis of **C2**, 2 compounds (400 Hz, $CDCl_3$, 25°C)

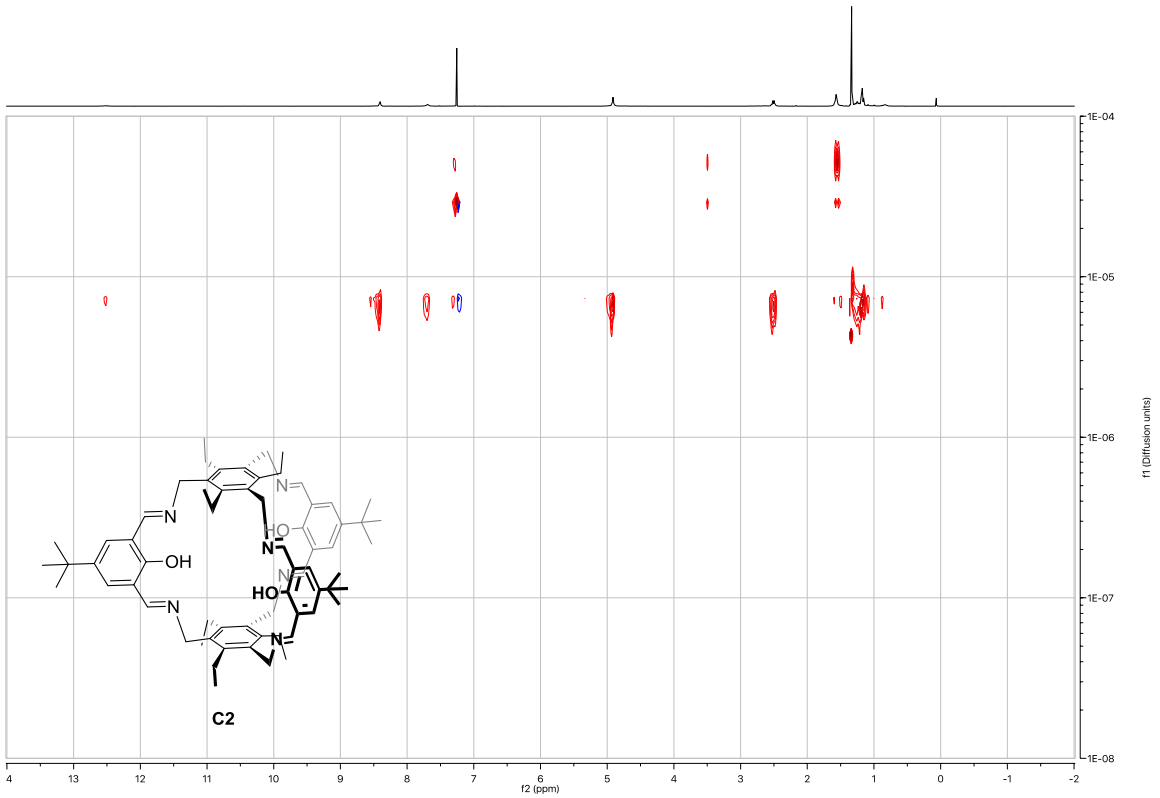

APPENDIX G

paramagmetic ^{1}H-NMR spectrum of coordinationexperiment with **C2** and $Cu(OAc)_2$ (1:3) on 60 ˚C. (400 Hz, $CDCl_3$, 25°C;. $t_{Relaxation}$ = 0.1 s; $t_{acquisition}$ = 0.1s.

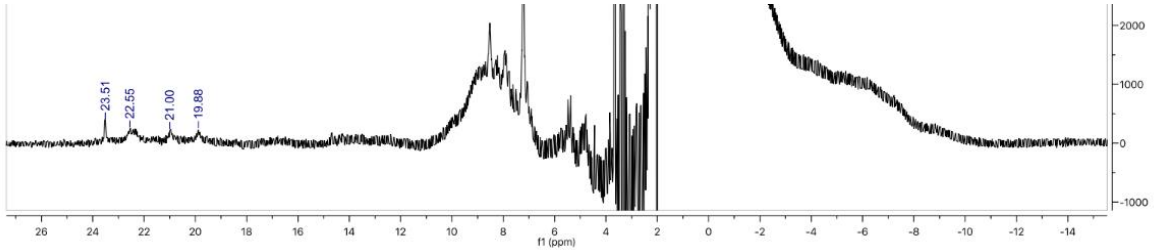

IR data

The spectra for copper-coordination show many other peaks. Some could be assigned with the use of literature [74] [17] (table 1). Peak **A** originates from an O-H vibration (phenol, water, acetate) or from a N-H vibration (NEt_3 or $HNEt_3^+$). Peak **C** and **D** could have two origins: aldehyde or $HNEt_3^+$. First, aldehydes are known to have a C-H comb of two peaks. Salt hydrolysis of $CuCl_2$ could have occurred, producing 2 eq acid and hydrolyzing the cage. Still, enough base should be present to neutralize the acid. In addition, the range is too high (2830-2810 cm^{-1}, 2750-2720 cm^{-1}) and no aldehyde peak is shown in the NMR spectrum. Therefore, the second origin is more likely, which is $HNEt_3^+$. Although, the reference is still slightly different. The overlapping peaks are partly caused by excesses of metal salts. To finalize, peak **F** and **H** in I. to III. come from the excess acetate ions and **G** and **I** might be from $CuCl_2$. This is all summarized in the table below.

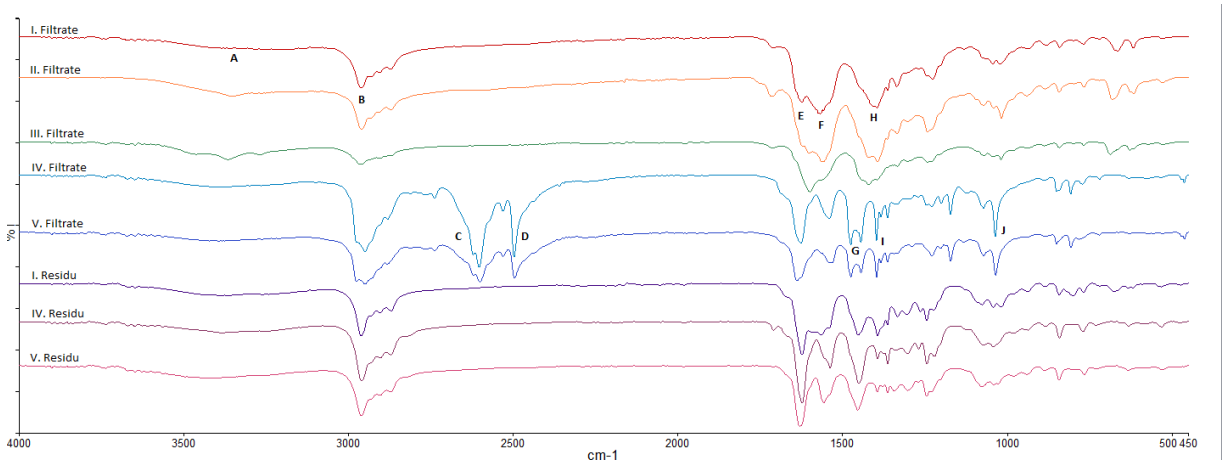

Figure 31: *Infrared spectra of copper coordination attempts.*

Peak	Assignment	Peak	Assignment
A	O-H stretch of phenol, water, acetate, NH	G	$CuCl_2$
B	C-H stretch alkane	H	$Cu(OAc)_2$
C	$HNEt_3^+$ st or aldehyde	I	$CuCl_2$
D	$HNEt_3^+$ st or aldehyde	J	?
E	C=N stretch of imine	K	C-O stretch phenol
F	$Cu(OAc)_2$		

Table 1: *Infrared spectra of copper coordination attempt*

[17] Peaks are assigned through probability, not evidence.

^{1}H-NMR spectrum of coordinationexperiment with **C2** and $Zn(OAc)_2 \cdot 2H_2O$ (400 Hz, CD_2Cl_2, 25°C).

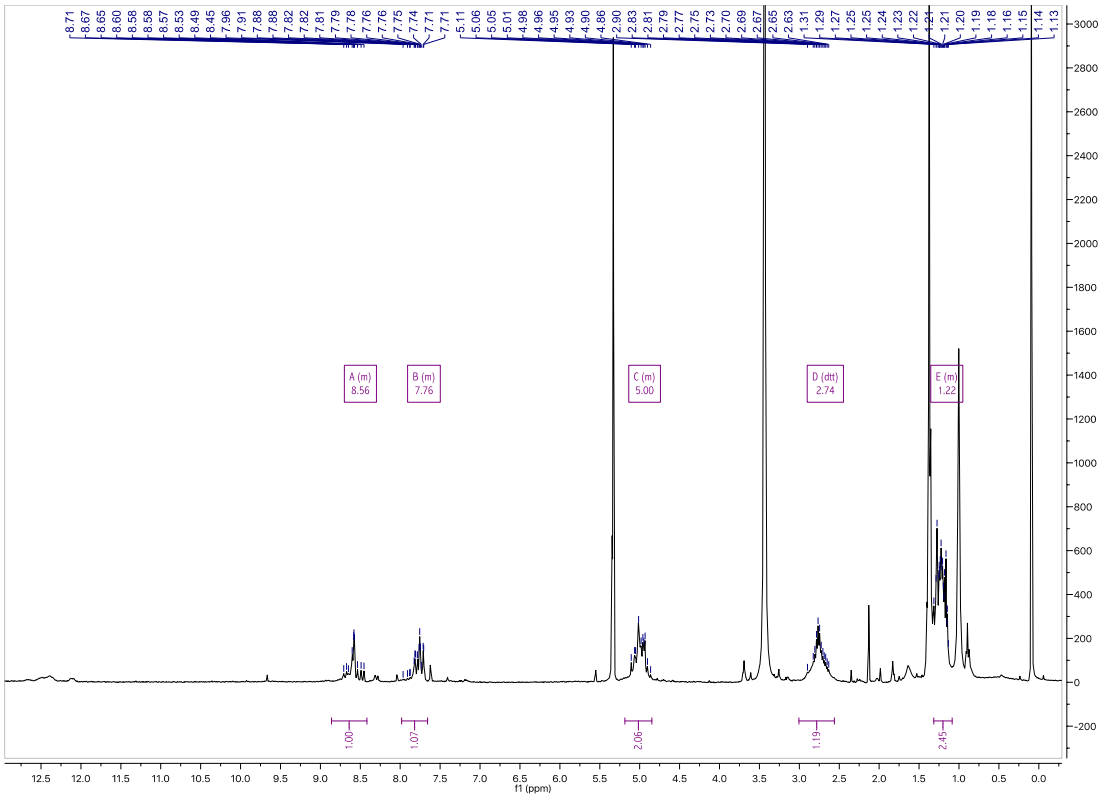

^{1}H-NMR spectrum of coordinationexperiment with **C2**, $ZnCl_2$ and NEt_3 (400 Hz, $CDCl_3$, 25°C).

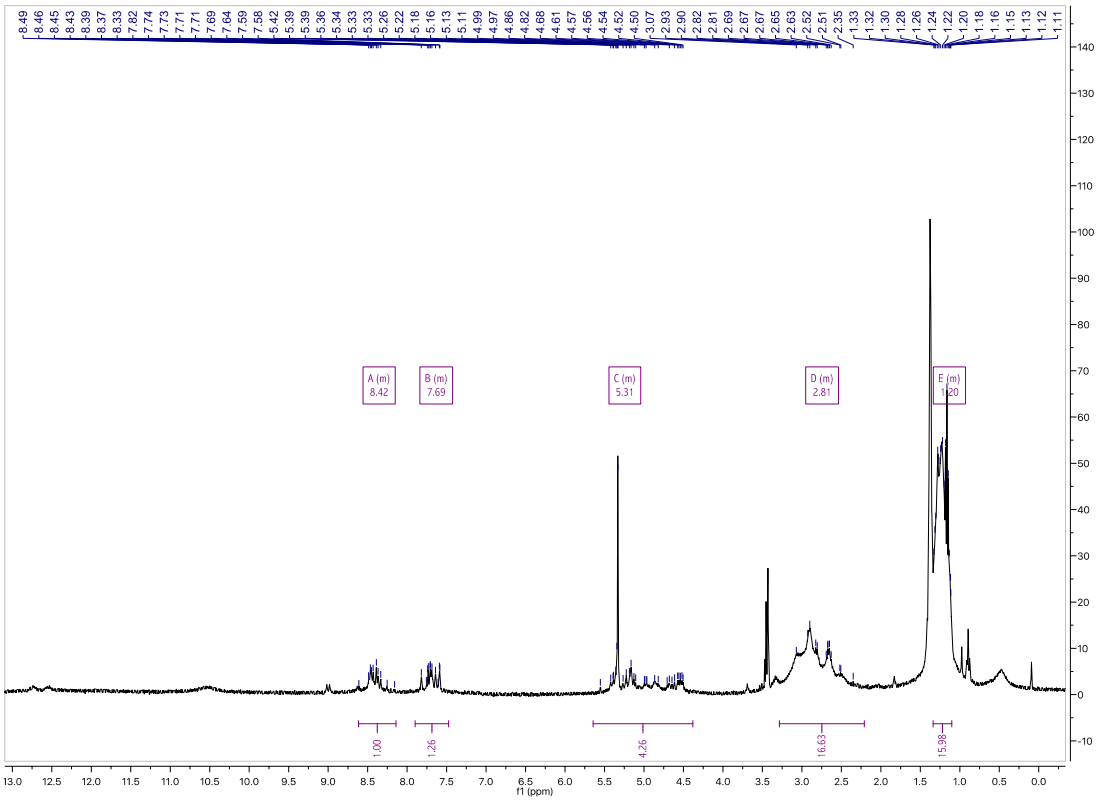

APPENDIX H

^{1}H-NMR spectrum of **C1** (400 Hz, $CDCl_3$, 25°C)

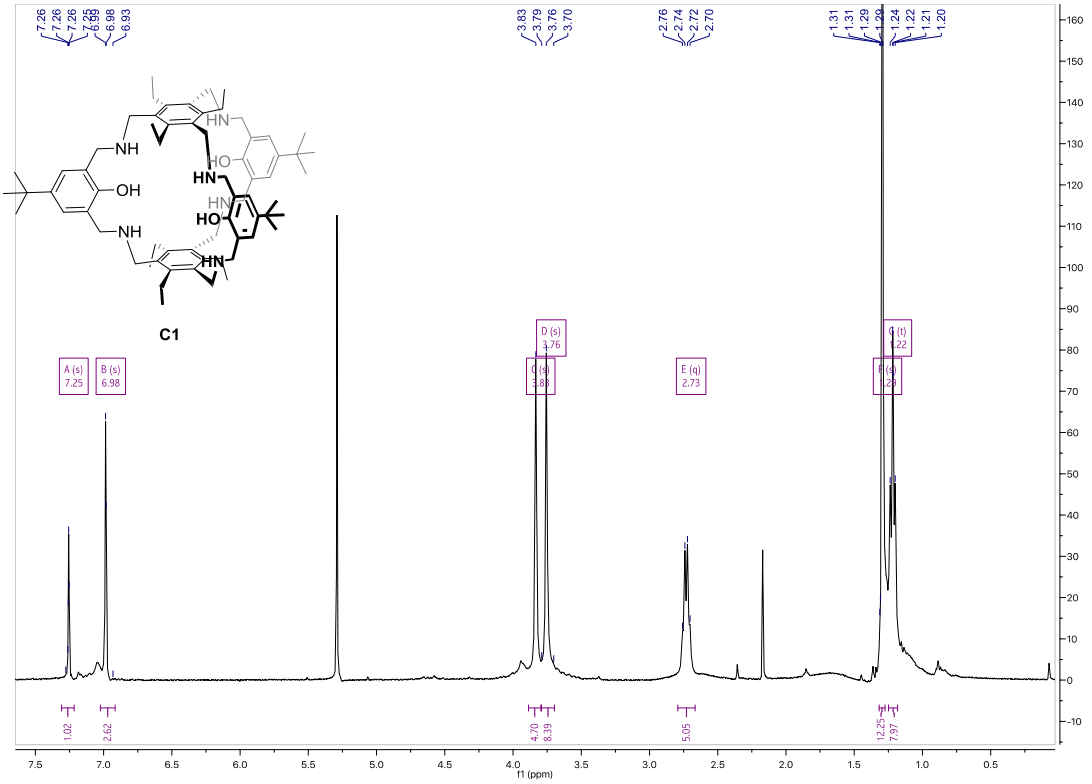

^{13}C-NMR spectrum of **C1** (100 Hz, $CDCl_3$, 25°C)

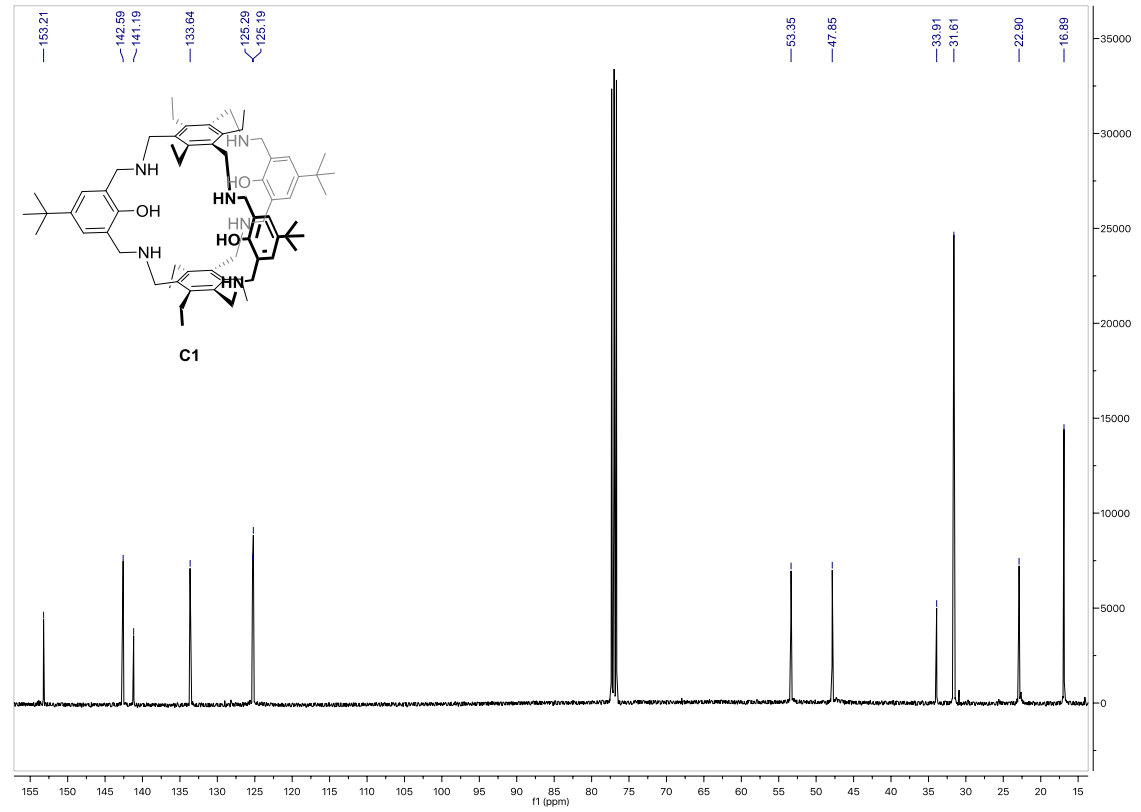

IR-spectrum of **C1** (neat, 25°C)

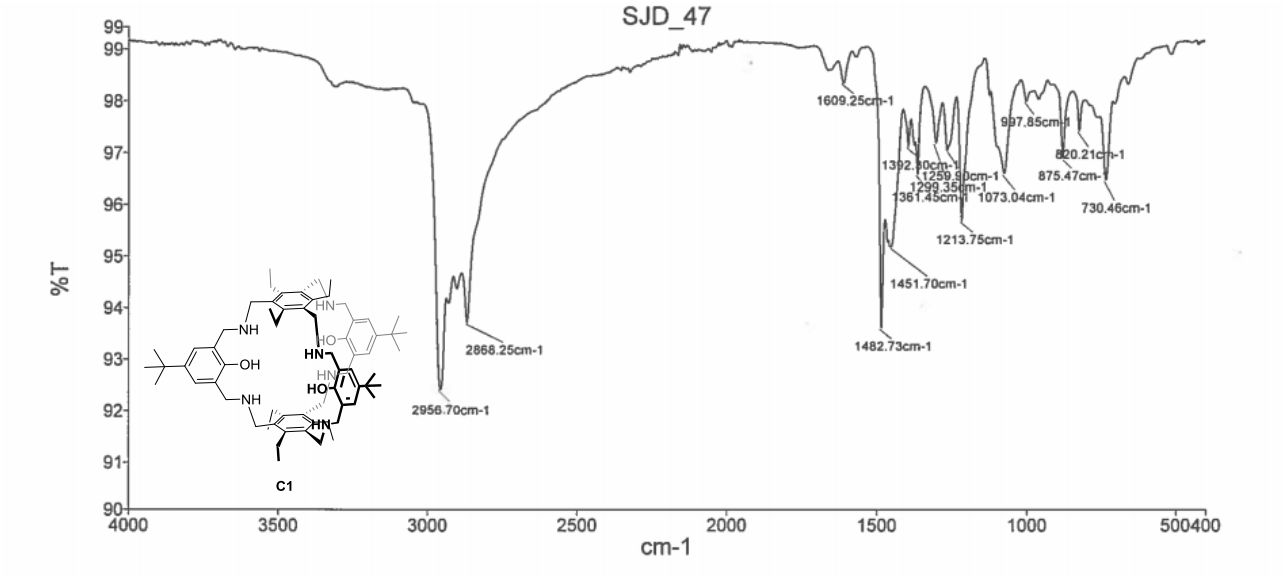

APPENDIX I

^{1}H-NMR spectrum of coordinationexperiment with **C1** and $Zn(OAc)_2 \cdot 2H_2O$ (400 Hz, $CDCl_3$, 25°C).

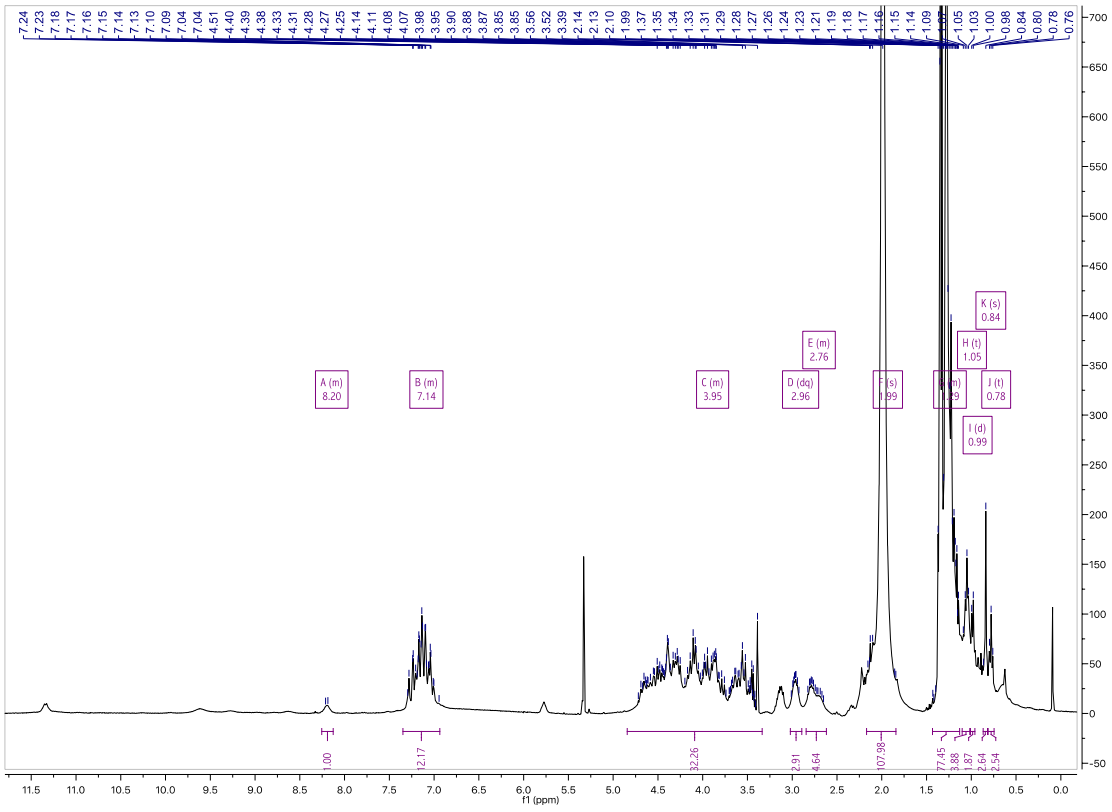

^{1}H-NMR spectrum of coordinationexperiment with **C1**, $ZnCl_2$ and NEt_3 (400 Hz, $CDCl_3$, 25°C).

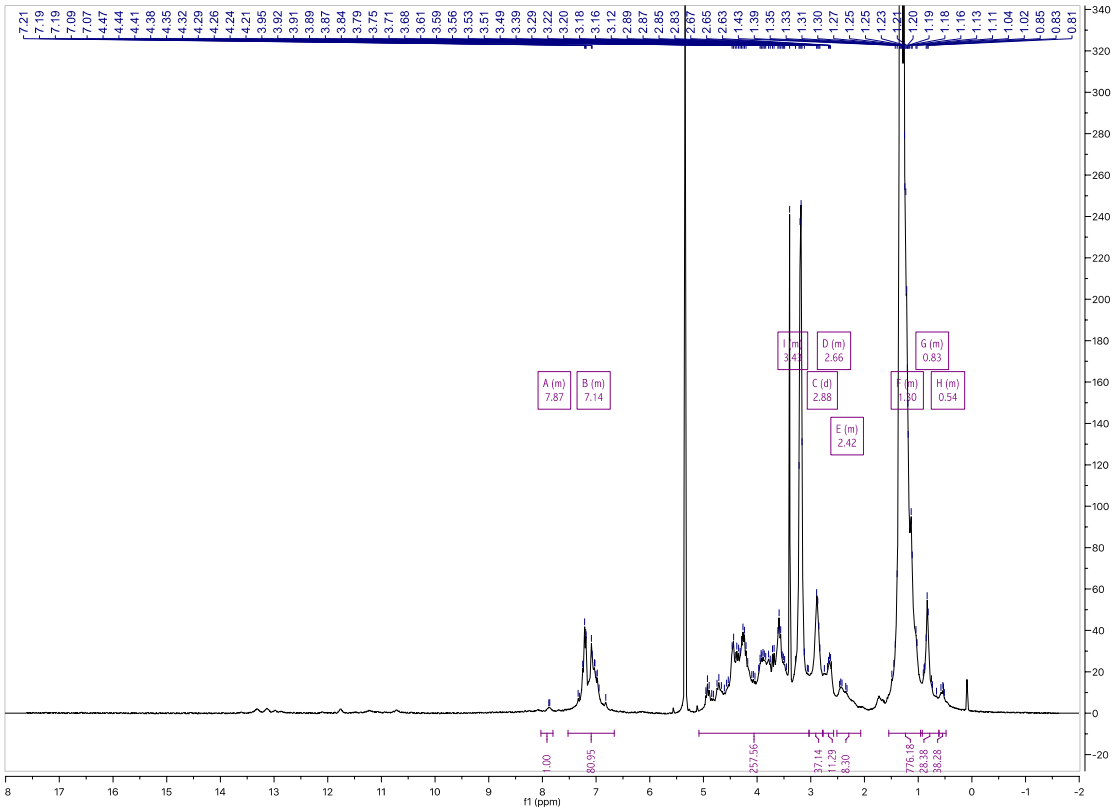

^{13}C-NMR spectrum of coordinationexperiment with **C1**, $ZnCl_2$ and NEt_3 (100 Hz, $CDCl_3$, 25°C).

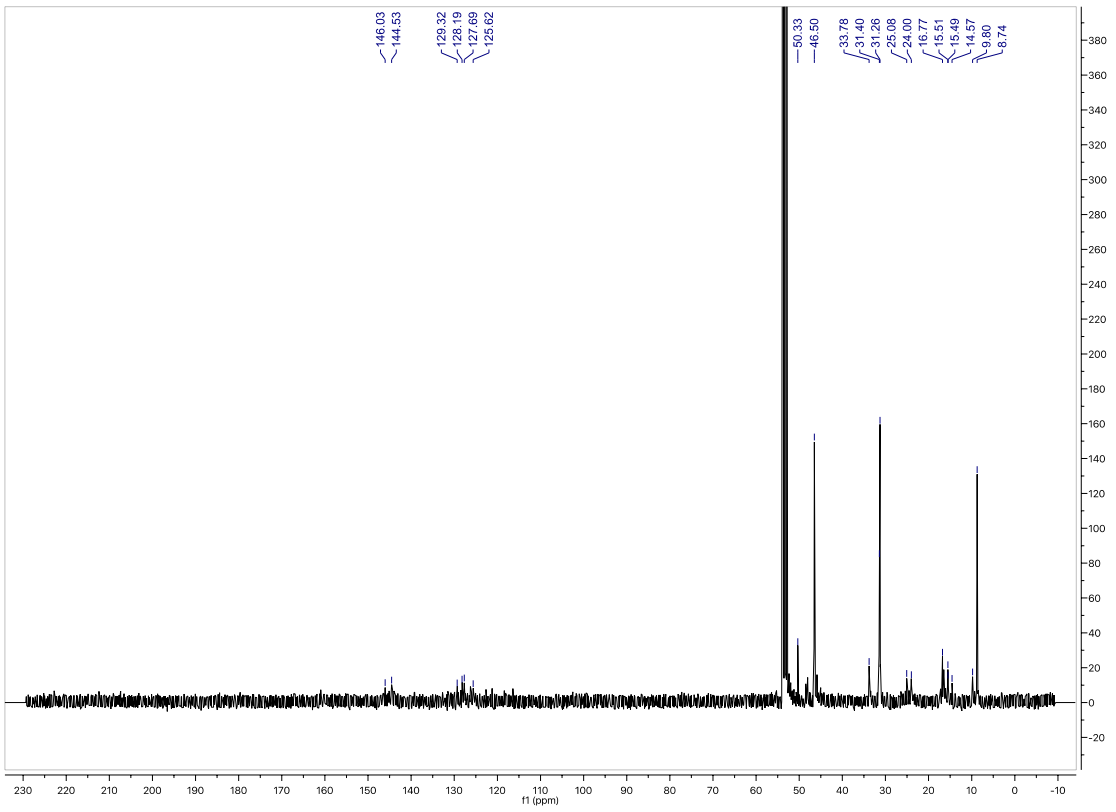

APPENDIX J

ESI-MS spectra of zinc-coordination experiments (CH_2Cl_2). (a) **C2** and $Zn(OAc)_2 \cdot 2H_2O$. (b) **C2**, $ZnCl_2$ and NEt_3. (c) **C1** and $Zn(OAc)_2$. (d) **C1**, $ZnCl_2$ and NEt_3.